

## **NanoVectors for Targeted Chemotherapy in Cervical Cancer**

---

**Az-Zamakhshariy Zardad**

A dissertation submitted to the Faculty of Health Sciences, University of the Witwatersrand,  
in fulfilment of the requirements for the degree of Master of Pharmacy



**Supervisor:**

Professor Viness Pillay, Department of Pharmacy and Pharmacology, University of the  
Witwatersrand, Johannesburg, South Africa

**Co-Supervisors:**

Associate Professor Yahya Essop Choonara, Department of Pharmacy and Pharmacology,  
University of the Witwatersrand, Johannesburg, South Africa

Associate Professor Lisa Clare du Toit, Department of Pharmacy and Pharmacology,  
University of the Witwatersrand, Johannesburg, South Africa

Mr Pradeep Kumar Department of Pharmacy and Pharmacology, University of the  
Witwatersrand, Johannesburg, South Africa

## DECLARATION

---

---

I, Az-Zamakhshariy Zardad, declare that this dissertation is my own work and done to the best of my ability. It is being submitted for the degree of Master of Pharmacy in the Faculty of Health Sciences at the University of the Witwatersrand, Johannesburg, South Africa. It has not been submitted before for any degree or examination at this or any other University.

\_\_\_\_\_  
Signature

This \_\_\_\_\_ day of \_\_\_\_\_, 2017 at \_\_\_\_\_

## DEDICATION

---

The effort and the work put into this project are dedicated to my parents Imran and Fatima Zardad. They always supported me throughout my academic years and encouraged me to do my best in everything I pursue. Thank you for your giving me the endless opportunities I received in my life, I could never repay you for what you have afforded me.

## RESEARCH PUBLICATIONS

---

1. A Review of Thermo- and Ultrasound-Responsive Polymeric Systems for Delivery of Chemotherapeutic Agents. Zardad A., Choonara Y. E., du Toit L. C., Kumar P., Mabrouk M., Kondiah P. P. D., Pillay V. Zardad, A.-Z.; Choonara, Y.E.; du Toit, L.C.; Kumar, P.; Mabrouk, M.; Kondiah, P.P.D.; Pillay, V. A Review of Thermo- and Ultrasound-Responsive Polymeric Systems for Delivery of Chemotherapeutic Agents. *Polymers* 2016, 8, 359
2. Facile Green Synthesis of Thermosonic injectable Organogels (TIO's). Zardad A., Choonara Y. E., du Toit L. C., Kumar P., Mabrouk M., Badhe R.V., Cheraja D.R., Kondiah P. P. D., Pillay V. (To be submitted to an international peer reviewed journal)
3. Synthesis, Characterization and Assembly of Solid Lipid Nanospheres into the Thermosonic Injectable Organogels (TINO's). Zardad A., Choonara Y. E., du Toit L. C., Kumar P., Mabrouk M., Kondiah P. P. D., Pillay V. (To be submitted to an international peer reviewed journal)

## ACKNOWLEDGEMENTS

---

I would like to express my gratitude to Professor Viness Pillay for always encouraging me through the trying times and being such an involved supervisor and showing interest in my work.

Professor Yahya Choonara, thank you for always providing me with helpful input and thorough feedback in my research and providing me with realistic solutions to overcome challenges I've faced.

Professor Lisa du Toit, I am very grateful to you for always being willing at any time to assist me with the operation of lab equipment and being available for immediate consultation in urgent times.

Mr Pradeep Kumar, thank you for being an inspiring example of a researcher, supervisor and mentor, observing what you achieve everyday always gives me courage to start a new day in the lab.

Dr Mostafa Mabrouk, I appreciate all the time you took to guide me throughout my research and assisting me to understand important concepts in our field.

Thank you to Dr Ravindra Badhe for assisting me with my cytotoxicity studies, Dr Thashree Marimuthu, Dr Lomas Tomar, Dr Charu Tyagi and Dr Dharmesh Chereja for always advising me well.

Thank you to all my colleagues, Simphiwe Mavuso, Fatema Mia, Pakama Mahlumba, Margaret Siyawamwaya, Khuphukile Madida, Khadija Rhoda, Latavia Singh, Dr Pierre Kondiah, Karmani Murugan, Fatima Bibi Choonara, Poornima Ramburran, Dr Mershen Govender, Dr Sunaina Inderman, Dr Femi Akilo, Mduduzi Sithole, Zikhona Hiyayana and Sam Adayoni for being so helpful during the course of my research

Thank you to all lab staff members, Mr Sello Ramamrumo, Pride Mothobi, Bafana and Kleinbooi, for always being helpful when assistance is needed in the lab.

Thank you to my parents and siblings for all the support and endless encouragement they've given to me throughout my academic years.

I want to express my deepest gratitude to my dearest Faatimah Ismail for believing in me and being my pillar of strength every single day to take on new challenges.

To one of my closest friends Muhammad Abu Bakr Reis thank you for always being there when I needed support and an extra push to get through the day.

Thank you to Professor Viness Pillay Chair Grant National Research Funding (NRF) of South Africa for funding my research and to the Wits Staff bursary for assisting me to complete my research.

In The Name of God The Most Gracious The Most Merciful

## ABSTRACT

---

Cervical Intraepithelial Neoplasia (CIN) or Human Papilloma Virus (HPV) is known as the precancerous stages of cervical cancer and may be treated with antineoplastic agents. Current treatment includes intravenous administration of Gemcitabine and 5-Fluorouracil however, these drugs have an undesirable side effect profile. This may be overcome by local administration of chemotherapeutic drugs to the site of the cancer. The purpose of this study was to design a drug delivery system that can be locally administered to the site of the cervical cancer and possess thermosonic properties. Designs of three Thermosonic Injectable Organogels (TIO's) were undertaken using ring opening polymerization (open ring reaction) to formulate three different gels to test the response ability of the gels against thermal and ultrasound exposure. The times taken for these gels to form were recorded at below 15 minutes. All three TIO's responded differently to thermal and ultrasound stimuli. Physical changes in the gels were noted and further studies were undertaken to confirm their responsiveness towards the dual-stimuli. All three TIO's showed a dense microstructure containing pores catering for the incorporation of drugs or drug-loaded carriers. Rheological studies showed that there was an increase in viscosity of the gels under increasing heat even though the response differed between TIO formulations. The gels were non-cytotoxic at distinct concentrations ranging between 6.1mg/ml-7.8mg/ml. Solid Lipid Nanospheres (SLN's) were then designed which encapsulated the model antineoplastic drug 5-Fluorouracil. The SLN's were spherical in shape and had an acceptable poly dispersion index (PDI) which was below 0.7 after ultrasonication and filtration of prepared samples. The SLN's were then incorporated by direct addition and dispersion into the TIO formulations before undertaking the open ring reaction to form Thermosonic Injectable Nano-Organogels (TINO's). The TINO's were analysed for its swelling and erosive properties. Results showed that the TINO's possess both swelling and erosive properties. Furthermore, the TINO's underwent dissolution studies that involved thermal and thermal with ultrasound stimuli to test the drug release rate and the stimuli responsiveness of the TINO. Results of the SLN's showed a very slow release rate whether exposed to a single (thermal) or both thermal and ultrasound stimuli, indicating that the addition of ultrasound stimuli did not alter the drug release from the SLN's. However, the incorporation of the SLN's into the TIO's prolonged the release rate. Hence increasing the SLN concentration in the TIO's reduced the response towards ultrasound stimuli. Therefore lower ratios of SLN:TIO provided superior responsiveness compared to higher concentrations of SLN:TIO. TIO 1 and TINO 2 released drug with thermal stimuli and higher drug release occurred with exposure to both thermal and ultrasound stimuli. These TINO's in conjunction with ultrasound responsiveness may be used as a potential platform for the delivery of antineoplastics in treating cervical cancer.

## LIST OF ABBREVIATIONS

---

AA	Acrylic Acid
AAM	Acrylamide
PBMA	Poly(butyl methacrylate)
BSA	Bovine Serum Albumin
CHC	Carboxymethyl-hexanoyl chitosan
CHOL	Cholesterol
CHOL(b)	Cholesterol Bodipy
DMDEA	2-(5,5-dimethyl-1,3-dioxan-2 yl oxy) ethyl acrylate
DPPC	1,2 -dipalmitoyl-sn-glycero-3-phosphatidylcholine
DPPE	Dipalmitoyl -sn-glycero-3-phosphatidylethanolamine
DPPG	Dipalmitoyl phosphatidylglycerol
DPSC	1,2-distearoyl-sn-glycero-phosphcholine
DPSE	1,2 distearoyl-sn-glycero-3-phosphoethanolamine
DSPC	1,2-distearoyl-sn-glycero-3-phosphotidylcholine
DSPE	1,2-distearoyl-sn-glycero-3-phosphoethanolamine
DSPG	1,2-dioctadecanoyl-sn-glycero-3-phospho-(1'-rac-glycerol)
HAP-1	Human Atherosclerotic Peptide-1
HMM	2-hydroxymethyl methacrylate
MOEGA	Monomethyl oligo (ethylene glycol) acrylate
MSPC	1 stearoyl-2-hydroxy-sn-glycero-3-phosphocholine
N DMAM	N Dimethylacrylamide
N-(hm)A	n-hydroxymethyl acrylamide
N'N DMAM	N,N Dimethylacrylamide
P( $\beta$ A)	Poly ( $\beta$ benzyl-L-Aspartate)
P(thfma)	Poly(2-tetrahydrofuranoloxo) ethylmethacrylate
P(thpma)	Poly(2-tetrahydropyranyl) methacrylate

PCL	Poly Caprolactone
PEG	Polyethylene Glycol
PEG'd	Polyethylene Glycolated
PEI	Polyethyleneamine
PEO	Polyethylene Oxide
PIBMA	Poly[(Isobutoxy) ethyl methacrylate]
PFC	Perfluorocarbon
PFH	Perfluorohexane
PFP	Perflouropentane
PLA	Poly (Lactide Acid)
PLa	Poly (D,L-lactide)
PLGA	Poly (D,L-lactide-co-glycolide)
PLLA	Poly L-lysine
PMA	Poly methacrylate
PMMA	Poly methyl methacrylate
P(NIPAM)	Poly (N-Isopropyl Acrylamide)
PPaa	Propylacrylic Acid
SLN	Solid Lipid Nanospheres
SPIO	Super Paramagnetic Iron Oxide
TIO	Thermosonic Injectable Organogel
TINO	Thermosonic Injectable Nano-Organogel



## LIST OF EQUATIONS

---

**Equation 2.1**  $UH = tR^{(43-T)}$

**Equation 3.1**  $CC = [\text{The number of cells (in the 4 corner quadrants)} / 4] \times \text{Dilution factor (4)}$

**Equation 3.2**  $\% CV = \text{Absorbance of sample} / \text{Absorbance of control} \times 100$

**Equation 4.1**  $\% \text{ Drug loading} = \text{Weight of the drug in the formulation} / \text{Weight of total formulation} \times 100$

**Equation 4.2**  $\% \text{ Encapsulated Drug} = \text{Actual drug loaded} / \text{Theoretical drug Loaded} \times 100$

## LIST OF FIGURES

---

**Figure 1.** Schematic representation of a) TINO units (drug-loaded SLN within the TIO) b) TINO injected into cervical cancer tumour site c) ultrasound application targeting the tumour site d) TINO responding to ultrasound, causing increased drug release and intracellular permeability of the tumour due to an increase in localized heat.

**Figure 2.1** Conceptual illustration representing the drug release mechanism of thermo-responsive systems with an LCST. Adapted from Nakayama *et al.* (2006).

**Figure 2.2** Schematic illustrating low and high power ultrasound assisting in drug delivery through microbubbles and cavitation. Adapted from Zhao *et al.* (2013).

**Figure 2.3** Image illustrating a Near InfraRed Laser being applied to the site of delivery and the mechanism of action that occurs with heat stimulus. Adapted from Zhang *et al.* (2014).

**Figure 2.4** Graphs representing the proliferation index and apoptosis index considering individual formulatory components and combinations of saline, nanobubbles, drug, antibodies and HIFU. Source: Zhang *et al.* (2014).

**Figure 2.5** Schematic of sonoporation of the vascular endothelia cells allowing the nanocapsules direct contact with the tumour cells and releasing drug into tumour cells. Adapted from Yang *et al.* (2014).

**Figure 2.6** Schematic illustrating focused ultrasound-mediated drug absorption into cancer cells leading to tumour cell death, Adapted from Gourevich *et al.* (2013).

**Figure 3.1** Bar Graph comparing the gelling time during preparation of TIO 1 TIO 2 and TIO 3.

**Figure 3.2** Figures illustrating the mechanism cycle of response to thermal and ultrasonic stimuli a) TIO 1 b) TIO 2 c) TIO 3.

**Figure 3.3** SEM Images TIO 1, a) and b), TIO 2 c) and d) and TIO 3 e) and f). Illustrating the general surface morphology of the gels.

**Figure 3.4** FTIR Spectra illustrating the chemical transformations of the monomers to the TIO formulations

**Figure 3.5** Thermal behaviour of TIO formulations and their parent monomers.

**Figure 3.6** X-ray Diffraction depicting the physicochemical nature of TIO 1, TIO 2, TIO 3 and the parent monomers of the gel.

**Figure 3.7** Frequency sweep of TIO 1, TIO 2, TIO 3 and a Reference.

**Figure 3.8** Temp ramp rheological characterization for TIO 1, TIO 2, TIO 3 and a Reference.

**Figure 3.9** Graphs illustrating the shear viscosity for TIO 1, TIO 2 and TIO 3.

**Figure 3.10** Compressive strength demonstrated by TIO 1, TIO 2 and TIO 3

**Figure 3.11** Deformation energy demonstrated by TIO 1, TIO 2 and TIO 3.

**Figure 3.12** Gel Resilience % given by TIO 1, TIO 2 and TIO 3.

**Figure 3.13** Graph Illustrating the EC 50 of TIO 1 TIO 2 and TIO 3.

**Figure 3.14** Graph illustrating the % cell viability on day 1 for TIO 1 TIO 2 and TIO 3

**Figure 3.15** Graph illustrating the % cell viability on day 3 for TIO 1 TIO 2 and TIO 3.

**Figure 3.16** Graph illustrating the % cell viability on day 5 for TIO 1 TIO 2 and TIO 3.

**Figure 4.1** Graph illustrating the surface molecular status of 1:1 PA:PLA plain and 1:1 PA:PLA drug encapsulated.

**Figure 4.2** Graph illustrating the surface molecular status of 2:1 PA:PLA (plain) and 2:1 PA:PLA (drug encapsulated)

**Figure 4.3** Graph illustrating the thermal behaviour for 1:1 PA:PLA (plain) and 1:1 PA:PLA (drug encapsulated).

**Figure 4.4** Graph illustrating the thermal behaviour for 2:1 PA:PLA (plain) and 2:1 PA:PLA (drug encapsulated).

**Figure 4.5** Molecular phase classification of 1:1 PA:PLA (plain) and 1:1 PA:PLA (drug encapsulated).

**Figure 4.6** Molecular phase classification of 2:1 PA:PLA (plain) and 2:1 PA:PLA (drug encapsulated).

**Figure 4.7** Scanning electron microscope images for a) 1:1 PA:PLA (drug encapsulated), b) 1:1 PA:PLA (plain), c) 2:1 PA:PLA (drug encapsulated), d) 2:1 PA:PLA (plain).

**Figure 4.8** A calibration curve for 5-FU in methanol.

**Figure 4.9** Graphs depicting zeta size and zeta potential for 1:1 PA:PLA (plain).

**Figure 4.10** Graphs depicting zeta size and zeta potential for 1:1 PA:PLA (drug encapsulated).

**Figure 4.11** Graphs depicting zeta size and zeta potential for 2:1 PA:PLA (plain).

**Figure 4.12** Graphs depicting zeta size and zeta potential for 2:1 PA:PLA (drug encapsulated).

**Figure 4.13** Degradation and swelling profile for TIO 1, NS: TINO 1 (1:5), (2:5) and (3:5).

**Figure 4.14** Degradation and swelling profile for TIO 2, NS: TINO 2 (1:5), (2:5) and (3:5).

**Figure 4.15** Degradation and swelling profile for TIO 3, NS: TINO 3 (1:5), (2:5) and (3:5).

**Figure 4.16** Drug release profiles for 1:5 NS: TIO ratio for TINO 1, TINO 2 and TINO 3. (T= Thermal, TU = Thermal + Ultrasound).

**Figure 4.17** Drug release profiles for 2:5 NS: TIO ratio for TINO 1, TINO 2 and TINO 3.

**Figure 4.18** Drug release profiles for 3:5 NS: TIO ratio for TINO 1, TINO 2 and TINO 3.

## LIST OF TABLES

---

**Table 2.1** Thermoresponsive systems in cancer therapy.

**Table 2.2** Polymeric drug delivery systems responsive to ultrasound in cancer therapy.

**Table 2.3** Delivery systems incorporating thermal and ultrasound components.

## TABLE OF CONTENTS

---

---

	Page
DECLARATION	i
DEDICATION	ii
RESEARCH PUBLICATIONS	iii
ACKNOWLEDGEMENTS	iv
ABSTRACT	v
LIST OF ABBREVIATIONS	vi & vii
LIST OF EQUATIONS	viii
LIST OF FIGURES	ix & x
LIST OF TABLES	xi

### CHAPTER 1

#### OVERVIEW, RATIONALE AND MOTIVATION FOR THE STUDY

---

---

1.1 Introduction	1
1.2 Rationale and Motivation of Study	2
1.3 Aim and Objectives	3
1.4 Overview of this dissertation	4
1.5 References	5

### CHAPTER 2

#### A REVIEW OF THERMO- AND ULTRASOUND-RESPONSIVE POLYMERIC SYSTEMS FOR TARGETED DELIVERY OF CHEMOTHERAPEUTIC AGENTS

---

---

2.1 Introduction	7
2.2 Advantages and Mechanisms of Cancer Targeting via Thermoresponsive Systems	8
2.3 Advantages and Stimulation Mechanism of Ultrasound-Responsive Polymers in Cancer Therapy	10
2.4 Properties of Thermoresponsive Polymer Systems: Temperature Ranges at Phase Transitions	11

2.5 Modification of Properties of Thermoresponsive Polymer Systems	13
2.6 Advancing Functional Trends in Thermoresponsive Polymers	15
2.7 Modification of Ultrasound-Responsive System Properties in Cancer Therapy	18
2.8 Pseudo-Ultrasonic-Responsive Systems in Cancer Chemotherapeutics: Advancing Trends in Ultrasonic-Responsive Systems	20
2.9 An Overview of Various Chemotherapeutic Delivery Systems Combining Thermal- and Ultrasound-Responsive Polymers	22
2.10 Conclusions and Future Perspective	26
2.11 References	27

## CHAPTER 3

### **FACILE GREEN SYNTHESIS OF THERMOSONIC INJECTABLE ORGANOGELS (TIO's)**

---

3.1 Introduction	36
3.2 Materials and Methods	37
3.2.1 Materials	37
3.2.2 N-isopropyl acrylamide and sebacic acid - TIO 1	38
3.2.3 N-isopropyl Acrylamide and 1,3 4-(Carboxyphenoxy) propane - TIO 2	38
3.2.4 N-isopropyl acrylamide, and 1,3 4-(Carboxyphenoxy) propane - TIO 3	38
3.2.5 Drying Protocol of the Organogels	38
3.2.6 Thermo and Ultrasound Response Analysis	39
3.2.7 Morphology Analysis of the TIO'S	39
3.2.8 Chemical Structure Integrity Analyses of the TIO'S	39
3.2.9 Thermoanalytical Analysis of the TIO'S	40
3.2.10 Phase Identification of the TIO'S	40
3.2.11 Rheological Analysis of the TIO'S	40
3.2.12 Physicomechanical Behaviour of the TIO'S	40
3.2.13 Cell culture and Fibroblast Proliferation Studies	41
3.3 Results and Discussion	42
3.3.1 Assessment of the Gelation Rate of the TIO's	42
3.3.2 Evaluation of the Stimuli-Responsiveness of the TIO's	43

3.3.3 Evaluation of the Morphological Structure of the TIO's	44
3.3.4 Chemical Structure Identification of the TIO's	46
3.3.5 Thermoanalytical Assessment of the TIO's	47
3.3.6 Physicochemical Integrity of the TIO's	49
3.3.7 Rheological Evaluation of the TIO's	51
3.3.8 Textural Analysis of the TIO's	54
3.3.9 Fibroblast Cell Proliferation Studies	56
3.4 Conclusions	59
3.5 References	60

## CHAPTER 4

### **SYNTHESIS, CHARACTERIZATION AND ASSEMBLY OF SOLID LIPID NANOSPHERES INTO THE THERMOSONIC INJECTABLE ORGANOGELS (TINO's)**

---



---

4.1 Introduction	65
4.2 Materials and Methods	66
4.2.1 Materials	66
4.2.2 Preparation of Solid Lipid Nanospheres (SLN's)	66
1:1 and 2:1 Nanospheres with Drug	66
4.2.3 Incorporation of the SLN's into the Organogels TIO's – TINO	67
4.2.4 Probing the Molecular Status Determination of the SLN's	67
4.2.5 Analyses of the Thermal Behavioural Analysis of the SLN's	68
4.2.6 Determination of the Molecular Phase Classification of the SLN's	68
4.2.7 Investigation of the Structural Morphology of the SLN's	68
4.2.8 Drug Entrapment Efficient Analysis of the SLN's	68
4.2.9 Determination of the Size and Zeta Potential of the SLN's	69
4.2.10 Evaluation of Erosive and Swelling Dynamics of the SLN's Incorporated into the TIO's	69
4.2.11 Drug Release Studies from the SLN's and the TINO's	69
4.3 Results and Discussion	70
4.3.1 Assessment of the SLN Molecular Status	70

4.3.2 Analysis of the Thermal Behaviour of the SLN's	71
4.3.3 Classification of the Molecular Phase Classification of the SLN's	73
4.3.4 Elucidation of the Structural Morphology of the SLN's	75
4.3.5 Drug loading and Encapsulated Efficiency Analysis	77
4.5.6 Determination of the Size and Zeta Potential of the SLN's	78
4.3.7 Swelling and Erosive Dynamics of the SLN's Incorporated into the TIO's (TINO's)	82
4.3.8 Drug Release Studies from the SLN's and the TINO's	85
4.4 Conclusions	88
4.5 References	88

## **CHAPTER 5**

### **CONCLUSIONS AND RECOMMENDATIONS**

---

---

5.1 Conclusions	92
5.2 Recommendations	93

### **APPENDICES**

Appendix A	94
Appendix B	95
Appendix C	96



## CHAPTER 1

### OVERVIEW, RATIONALE AND MOTIVATION FOR THE STUDY

---

#### 1.1 Introduction

Cancer was estimated by the World Health Organisation (WHO) to become the leading cause of deaths by 2010 (Bharali *et al.*, 2010). Whilst researchers and industry are making continuous efforts to overcome cancer, this non-communicable disease resulted in 8,200,000 deaths worldwide in 2012. Of all of types of cancer, cervical cancer is known to be the third most common cause of mortality in women (Gao *et al.*, 2014). It has been strongly associated with the Human Papillomavirus and therefore labelled the only cancer that has a definite cause (Hu *et al.*, 2013). Preceding cervical cancer, a condition referred to as Cervical Intraepithelial Neoplasia (CIN) surfaces. It consists of three grades, namely; CIN I, CIN II and CIN III. As the grade increases, the severity of the condition increases which ultimately leads to cervical cancer (Garbett *et al.*, 2014). There is a transformation which makes diagnosis of precancerous lesions possible. A change in morphology occurs within the squamocolumnar junction of the human cervix during puberty thus increasing the chances of developing CIN (Herfs *et al.*, 2012).

Modern medicine allows scientists to develop nanomedicines where structures of nanoscopic size are used for the diagnosis and treatment of cancer (Kateb *et al.*, 2010). Extensive investigation has been undertaken on nanoparticles with the intention to progress in diagnostic and therapeutic procedures. Progress has developed with nanoparticles via creating novel structural and multi-polymer design. Through this, multifunctional systems can be engineered and used for anti-cancer drug delivery (Jia *et al.*, 2013).

Stimuli-responsive materials have shown beneficial results to advance the world of in drug delivery science due to their rapid response to environmental physicochemical stimuli such as ultrasound or temperature (Zhao *et al.*, 2013). For decades, High Intensity Focused Ultrasound (HIFU) therapy attracted the interest of the medical fraternity for cancer therapy and is considered favourable over many other cancer therapies such as radiation due to the minimal or complete non-invasive process. During this process a rapid increase of temperature occurs at the site where the ultrasound is focused. This is an advantageous procedure and can be used in combination with drug delivery systems that are responsive to heat in a synergistic manner and contribute to site specific targeted drug delivery (Li *et al.*, 2011). Additionally, ultrasound enhances the delivery of drugs using nanocarriers via

sonoporation, which is the formation of temporary pores in the cell membrane induced by ultrasound, enabling enhanced intracellular delivery of drugs to viable cells (Pan *et al.*, 2004). Initially, HIFU was invented with the intention of performing extracorporeal medical procedures in tumour treatment. The waves from the ultrasound are able to penetrate deeper into the body than light (Li *et al.*, 2010). It was suggested by Burov in 1956 that HIFU be used for the treatment of malignant tumours (Dogra *et al.*, 2009).

Anticancer drugs possess a high elimination rate and therefore high doses are required for cancer therapy. Furthermore, anticancer drugs are non-specific and results in damage to healthy tissue (Bharali *et al.*, 2010). Cancer drugs also have extreme side-effects. Furthermore, HPV lesions in particular cause modification in the Human Leukocyte Antigen-G (HLA-G) expression that leads to inhibition of immune function (Bortolotti *et al.*, 2013).

Therefore, this study explored the design of a novel drug delivery system incorporating Solid Lipid Nanospheres into Thermosonic Injectable Organogels (TIO's) to form Thermosonic Injectable Nano-Organogels (TINO's), which maybe injected at the site of the tumour and upon exposure to stimuli, react and release the anti-neoplastic drug. In this work, 5-Fluorouracil was used as the model drug for potential targeted treatment in cervical cancer. Thermosonic is used to describe the thermo-ultrasound dual-responsiveness of the TINO's

## **1.2 Rationale and motivation for this study**

The proposed TINO's were designed to function as a controlled released system; this can produce a significant result in controlling the challenge of side-effect profiles faced in cervical cancer chemotherapy and contribute to decreasing drug resistance. The advantages of the TINO formulation include its ultrasound-responsive capabilities; its efficiently high drug-encapsulating properties, high cellular uptake, increased permeability and retention capabilities via ultrasound application and stimulation.

Thermo-responsive and ultrasound-responsive polymers was used to design the TINO's that are controlled and self-regulated by responding to ultrasound stimulus in order to activate drug delivery of treatment. HIFU is considered an efficient and safe method of treatment for cancer. As ultrasound energy was focused, it increased heat towards the desired target where a TINO containing the chemotherapeutic drug is administered. The TINO will react to the heat produced by ultrasound energy at the tumour site. This will result in drug being released at the targeted site. Synergistically, sonoporation may enhance the uptake of the drug intracellularly into the tumour site. Therefore this formulation is intended to be used with

HIFU which is less invasive. Figure 1 provides a schematic the process of how the TINO's were intended to be used.

This novel system is an advancement to current nanotechnology delivery systems with multiple advantages as it aims at decreasing invasive procedures and undesirable side effects during ultrasound application e.g. HIFU treatment, while synergistically treating cervical cancer through localised administration with enhanced permeability for positive therapeutic outcomes.

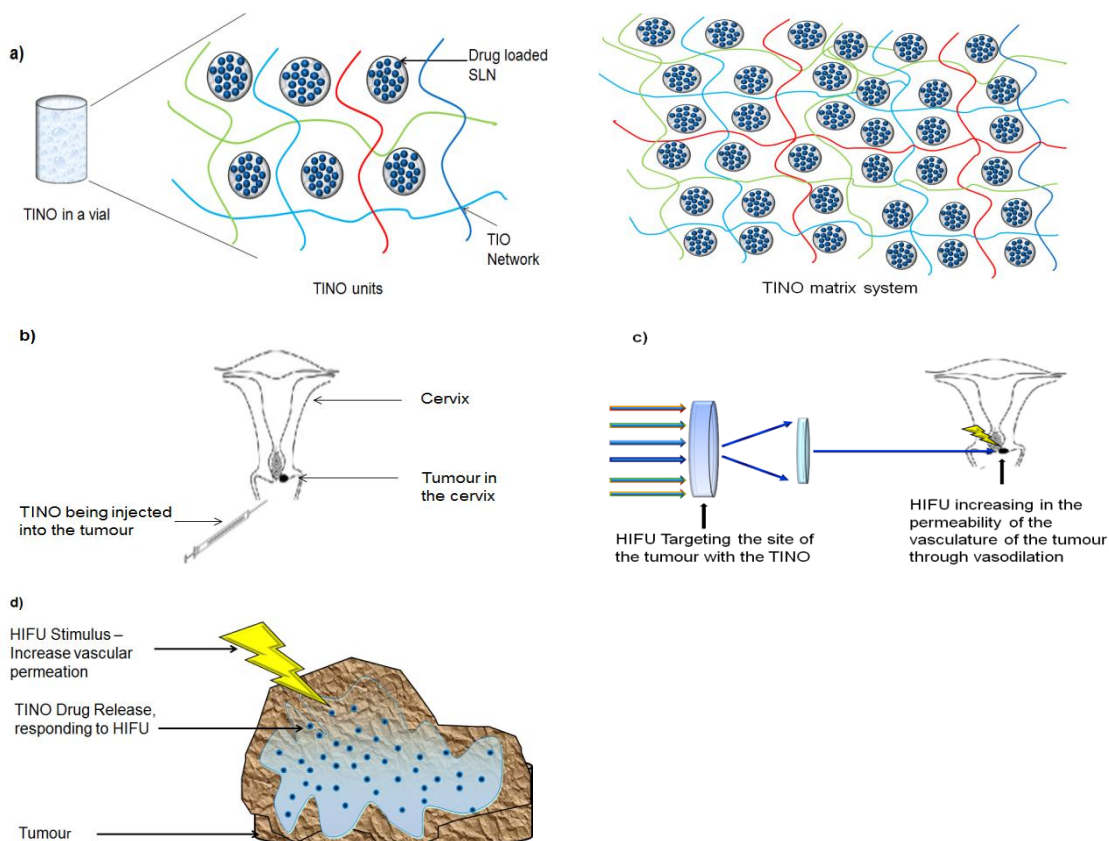


**Figure 1.** Schematic representation of a) TINO units (drug-loaded SLN within the TIO) b) TINO injected into cervical cancer tumour site c) ultrasound application targeting the tumour site d) TINO responding to ultrasound, causing increased drug release and intracellular permeability of the tumour due to an increase in localized heat.

### 1.3 Aim and objectives

The aim of this project was to design a novel Thermosonic Injectable Nano-Organogel responding to thermal change produced by ultrasound such as HIFU High Intense Focused

Ultrasound. This would cause drug to be released in a controlled manner at the tumour site in cervical cancer. The following objectives were fulfilled:

1. The selection of appropriate stimuli-responsive polymers with properties which responds to thermal changes together with ultrasound application through gellation and degradation.
2. A novel organogel (TIO) was formulated with the stimuli-responsive polymers selected using a developed method, such that the TIO forms a dense network from a polymer complex that is able to entrap the drug securely and the structure of the TIO was determined.
3. Solid Lipid Nanospheres were formulated as a vehicle for the chemotherapeutic drug and was incorporated into the TIO.
4. An appropriate anti-neoplastic drug was incorporated into the Solid Lipid Nanospheres. The compatibility of the anti-neoplastic drug towards the polymers and the efficacy of the drug with regards to cervical pathology were considered. The consistency of the drug distributed throughout the TIO was achieved.
5. The physico-chemical and physicommechanical properties of the TIO were determined including; viscosity, swelling, resilience.
6. *In vitro* studies were performed and the drug release pattern was determined by analysing the comparative drug release for thermal as well as thermal and ultrasound combined stimuli on the TIO.
7. Proliferation studies on fibroblasts were undertaken using the organogel.

## **1.4 Overview of this Dissertation**

### **1.4.1 Chapter One**

This chapter introduced cervical cancer, its causes and the pathology of how cervical cancer develops. It discussed how medical procedures and developing drug delivery has successfully assisted with overcoming the progression of cancer. It also outlined the rationale and the aim and objectives in this study.

### **1.4.2 Chapter Two**

This is a review paper that discussed targeted delivery of chemotherapeutic agents and current trends through thermal and ultrasound responsive systems.

### **1.4.3 Chapter Three**

This chapter is focused on the design of TIO's using a ring opening polymerization method. Characterization of the TIO's were undertaken and reported.

### **1.4.4 Chapter 4**

This chapter discussed the synthesis and characterization of SLN's and the assembly of the SLN's with the TIO's. The drug release of the TINO's was analysed.

### **1.4.5 Chapter 5**

This chapter concluded the dissertation with the provision of possibilities and recommendations to improve this study.

## **1.5 References**

Bharali, D.J., Mousa, SA., 2010. Emerging nanomedicines for early cancer detection and improved treatment: Current perspective and future promise. *Pharmacology & Therapeutics*. 128, 324-335.

Bortolli, D., Gentilli, V., Rotola, A., Di Lucia, D., Rizzo, R., 2013. Implication of HLA-G3' untranslated region polymorphisms in human papilloma virus infection. *Tissue Antigens*. 83, 113–118.

Dogra, VS., Zhang. M., Bhatt ., 2009. High-Intensity Focused Ultrasound (HIFU) Therapy Applications. *Ultrasound Clin* 4, 307-321.

Garbett.NC., Merchant.LC., Helm CW., Jenson, AB., Klein,JB., Chaires.JB., 2014. Detection of Cervical Cancer Biomarker Patterns in Blood Plasma and Urine by Differential Scanning Calorimetry and Mass Spectrometry. *PLOS ONE*. 9(1), 1-12

Gao, Q., Liu, W., Cai, J., Li, M., Gao, Y., Lin, W., Li, Z., 2014. EphB2 promotes cervical cancer progression by inducing epithelial-mesenchymal transition. *Human Pathology* 45, 372-381.

Herfs, M., Yamamoto, Y., Laury, A., Wang, X., Nucci , MR., McLaughlin-Drubin, ME., Münger, K., Feldman, S., McKeon, FD., Xian, W., Crum, CP., 2012. A discrete population of squamocolumnar junction cells implicated in the pathogenesis of cervical cancer. *PNAS*. 109(26), 10516-0521.

Hu, Y-X., Li, M., Jia, X-H., Du, Q-X., Miao, F-T., Yao, L., Shen, JD., 2013. HPV16 CTL Epitope Peptide-activated Dendritic Cell and Natural Killer Co-culture for Therapy of Cervical Cancer in an Animal Model. *Asian Pacific Journal of Cancer Prevention*. Vol 14 (12), 7335-7338.

Jia, F., Liu, X., Li, L., Mallapragada, S., Narasimhan, B., Wang, Q., 2013. Multifunctional nanoparticles for targeted delivery of immune activating and cancer therapeutic agents. *Journal of Controlled Release* 172, 1020-1034.

Kateb, B., Chiu, K., Black, KL., Yamamoto, V., Khalsa, B., Ljubimova, JY., Ding, H., Patil, R., Portilla-Arias, JA., Modo, M., Moore, DF., Farahani, K., Okun, MS., Prakash, N., Neman, J., Ahdoot, D., Grundfest, W., Nikzad, S., Heiss, JD., 2010. Nanoplatforms for constructing new approaches to cancer treatment, imaging, and drug delivery: What should be the policy?. *NeuroImage* 54, S106–S124.

Li, Y., Tong, R., Xia, H., Zhang, H., Xuan, J., 2010. High intensity focused ultrasound and redox dual responsive polymer micelles. *The Royal Society of Chemistry* . 46, 7739–7741.

Li, W., Cai, X., Kim, C., Sun, G., Zhang, Y., Deng, R., Yang, M., Chen, J., Achilefu, S., Wang, LV., and Xia, Y., 2011. Gold Nanocages Covered with Thermally-responsive Polymers for Controlled Release by High-intensity Focused Ultrasound. *NIH Public Access Author Manuscript* 3(4),1724-1730.

Pan H, Zhou Y, Sieling F, Shi J, Cui J, Deng C. Sonoporation of Cells for Drug and Gene delivery. *Proceedings of the 26th Annual International Conference of the IEEE EMBS; San Francisco, CA, USA; September 1-5, 2004.*

Zhao, L., Xiao, C., Ding, J., He, P., Tang, Z., Pang, X., Zhuang, X., Chen, X., 2013. Facile one-pot synthesis of glucose-sensitive nanogel via thiol-ene click chemistry for self-regulated drug delivery. *Acta Biomaterialia* 9, 6535–6543.

## CHAPTER 2

### A REVIEW OF THERMO- AND ULTRASOUND-RESPONSIVE POLYMERIC SYSTEMS FOR TARGETED DELIVERY OF CHEMOTHERAPEUTIC AGENTS

---

---

#### 2.1 Introduction

Through the decades of development in cancer treatment, chemotherapy has proven to be the world's standard management for most cancer conditions (Deckers & Moonen, 2010). Due to the high cost challenges that arise with new therapeutic approaches, the healthcare fraternity faces difficulty in achieving significant success rates (Yudina *et al.* 2012). Escalating efforts are being made by pharmaceutical scientists to advance cancer drug delivery through nanotechnology and the evolution of polymer sciences of biodegradable polymeric nanocarriers. These carriers propose an appropriate approach for transferring chemotherapeutic drugs and proteins in a desirably controlled manner to the target site (Chen *et al.* 2014). Two classes of polymers, namely thermal- and ultrasound-responsive polymers are in many ways associated with advancing cancer therapy (Bawa *et al.* 2009). They have also proven to be of value in biomedical applications, ranging from tissue engineering to drug delivery, including gene therapy (Ward & Georgiou, 2011).

Thermoresponsive polymers feature in most copolymeric drug delivery systems, with well-known examples including P(N-Isopropyl Acrylamide), Pluronic-F127 and chitosan (Cooperstein & Canavan, 2013; Hoare & Kohane, 2008; Li, Lim & Wang, 2008; Qui & Park, 2012; Ward & Georgiou, 2011; Yannic *et al.* 2008). In most cases these thermo-responsive polymers are used to design hydrogels as 3D networks formed by crosslinking of water-soluble polymers (Hoare & Kohane, 2008). Thermoresponsive hydrogels have been of much interest for decades in the field of drug delivery (Kost & Langer 2012). Their properties include phase transitioning, altering drug solubility, and controlling drug release at a desired rate (Banerjee, Chaurasia & Ghosh, 2010). Internal stimulation of smart polymer delivery systems is ideal for drug delivery from a safety perspective, however careful external control of a temperature stimulus is the standard by which thermo-responsive hydrogels respond to modulate drug release (Nazar, 2013; Zhu & Torchilin, 2013). An example of employment of heat as an external stimulus is Hyperthermia Treatment (HT) where accurate and focused heat at temperatures  $\geq 42^{\circ}\text{C}$  is produced at specific radio frequencies. The induced heat alters the morphology of the target tissue which assists in increased blood vessel permeability for enhanced drug delivery or ablation of cancerous tissue (Schmaljohann, 2006).

Ultrasound is also applied in advanced medical procedures for tumour therapy through heat production. This has proven to be a potentially effective and a safe method of tumoural ablation, as well as promoting tissue generation (Curley *et al.* 2014). Ultrasound-responsive polymers can be classified into biodegradable (polylactides, polyglycolides) and non-biodegradable polymers (ethylene vinyl acetate, poly(lactide-co-glycolide)). Zhou and co-workers suggested the forward-thinking approach of nanocarriers in combination with ultrasound for diagnostic and/or therapeutic applications (Zhou *et al.* 2014).

In keeping with the fact that these two advanced classes of polymers are commonly applied for chemotherapeutic delivery systems, it is pertinent that a concise review of research in this area is assimilated as a foundation of work that has been undertaken, as well as highlighting the potential to make advancements in this field. This review provides a concise and critical exploration into the subject matter by discussing the advantages and shortcomings of thermal- and ultrasound-responsive drug delivery in cancer therapy; in addition to the functional properties, phase transitions, as well as underlying scientific mechanisms of these delivery systems.

## **2.2 Advantages and Mechanisms of Cancer Targeting via Thermo-responsive Systems**

There are many other advantages that exist with regard to thermo-responsive polymers from their function and design to their application and administration. They are widely used in biomedical application in drug delivery and gene therapy and also branches into tissue engineering. This smart polymer has the ability to be developed and transformed into different formulations in order to carry out their function as intended, these include; micelles, hydrogels, particles, films etc (Gandhi *et al.* 2015). These formulations can be modified by adding additional elements such as gold or magnetic material for enhanced performance e.g. good heating properties. External sources of stimulation such as laser power can be used to create the desired response i.e. tumour specificity. Cancer is known to increase normal body temperature, augmenting the thermal stimulus towards thermo-responsive systems (You, Almeda & Auguste, 2010).

P(NIPAM) is amphiphilic with a lower critical solution temperature (LCST) between 30-34°C, often used in cancer chemotherapeutics due to its excellent thermo-responsive behaviour. At room temperature, the structural network of P(NIPAM) hydrogel exists as an aqueous gel network. P(NIPAM) hydrogel is generally administered as a depot or an injectable implant exposed to body temperature (37°C). At 32°C the hydrophilic fragments of the gel network



become hydrophobic due to the presence of the isopropyl group that the polymer contains and the gel expels the aqueous content from the network, resulting in polymer-solvent interaction (Iyer *et al.* 2013). These are osmotic mechanisms that are dependent on the polymer-polymer affinity, hydrogen ion pressure and the rubber elasticity of individual strands of the polymer, resulting in shrinkage of the network until all chains within the matrix collapse to form a solidified gel (Kimita, Braithwaite & Luckham, 1999). Once the matrix collapses the drug entrapped within the network is released into the tumour tissue (Figure 2.1). Pluronics also function via this mechanism, being used in long-term anti-cancer therapy as demonstrated by Chen and co-workers (2013).

Several amphiphilic block copolymers also exist as aqueous soluble systems in water at low temperature and have reversible phase transition properties after sol-gel conversion has occurred. This property is known as thermoreversibility, which is composition and concentration dependent. Thermogels were produced from poly ethylene glycol (PEG)/polyester copolymers via the introduction of hydrophobic blocks onto the copolymer. Examples include PLGA, PCL, poly ( $\epsilon$ -caprolactone-co-D,L-lactic acid) (Yu *et al.* 2014). There is a fine line between the hydrophilic and hydrophobic ratio composition which falls within the viable region to produce a thermoreversible network for cancer therapy application (Galaev & Mattiasson, 2007). A PLGA-PEG-PLGA amphiphilic co-polymeric injectable thermogel designed by Ci and co-workers loaded with irinotecan, proved to regress colon tumours through a sustained release mechanism (Ci *et al.* 2014). The team demonstrated that the drug encapsulated within the thermogel provided improved bioavailability compared with drug unaided by the thermogel mechanism (Ci *et al.* 2014).

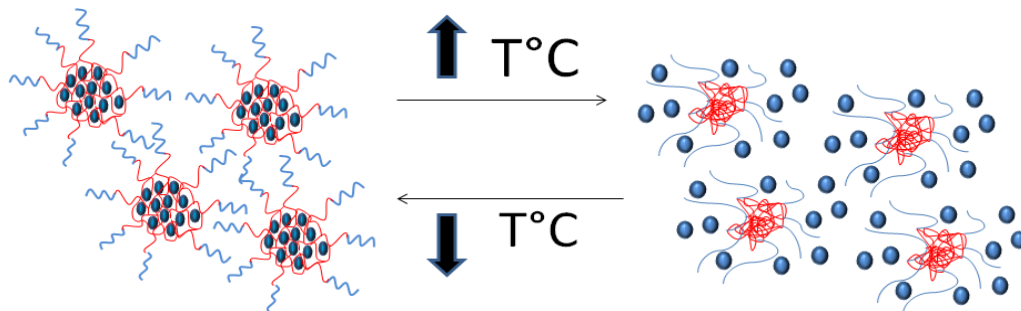


**Figure 2.1** Conceptual illustration representing the drug release mechanism of thermo-responsive systems with an LCST. Adapted from Nakayama *et al.* (2006).

### 2.3 Advantages and Stimulation Mechanism of Ultrasound-responsive Polymers in Cancer Therapy

Ultrasound promotes a few advantages to drug delivery. As discussed earlier, ultrasound offers more than one mechanism of stimulation i.e. through thermal induction, mechanical stimulus or gas vapourisation through micro bubbles. These three mechanisms could also work as an adjunctive stimulus during drug delivery. Due to these multi-mechanisms and the ability to combine them, ultrasound stimulates enhanced permeation of tissue, cell membranes and also the blood brain barrier in certain cases ultrasound can act as an activator of drugs such as 5-aminoevulinic acid and hematoporphyrin, and can also be used for guided therapy (Couture *et al.* 2014).

Ultrasound is not only known for its safety and inexpensive diagnostic capabilities through real-time imaging but also for its therapeutic proficiency through focusing high frequencies of ultrasound directed to malignant tumour tissue (Miller *et al.* 2012). The tissue is ablated owing to the thermal, chemical and mechanical effects of HIFU, with minimal side effects. Furthermore, ultrasound is a means of promoting healthy tissue regeneration as synergistic therapy (Phenix *et al.* 2014). Recent studies covered in this review highlight that ultrasound in cancer therapy is valuable for chemotherapeutic drug delivery and provides the positive desired outcomes from decreasing tumour growth and size to eradicating tumours completely. Ultrasound plays a role in advancing cancer therapy due to its ability to be easily combined in thermo-responsive systems producing a dual functioning for cancer therapy. Ultrasound is a stimulus that produces heat, a 'secondary stimulus' by energy vibration through acoustic cavitation initiated by acoustic vibrational waves. This heat (UH) calculated via a collective time period at 43°C based on the Equation 1:

$$UH = tR^{(43-T)} \quad \text{Equation 2.1}$$

Where  $t$  represent the time of the treatment,  $R$  is the constant equivalent to 0.25 for temperatures 37-43°C and 0.5 for temperatures above 43°C and  $T$  is the average temperature throughout the treatment; this increases the blood flow in the tumour vasculature (Lai, Fite & Ferrara, 2013). These acoustic waves employ a release mechanism through cavitation which increases the accumulation of chemotherapeutic drug within the site of the tumour. Once the ultrasound activates the polymer, the polymer responds by creating air filled microbubbles that eventually burst causing temporary pores in the tissue cell membrane at the focal point of application, enhancing tissue permeability which allows increased passive targeting into tissue (Legay *et al.* 2011; Peteu *et al.* 2010).

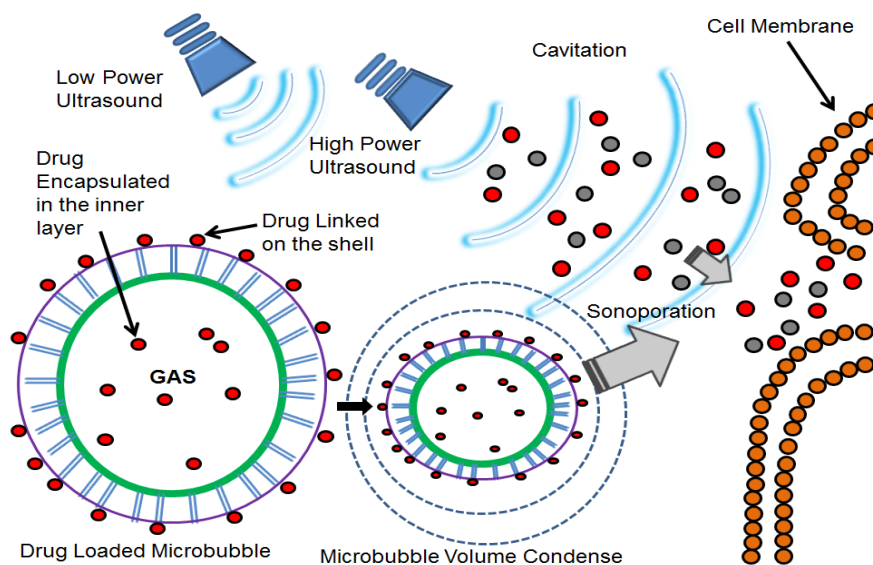


**Figure 2.2** Schematic illustrating low and high power ultrasound assisting in drug delivery through microbubbles and cavitation. Adapted from Zhao *et al.* (2013).

#### 2.4 Properties of Thermoresponsive Polymer Systems: Temperature Ranges at Phase Transitions

The range of LCST's for thermoresponsive polymers varies significantly. The LCST can be modified by blending various thermoresponsive polymers in order to customise the physicochemical properties of the system. These include the structural density, surface charge, toxicity and transfection efficiency within cancer cells (Cho 2012; Mao *et al.* 2007). Copolymerisation of polymers has also been explored to synthesise thermoresponsive polymers with various LCST's. Lai and co-workers have co-polymerised a total of ten thermoresponsive polymers with different LCST's to observe how these polymers changed the 3D structure of a blood clot (Lai *et al.* 2014; Yang *et al.* 2009). Chen and co-workers co-polymerized poly(glycidyl methacrylate) with poly(NIPAM) as a pendant to provide a thermo-responsive gating system for the design of nanotubes with a LCST of 32°C. They also demonstrated that above the LCST (37°C), the nanotubes remain open sufficiently long enough for the activation of proficient drug release. Below the LCST (25°C), the gates were in a closing state with no drug release until the activation temperature is once again reached (Chen *et al.* 2014).

Optimal cancer therapy focuses on targeted systems for clinical application. Thermoresponsive systems are designed with the LCST responding to the local tumour tissue temperature (~40°C) that is required for the release of drugs into the cancer cells

(Rezaei *et al.* 2012). A common challenge with thermoresponsive systems is duration they require to undergo phase transition that results in a burst phase of drug release. However, in recent developments a study has shown that altering the hydrophilic and hydrophobic fragments of the system can enhance the control of drug release by decreasing the thermogelling response time (Banerjee, Chaurasia & Ghosh, 2010; James *et al.* 2014).

Phase transitions in thermoresponsive systems relate to the solubility properties that grounds the common concepts of LCST's and upper critical solution temperature's (UCST), also known as the cloud point (Abulatefeh *et al.* 2011; Kikuchi *et al.* 2014). Below the LCST temperature, the structural network of thermoresponsive systems is loosely arranged. As the system is exposed to heat, the network becomes denser until it reaches and surpasses the LCST with solidification at the site of action e.g. solid tumours or cancerous tissue. This subsequently produces an environment for sustained drug delivery, a common goal in cancer chemotherapy.

Colloidal-based thermoresponsive drug delivery systems designed for cancer therapy utilise polymers with a LCST due to the temperature difference between the body and the exterior environment. This facilitates the controlled delivery of the drug to the targeted site. These colloid-based thermoresponsive systems encompass liposomes, micelles and nanoparticles. Thermoresponsiveness of nanosystems could also occur through thermoreversible swelling via cryotherapy or cold shock, which is used in tumour ablation therapy. This allows increased porosity of the system and promotes drug release from a state of encapsulation (Mura, Nicolas & Couvreur, 2013).

There are very few thermoresponsive polymers that have UCST properties. These polymers become soluble at temperatures beyond UCST, whereas LCST polymers become insoluble (Mishra *et al.* 2014). Poly(acrylic acid-co-acrylamide) (P(AAA)) is a thermoresponsive polymer that has an UCST due to hydrogen bonding between the acrylic acid and acrylamide units (Gandhi *et al.* 2015). The UCST can vary between 2.5 - 25°C depending on the ratio of the two monomers. Phase transitions occur due to hydrogen bonding of macromolecules creating intermolecular networks (Yang *et al.* 2010). Unlike most thermoresponsive polymers that work on a negative temperature responsive phase transition system, this polymer functions on a positive temperature responsive phase transition system. A comparison between normal hydrogel and hydrogel nanoparticles produced from P(AAA) was made. The study showed that with an increase in acrylamide, drug entrapment of 5-FU was enhanced in both hydrogel and hydrogel nanoparticles but the nanoparticles

were more effective in colon cancer due to a higher concentration of 5-FU reaching the colon (Ray *et al.* 2008). Phase transitions of thermoresponsive hydrogels occur through very specific mechanisms due to the microscopic nature of the gels. These mechanisms are modified in various ways by altering compositions of polymers and by including new functional groups into the system.

## 2.5 Modification of Properties of Thermoresponsive Polymer Systems

The physical interaction of polymers with its environment and a change in functional group chemistry are affected by the modification of the polymers conformational state and its solubility during formulation (Yang *et al.* 2012). The most altered and well known property of thermo-responsive polymers is the drastic and reversible changes in solubility (Fuchise, 2014). The advantages of using thermoresponsive polymers for cancer therapy are attributed to the mechanisms of targeted chemotherapy. Zhang and co-workers fabricated gold nanorods loaded with doxorubicin for breast cancer which is induced through a thermo-chemotherapy mechanism activated through a Near InfraRed (NIR) Laser at 760nm, 500mW, and 16W/cm<sup>2</sup> (Zhang *et al.* 2014). Their studies showed a higher accumulation of doxorubicin, in tumours that were heated compared to those that were not exposed to heat (Zhang *et al.* 2014) (Table 2.1).

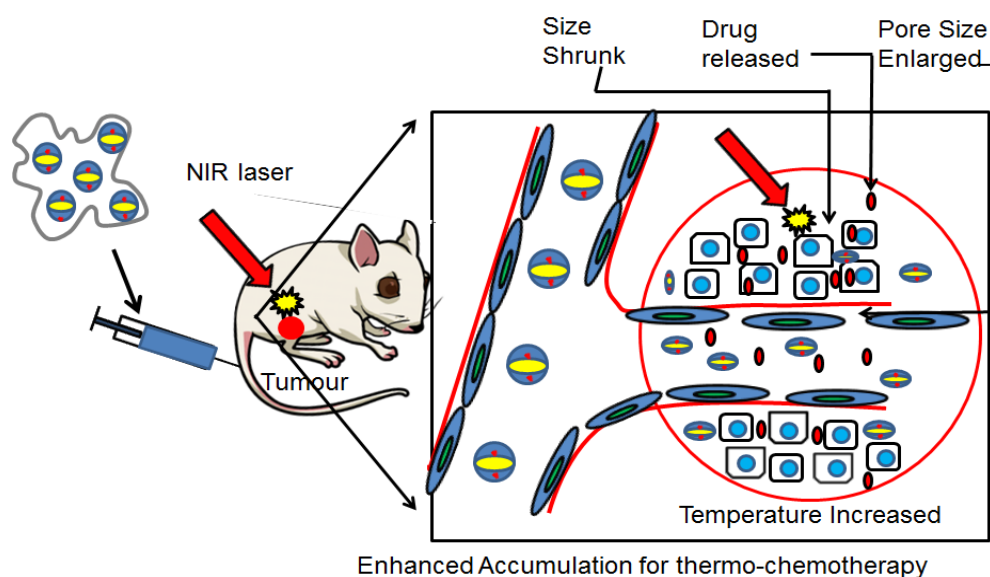


**Figure 2.3** Image illustrating a Near InfraRed Laser being applied to the site of delivery and the mechanism of action that occurs with heat stimulus. Adapted from Zhang *et al.* (2014).

Several types of thermoresponsive colloidal carriers were designed for optimum use in cancer therapy. These carriers enhance the chemotherapeutic effect by decreasing renal clearance due to increased size, which in turn leads to increased circulation time. Increased

circulation times are advantageous when the drug is targeted to function at the site of action to achieve tumour specificity. These colloidal carriers have the ability to extravasate from the tumour vasculature into the tumour tissue, concurrently avoid entering healthy tissue and therefore creating a higher quality efficient means of therapy. Furthermore, tumour tissue has a slightly higher temperature than normal tissue and therefore these delivery systems can be designed to respond to tumour temperature (Abulateefeh *et al.* 2011).

In many drug delivery developments thermoresponsive polymers are employed as a shell or outer layer with the intention of using heat as the drug release stimulus. In a development by Purushotum and co-workers, thermoresponsive core-shell magnetic nanoparticles were designed for the treatment of multi-modal cancer (Purushotham *et al.* 2015). These magnetic nanoparticles proved to possess good heating properties without the thermoresponsive coat, whereas the coated multifunctional system presented with a significant drug accumulation and release within the tumour and therefore proved to be a promising system for multi-modal cancer therapy (Purushotham *et al.* 2015) (Table 2.1).

Photothermal Ablation (PTA) of laser origin applied in cancer therapy, coupled with a doxorubicin-loaded hollow gold nanoshell system, was used to treat breast cancer. This thermally-responsive drug release was initiated by a 3W laser that produced temperatures between 54-55°C. However, temperatures between 40-45°C are said to cause extensive protein denaturation (Lepock, 2003) (Table 2.1). These temperatures are known to be high enough to cause cell death and tumoural ablation (Table 2.1) (Lee *et al.* 2013). This combinatory mechanism has proven to be efficient through histological analysis, tumour necrosis was >60% in mice that were treated in conjunction with laser treatment compared to mice without laser application (<10%). In evaluating the above systems, the variety of stimulating methods requires an understanding of the applicable chemistry that gives rise to specific properties through functional structures and trends in polymer sciences.

Thermoresponsive polymers vary in properties according to synthesis of different copolymer blends, as well as side-chain or element attachment to existing polymers to produce a new polymer or derivative. Modifications of methods of synthesis also alter the structure of polymer formation, having an effect on the thermoresponsive ability of the polymer. In a study undertaken by Chen and co-workers (2013), di(ethylene glycol) methyl ether methacrylate (DEGMA) and oligo ethylene glycol methyl ether acrylate (OEGA) diblock copolymers were fabricated with a gold nanoparticle core for cancer therapy (Chen, Xiang & Heiden, 2013). It was established that attachment of DEGMA to the gold nanoparticle core

had a greater effect in altering the thermoresponsive properties of the system compared to OEGA. Steric bulk and polymeric arrangement towards a metal core caused significant adjustments to the thermo-responsive properties of polymers. Possessing the gold nanoparticle as the core provided value to the systems' drug release control mechanism by converting light waves of 527nm to heat for thermo-responsive drug release into tumour tissue and minimal drug diffusion into the blood stream (Chen, Xiang & Heiden, 2013).

Synthesising polymeric derivatives also plays a part in altering the properties of a polymer. Kikuchi and co-workers designed four derivatives of a multi-armed star-shaped thermoresponsive delivery system from poly[2-(dimethylamino) ethyl methacrylates] (s-PDMAEMAs) (Mao *et al.* 2007). It was concluded that in s-PDMAEMAs with a low degree of polymerisation a trend of increasing transition temperature was observed (Mao *et al.* 2007). Attaching functionalised groups to a polymer could also change the phase transition temperature. Both phenyl and hydroxyl groups were polymerised terminally to P(NIPAM) for comparative studies. P(NIPAM) with the phenyl termination had a greater effect on lowering the LCST temperature than the P(NIPAM) with hydroxyl termination (Nakayama & Okano, 2005). Star-shaped amphiphilic co-block polymer micelles were also used in anticancer therapy by Rezaei and co-workers (2012). A novel designed paclitaxel-loaded folate-decorated system demonstrated an improved efficacy in terms of delivery and specificity. It has been suggested by Kikuchi *et al.* that these positive results presented by the micelles promote the application for chemotherapeutic drug delivery to achieve high intracellular uptake and a significant cytotoxic profile in cancer cells (Rezaeia *et al.* 2012). The flexibility of being able to modify thermoresponsive drug delivery systems in these numerous ways allows for greater advantages of these systems in cancer chemotherapeutics.

## **2.6 Advancing Functional Trends in Thermoresponsive Polymers**

Structurally, thermoresponsive polymers are known to have methyl, ethyl and propyl groups (Qiu & Park, 2012). Amide functional groups and amide-amide interactions tend to produce hydrogen bonding and dipole interactions between polymers and allows for thermophilic behaviour (Mah & Ghosh, 2013). Well established trends of functionalising thermoresponsive polymers is the attachment of antibodies for passively targeted specific delivery which leads to longer circulation time and accumulation of chemotherapeutic drugs in the desired pathological areas (Shao *et al.* 2011). Antibody attachment also assists with masking the release of drug without any interference by the body's natural defence. This is achieved through surface modification of the hydrophobic segment of the carrier system (Haidar, 2010).

Introducing thermoresponsive systems, such as P(NIPAM), with novel properties has been extensively researched in cancer therapy (Kokarderkar *et al.* 2012). Iron oxide nanoparticles with a thermoresponsive copolymer coating were produced with a second set engineered with R11 peptides for prostate cancer targeting. The iron oxide nanoparticles are guided to the desired site of accumulation via a magnetic field. The R11 conjugated nanoparticles proved to have a higher accumulation in the tumour compared to the nanoparticles without the R11 conjugated peptides (Wadajkar *et al.* 2013).

Furthermore, Bao and co-workers developed a multi-functionalised chitosan-grafted polyethyleneimine candesartan (CPC) conjugated nano-delivery system for use in the treatment of pancreatic cancer (Bao *et al.* 2014) (Table 2.1). The nanovectors employed multiple mechanisms toward chemotherapy by co-delivery of bafilomycin and the wild type-p53 gene complexed to CPC for the reduction in tumour size. Moreover, the nanovectors hinder tumour growth by promoting anti-angiogenesis via reduction of Vascular Endothelial Growth Factor (VEGF) secretions due to the candesartan. This synchronised approach of hindering tumour growth and reducing tumour size may contribute to elevated success in the development of targeted tumour therapy.

Although many researchers have explored chemotherapeutic delivery systems, brachytherapy, where radioactive seeds or sources are placed in or near the tumour itself for high dose radiation to the tumour and reduced exposure in the surrounding healthy tissues, cannot be ruled out from successful delivery in cancer therapy. A thermally-responsive elastin-like polypeptide that contains a therapeutic conjugated radionuclide has been fabricated by Lui and co-workers (2010) (Table 2.1). The system is suggested to have a suitable administration route, a well-controlled delivery mechanism and an increase in survival rate. As observed in the above-mentioned systems, heat can be produced and transferred in more than one way, significantly generating heat for cancer therapy through the exposure of ultrasound.



**Table 2.1.** Thermo-responsive systems in cancer therapy

Thermo-responsive system	Bioactive	Cancer type	Reference
Chitosan-g-PEI	Bafilomycin	Pancreatic Cancer	(Bao <i>et al.</i> 2014)
Elastin-Like peptide	Candesartan Radionuclide	Advanced stage tumoral cancers	(Liu, <i>et al.</i> 2010)
P(Nipam-co-AA)	Doxorubicin	Breast Cancer	(Yang <i>et al.</i> 2012)
P(Nipam)	Doxorubicin	Multimodal Cancer	(Purushotham <i>et al.</i> 2015)
PEG-HAuNS	Doxorubicin	Breast Cancer	(Lepock, 2003)
P(Nipam-acrylamide-allylamine)	–	Prostate Cancer	(Lee <i>et al.</i> 2013)
P(Nipam-co-N,NDMAM), CHOL-g-P[Nipam-co-N-(hm)A]	Indomethacin		(Chaw <i>et al.</i> 2004)
P(Nipam-co-N,NDMAM)-b-PLGA	Doxorubicin	Cancer	(Liu, Tong & Yang, 2005)
P(Nipam-co-N,NDMAM)-b-PLa	Adriamycin	Bovine aorta endothelial	(Kohori <i>et al.</i> 1999)
P(Nipam-co-AAm)	- , Doxorubicin	Ovarian Cancer, Colon Cancer	(Meyer, Shin & Kong, 1999; Strong, Dahorte & West, 2014)
P(MOEGA –DMDEA)	Paclitaxel, Doxorubicin	-	(Qiao <i>et al.</i> 2011)
P(Nipam-co-N,NDMAM)-b-P(LA-co-CL)	Doxorubicin	-	(Nakayama <i>et al.</i> 2006)
P(Nipam-b-PBMA)	Adriamycin	-	(Chung <i>et al.</i> 1999)
Pluronic F127 – chitosan	Curcumin	Prostate Cancer	(Rao <i>et al.</i> 2004)
(Fe <sub>3</sub> O <sub>4</sub> )-P(NIPAM)	Doxorubicin	Cancer	(Purushotham & Ramanujan, 2010)
PEG'd Liposomes	Doxorubicin	Liver Cancer	(Yahuaifai <i>et al.</i> 2014)
DPPC:DPPG:MSPC:mPEG <sub>2000</sub> -DSPE (HTLC)	Cisplatin	Cervical Cancer	(Dou <i>et al.</i> 2014)
DPPC/MSPC/DSPE-PEG <sub>2000</sub>		Breast Cancer	(Tagami <i>et al.</i> 2012)
P(NIPAM)-NH <sub>2</sub> (Amino-terminated)	Adriamycin	-	(Cammass <i>et al.</i> 1997)
Pluronic 127	Paclitaxel, Docetaxel	Breast Cancer, Ovarian Cancer	(Lin <i>et al.</i> 2014; Yang <i>et al.</i> 2009)
DPPC:DSPC:DPTAP:DSPE:PEG <sub>2000</sub>	Doxorubicin	Lung Carcinoma	(Dicheva <i>et al.</i> 2014)
DPPC:MPPC:DPPE-PEG <sub>2000</sub> , DPPC:HSPC:CHOL:DPPE-PEG <sub>2000</sub>	[Gd(HPDO3A)(H <sub>2</sub> O)] <sup>+</sup> (Doxorubicin)	Squamous Cell Carcinoma	(de Smet <i>et al.</i> 2010)
DPPC:CHOL:DSPE-PEG <sub>2000</sub> :DSPE-PEG <sub>2000</sub> -Folate	Doxorubicin	Epidermoid Cancer, Cervical Cancer	(Pradhan <i>et al.</i> 2010)

## 2.7 Modification of Ultrasound-Responsive System Properties in Cancer Therapy

Microbubbles have become a common trend in cancer therapy used in conjunction with ultrasound therapy. These microbubbles were conventionally used as ultrasound imaging diagnostic tools, demonstrating a positive contribution to the advancement in drug delivery through overcoming limitations of stimuli responsive systems. Numerous delivery systems, as provided in Table 2.3, employ phospholipid microbubbles such as 1,2 di-stearoyl-sn-glycerol-3-phosphoethanolamine (DPSE), Perfluorocarbon (PFC), Perfluoropentane (PFP), 1,2 -di-stearoyl-sn-glycerol-3-phosphotidylcholine (DSPC), 1,2-dioctadecanoyl-sn-glycero-3-phospho-(1'-rac-glycerol) (DSPG) and many more.

Zhang and co-workers designed methotrexate-loaded nanobubbles composed of a copolymer, poly(lactic acid-co-glycolic acid) better known as PLGA. Both individual units, i.e. poly(lactic acid) and poly(glycolic acid), are classified as ultrasound-responsive polymers (Zhang *et al.* 2014). This system was designed for targeted therapy in combination with the use of tumour ablative therapy through high intense focused ultrasound for placental choriocarcinoma. As depicted in Figure 2.4, when the combination therapy of antibody, nanobubbles, drug, polymer and HIFU are combined, the proliferation index is decreased and the apoptosis index increases significantly (Zhang *et al.* 2014). It can be deduced that adding a nano/microbubble component to the formulation assisted with responsiveness to ultrasound stimulation.

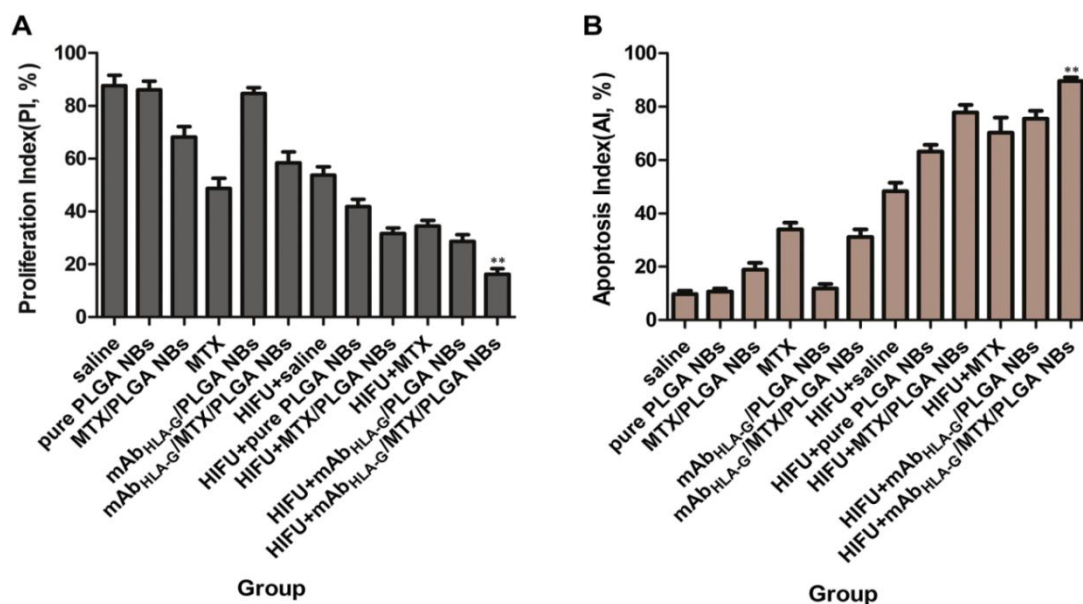


**Figure 2.4** Graphs representing the proliferation index and apoptosis index considering individual formulatory components and combinations of saline, nanobubbles, drug, antibodies and HIFU. Source: Zhang *et al.* (2014).

In delivery systems fabricated from polymers that are not ultrasound-responsive, ultrasound delivery is achieved through the addition of agents such as Levovist, an ultrasound contrast agent that contains microbubbles or Perfluoropentane (PFP) (Kudo, Okada & Yamamoto, 2009; Zong *et al.* 2013). Those microbubbles are then coated with the drug-loaded polymer via formation of emulsions to acoustically trigger delivery of chemotherapeutic drugs, for example, chlorambucil (Fabiilli *et al.* 2010). Through a similar mechanism, the drug is delivered with efficiency to the intended site. When the ultrasound is transmitted, it interacts with the PFP and vaporisation occurs, thus causing the formation of microbubbles. As the microbubbles increase in volume and surface area, they facilitate drug release by bursting; causing temporary pores within the desired cell layers releasing the drug into the targeted cancerous tissue as seen in Figure 2.2 (Cheng *et al.* 2014).

Yang and co-workers (2014) (table 2.2) designed Poly methylmethacrylate (PMMA)-based nanocapsules infused with Perfluorohexane (PFH), a well-known ultrasound contrasting agent used to conduct image guided therapy in liver cancer. The nanocapsules were uniformly shaped and arranged suggesting easy diffusion into cancer cells, with a high drug-loading ability of > 90%. Figure 2.5 below illustrates how ultrasound causes drug release and sonoporation to assist with drug transfusion into the cells. This may also be seen in Figure 2.6 in step [2] and step [3].

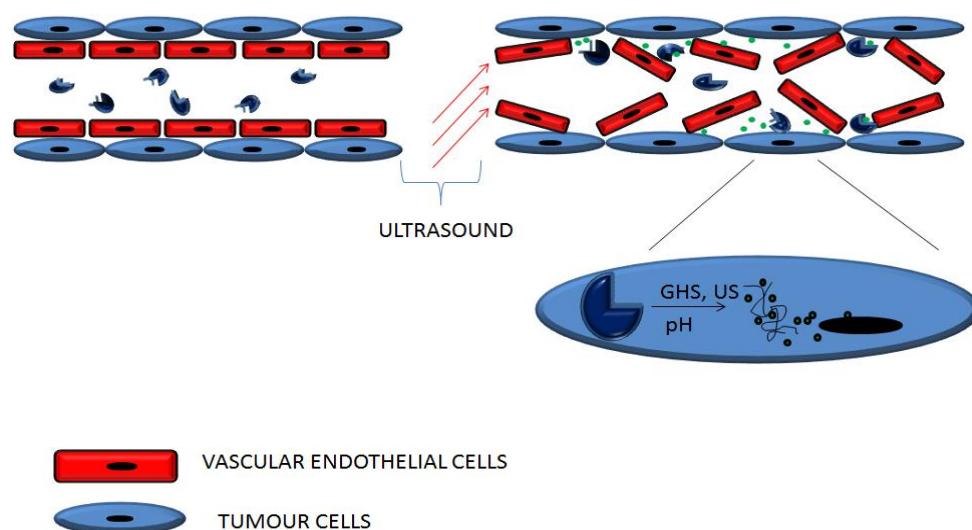


**Figure 2.5** Schematic of sonoporation of the vascular endothelia cells allowing the nanocapsules to be in direct contact with the tumour cells which will allow drug into tumour cells. Adapted from Yang *et al.* (2014).

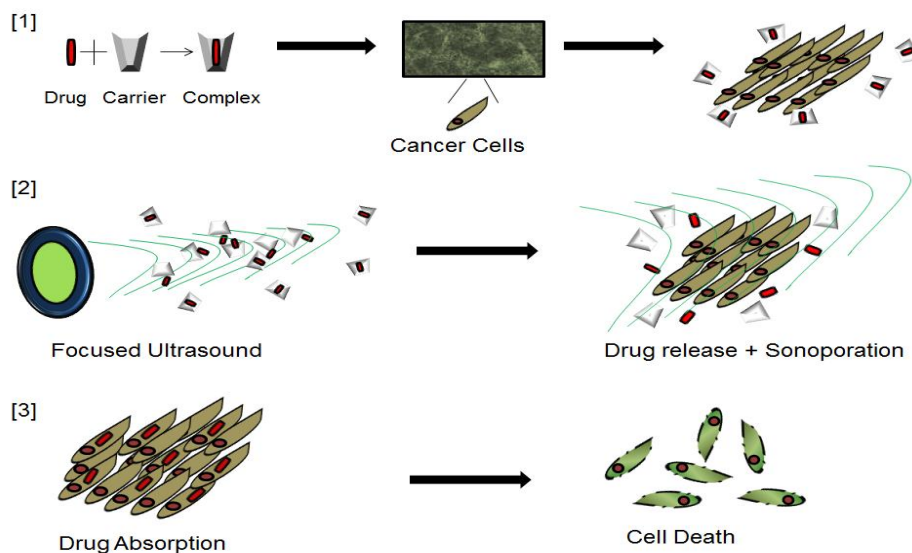


**Figure 2.6** Schematic illustrating focused ultrasound-mediated drug absorption into cancer cells leading to tumour cell death, Adapted from Gourevich *et al* (2013).

Gourevich and co-workers (2013) undertook a study considering both the mechanical and thermal stimuli emanating from ultrasound and tested the stimuli individually on a doxorubicin  $\gamma$ -cyclodextran nanocarrier system that was designed for the treatment of breast cancer. Each of these stimuli were compared to a control group and proved to cause an increase in encapsulated drug uptake i.e. mechanical, hyperthermia and focused ultrasound induced heat respectively. Focused ultrasound (1.35 MHz) in conjunction with MRI guidance allowed the drug delivery process to be more efficient, safer and accurate. Introduction of SonoVue (sulphur hexafluoride) microbubbles permitted a significant increase in intracellular doxorubicin uptake (table 2.3) (Gourevich *et al.* 2013). Ultrasound-responsiveness branches throughout a broad spectrum of stimuli allowing many other smart polymer systems to respond through heat production and chemical hydrolysis via a pH change.

## 2.8 Pseudo-Ultrasonic-Responsive Systems in Cancer Chemotherapeutics: Advancing Trends in Ultrasonic-Responsive Systems

Due to the heat ultrasound generates during its application, thermoresponsive systems could also be employed in conjunction with ultrasound therapy as a complementary action. As highlighted in Table 2.3, Ninomiya and co-workers (2014) designed Thermosensitive Liposomes (TSL) from N-isopropyl acrylamide and N-isopropyl methacrylamide whereby, upon exposure to locally focused ultrasound (1MHz, 30 s,  $0.5\text{W}/\text{cm}^2$ ), heat was produced which stimulated the TSL to release doxorubicin for the treatment of breast cancer.

Focused ultrasound employed in cancer therapy is useful due to its ability to initiate hyperthermia or ablative therapy for tumours. Yang and co-workers [90] designed a doxorubicin liposomal delivery system that works in conjunction with pulsed focused ultrasound for the treatment of brain tumours (glioblastoma). Results showed that pulsed HIFU reduced the tumour growth rate significantly in comparison to chemotherapy alone. When the doxorubicin-loaded liposome was introduced unaided by HIFU, it had a longer survival rate. When the liposomes were introduced and combined with pulsed HIFU, it resulted in an even longer survival rate than the individual approaches (Yang *et al.* 2012).

Pluronic is a well-known thermoresponsive triblock polymer (PEO-PPO-PEO) composed of basic poly(ethylene oxide) and poly(propylene oxide) units. A study was undertaken by Hussein & Pitt (2008) using Pluronic P-105 micelles loaded with doxorubicin. An *in vitro* release test was undertaken upon continuous wave and pulsed ultrasound exposure to the micelles. Conclusive results proposed that cavitation played a vital role in the disturbance of the micelle structure that resulted in drug release of doxorubicin and upon withdrawal of the acoustic waves allowed the reformation of micelles and re-encapsulation of drug.

The delivery systems discussed above are stimulated by the 'secondary' stimulus, heat, generated via ultrasound, to temperatures high enough to activate drug release from these systems. Differentiating between whether the system responds to the thermal or ultrasound stimulus is important for future investigations for understanding and improvement of ultrasound-responsive drug delivery systems. Due to these thermoresponsive systems responding to ultrasound stimuli or being guided by ultrasound, it could be termed 'pseudo-ultrasonic' responsive.

An interesting study was undertaken by Rapoport and co-workers (2013). Their group had synthesised paclitaxel-loaded Perfluorocarbon (PFC) nanodroplets in combination with a PEO-co-PLA block copolymer and employed these subsequently to the application of focused ultrasound for the treatment of pancreatic cancer. It was suggested that the time between injecting the formulation and applying the magnetic resonance imaging guidance focused ultrasound (MRgFUS), played a significant role in positive cancer treatment. This was due to the time that the formulation required to accumulate in the tumour tissue in order for an appropriate concentration of drug to be present for release prior to MRgFUS application. If this time is not considered, applying the ultrasound may lead to collateral damage to normal tissue (Rapoport *et al.* 2013).

**Table 2.2** Polymeric drug delivery systems responsive to ultrasound in cancer therapy

Ultrasound-responsive system	Bioactive	Cancer type	Reference
PMMA	Doxorubicin	Liver Cancer	(Yang <i>et al.</i> (2014))
$\gamma$ Cyclodextran	Doxorubicin	Breast Cancer	(Gourevich <i>et al.</i> 2013)
L- $\alpha$ -phosphatidylcholine: CHOLI: DSPE-PEG <sub>2000</sub> PDA:PDLA-PFC	Doxorubicin Paclitaxel	Glioblastoma Pancreatic Cancer	(Yang <i>et al.</i> 2012) (Rapoport <i>et al.</i> 2013)
PLGA	Methotrexate	Placental choriocarcinoma	(Zhang <i>et al.</i> (2014))
APT:P(NIPMAM-co-NIPAM)	Doxorubicin	Breast Cancer	(Ninomiya <i>et al.</i> 2014)
Pluronic	Doxorubicin	-	(Husseini & Pitt 2008)
(DSPE-PEG <sub>2000</sub> -Biotin)	Paclitaxel	Breast Cancer	(Yan <i>et al.</i> 2013)
DSPC:DSPE-PEG <sub>2000</sub> :DSPG	Doxorubicin	Brain Cancer	(Fan <i>et al.</i> 2013)
DPPC:DPSE:PEG <sub>2000</sub> :Biotin	(1,3-bis(2-chloroethyl)-1-nitrosourea	Glioma (Brain/Spinal tumor)	(Fan <i>et al.</i> 2013)
CHC:SPIO:BSA (MB)	Camptothecin	Breast tumour cells	(Lui <i>et al.</i> 2013)
DPPC-DSPE-PEG-MALEIMIDE:CHOL PLA	Doxorubicin Paclitaxel, Doxorubicin	Lung Cancer Breast Cancer, Liver Cancer	(Geers <i>et al.</i> 2011) (Cochran <i>et al.</i> 2011; Einsbery <i>et al.</i> 2010)
DPPC:DPPG:DPPE-PEG <sub>2000</sub>	Doxorubicin	Cancer	(Tinkov <i>et al.</i> 2010)
DPPC:DPPA:DPPE-PEG <sub>2000</sub>	10-HydroxyCamptothecin	Liver Cancer	(Li <i>et al.</i> 2012)
lyso-lecithin : LTSL:ThermoDox <sup>®</sup>	Doxorubicin	Squamous Cell Carcinomas (Tumour)	(Yang <i>et al.</i> 2012)
DPPC:MSPC:DSPE-PEG <sub>2000</sub>	TO-PRO-3 (DNA-intercalating agent)	Glioma	(Yudina <i>et al.</i> 2011)
DSPC: DSPE-PEG(2k)-OMe	HLA (Antigen)		(Suzuki <i>et al.</i> 2009)
DSPC: DSPE-PEG(2 k)-OMe	IL-12	Ovarian Cancer	(Suzuki <i>et al.</i> 2010)

### 2.9 An Overview of Various Chemotherapeutic Delivery Systems Combining Thermal- and Ultrasound-Responsive Polymers

N,N-Diethylacrylamide (NNDEA) core Pluronic micellular solution (Plurogels<sup>®</sup>) and regular Pluronic P-105 micelles at low concentrations were formulated to release doxorubicin in response to low frequency ultrasound for synergistic therapy against leukaemia cells. The

Plurogel, being stabilised in comparison to the unstable Pluronic micelles, provided enhanced protection of normal cells against the drug through micelle reformation and reuptake of drug into the micelle after removal of the ultrasound stimulus, leading to less exposure to the drug and lowering the possibility of side effects (Table 2.4) (Pruitt & Pitt 2002).

PLGA as well as Pluronic proved to be responsive to ultrasound. According to Liu and co-workers (2005) [107], thermoresponsive micelles fabricated from the block copolymer, poly (N-isopropylacrylamide-co-N, N-dimethylacrylamide)-b-poly(D,L-lactide-co-glycolide) contained both thermoresponsive and ultrasound responsive components (Liu, Tong & Yang, 2005). In addition to PLGA's superior biodegradability and drug-loading capacity, an increase in drug delivery could be achieved via application of ultrasound.

Polymethacrylate polymers are ionic polymers and are pH-responsive (Chen *et al.* 2013). Research involving application of ultrasound by Wang and co-workers (2009) has been undertaken with micelles assembled from a diblock copolymer of thermal- and pH-sensitive polymers. Their research demonstrated that applying HIFU to the micelles in an aqueous solution produced thermal and mechanical effects that initiated chemical hydrolysis that resulted in a decrease in pH and promoted drug release. This delivery system could be effective for tumoural delivery due to their lower pH ~5.7 and higher temperatures than normal tissue, possibly responding to natural tumour milieu (Gao, Zhang & Sun, 2012). HIFU combined with this delivery system would be complementary and may have significant potential for tumour therapy.

Stover and co-workers (2008) developed sphingolipid ceramide loaded linear-dendritic nanoparticles by grafting P(N-Isopropyl Acrylamide)-P(Lactic Acid),P(NIPAM)-PLA with Poly-L-lysine-Poly-L-lactide PLLA-PLA for apoptotic action in solid tumours, both of which contained PLA, that could be considered an ultrasound component. This system proved to be thermoresponsive and provided a long term sustained release ceramide which occurs successfully with hyperthermia (Stover *et al.* 2008). This system therefore, could be triggered via a focused ultrasound stimulus since it is a source of hyperthermia.

A novel intravenous paclitaxel-loaded nano-emulsion was designed by Rapoport and co-workers (2009), providing pancreatic and ovarian cancer chemotherapy through a conversion method technique from nano-emulsion to microbubbles via ultrasonic energy ranging between 90KHz-1MHz. Nano-emulsions containing paclitaxel decreased the tumour

size significantly whereas the nano-emulsion that did not contain paclitaxel had no effect on tumour shrinkage. It was, however, reported that although tumour size reduction did occur, tumour resistance was an emerging factor and current research is being undertaken to eliminate resistance completely (Rapoport *et al.* 2009).

Another study undertaken demonstrated that the efficacy of ultrasound was dependent on the time allowed for accumulation of the drug at the site of the tumour subsequent to administration. This resulted in an increased uptake of drug into the tumour through micelle degradation or tumour perturbation (Gao, Fain & Rapoport 2005). Interestingly, even though the system partially comprised of Pluronic-105, ultrasound did not increase extravasation of the micelles even 30 minutes after the injection. It was further demonstrated that the mixed micelles retained 65% of drug in the core whereas standard Pluronic micelles release most of the drug encapsulated. It was indicated that these micelles are effective in the early stages of tumour appearance, however once the tumour has metastasized, surgical or ablative therapy should be considered before applying this delivery system.

It is reported that nano-sterically stabilised liposomes (nSSL) are known to be very efficient in tumours due to their 'leakage' into the tumour (Schroeder *et al.* 2009). A study of Cisplatin loaded nSSLs in the presence of low focused ultrasound was conducted for chemotherapy in colonic cancer in Albino Laboratory-bred (BALB/c) female mice. The cholesterol composition in these liposomes decreases the porosity as well as their sensitivity to heat. Using LFUS in the presence of drug loaded nSSLs, enhanced the therapeutic effect of delivery systems such as these, which do not release drug into the circulation (Gabizon *et al.* 1994). According to Lin and co-workers (2006) cholesterol and PEG-lipid content or lipid packing, contributes greatly to ultrasound responsivity in a system. When the temperatures increases, it inherently assists with the ultrasound-responsive sensitivity, making it challenging to distinguish the quantification of ultrasound- to thermoresponsive sensitivity (Lin & Thomas, 2004).

A dually-responsive ultrasound-pH responsive polymeric vesicle was synthesised as an antineoplastic delivery system. Poly ethylene oxide (PEO) is classified as thermoresponsive and poly (2-tetrahydrofuranolxyethyl methacrylate), a pH-responsive polymer. As previously mentioned, ultrasound can activate thermoresponsive systems via heat production and stimulate pH-responsive systems via chemical reactions; thus overlapping heat and ultrasound. This novel polymeric vesicle proved to have the ability to encapsulate anticancer drugs, and release them at a controlled drug release rate, being non-cytotoxic to liver cells



below a concentration of 250µg/mL but decreasing liver cell viability (by 25%) above 500µg/mL. The DOX encapsulated polymers tested against liver cancer cells and proved to successfully decrease these cells viability as ascertained via CCK-8 *in vitro* quantification method (Chen & Du, 2013).

Husseini and Pitt (2008) reported on a study undertaken by Howard et al. (2006) based on determining the effects of ultrasound on paclitaxel-loaded copolymeric micelles, designed from the thermoresponsive PEO, and PLA-tecopherol, where PLA is reported to be ultrasound-responsive in nature. When evaluated against breast tumour progression in combination with ultrasound (1MHz), not only were normal cells protected from the toxic effects of the chemotherapeutic drugs, but the ultrasound assisted in the increasing drug uptake in cancer cells ascertained via *in vitro* studies, and increased tumour regression when tested on nude mice (Husseini & Pitt, 2008).

Micelles fabricated from PEO combined with different methacrylates were tested in response to HIFU, of which neither of the polymers are ultrasound responsive classified. These micelles were encapsulated with Nile red (NR) of lipophilic nature and upon exposure to HIFU, the micellar structure is disrupted through chemical hydrolysis and causes release of NR in a controlled manner (Ayano *et al.* 2012). Therefore, loading hydrophobic substances such as chemotherapeutic drugs in these micelles may be considerable for cancer therapy.

A multifunctional nanoparticle injectable polymeric perfluorocarbon nanoemulsion comprising of a PEO-b-PLA diblock copolymer, a thermoresponsive and ultrasound-responsive classified combination, were synthesised to release encapsulated doxorubicin in response to therapeutic ultrasound to treat breast cancer. In conjunction with diblock delivery system, drug-loaded, targeted nanobubbles were included during which the bubbles expand to become microbubbles upon heating. Upon rupturing, cavitation occurs and ultimately intracellular drug uptake is enhanced; through these mechanisms chemotherapy was effectively undertaken (Zeng & Pitt, 2006). Providing an overview of thermoresponsive and ultrasound-responsive drug delivery systems assists to create predictable perspectives and outlooks. These are vital for discovering innovative approaches to further develop drug delivery and research within the field of cancer chemotherapeutics. Table 2.3 provides a summary of chemotherapeutic delivery systems with ultrasound and thermoresponsive attributes.

**Table 2.3** Delivery systems incorporating thermal and ultrasound components

Thermo-Responsive Component	Ultrasound-Responsive Component	Bioactive	Cancer type	References
N,N-DEAM	Pluronic	Doxorubicin	Leukaemia (HL-60)	(Pruitt & Pitt, 2002)
P(Nipam)-co-N,NDMAM.	PLGA	Doxorubicin	Breast Cancer	(Liu, Tong & Yang, 2005)
PEO	Poly(thpma)	-	-	(Wang <i>et al.</i> 2009)
P(Nipam) -PLA	PLLA-PLA	Sphingolipid ceramide	Cancer	(Stover <i>et al.</i> 2008)
PEO	PLA	Paclitaxel	Pancreatic, ovarian, Breast cancer tumours	(Rapoport <i>et al.</i> 2009)
PEG <sub>2000</sub> -diacylphospholipid	Pluronic P-105	Doxorubicin	Ovarian Cancer	(Gao, Fain & Rapoport, 2005)
PEG	P( $\beta$ A)	Doxorubicin	Ovarian Cancer	(Gao, Fain & Rapoport, 2005)
PE: DSPE	CHOL	Cisplatin	Colon Cancer	(Gabizon <i>et al.</i> 1994)
DPPC	(DPPE-PEG <sub>2000</sub> )	Calcein	-	(Lin & Thomas, 2004)
PEO	P(2-thfma)	Doxorubicin	Liver Cancer	(Chen & Du, 2013)
PEO	PLa-tocopherol	Paclitaxel	Breast Cancer	(Husseini & Pitt, 2008)
P(Nipam)	PLA	-	-	(Ayano <i>et al.</i> 2012)
PEO, P(Nipam)	2-hydroxymethyl methacrylate	Doxorubicin	-	(Zeng & Pitt, 2006)
PEO	PIBMA, P(2-THMA)	-	-	(Xuan <i>et al.</i> 2011)
PEO	PLa, PCL	Doxorubicin	Breast Cancer	(Gao <i>et al.</i> 2008)
P(Nipam-co-PAA)	Propylacrylic acid	Doxorubicin	Breast Cancer	(Ta <i>et al.</i> 2014)

## 2.10 Conclusion and Future Perspective

Understanding the mechanisms of operation these drug delivery systems is essential for the advancement in stimuli-responsive system modification. Thermo-responsive delivery systems are widely developed and employed due to their efficient outcomes in drug delivery owing to internal and external stimulation i.e. body temperature and laser or ultrasound respectively. In terms of external stimulation, drug delivery systems will evolve to an extent where most stimuli-responsive systems of various classes of smart polymers could be

attuned to ultrasound-mediated delivery, but not necessarily be ultrasound-responsive, as ultrasound serves as a source of mechanical impulses that may simulate an environment similar to electric impulses, generate a change in heat to stimulate thermo-responsive delivery systems, and initiate chemical reactions in certain mediums to cause a pH change allowing drug release into the targeted site. Ultrasound, being a well known safe diagnostic tool for biomedical applications such as imaging and therapy such as hyperthermia, could be used in for many multi-responsive drug delivery systems. The application of ultrasound in futuristic approaches to drug delivery would extensively contribute to the enhancement of chemotherapeutic drug delivery. In stating that ultrasound induces mechanical effects, future research branching into investigating the effect of ultrasound on thixotropic properties of drug delivery systems, and responsivity and the efficiency to ultrasound in chemotherapeutic delivery systems derived from intelligent materials other than ultrasound-, thermal- and pH-responsive materials.

## 2.12 References

- Abulateefeh, S.R. Spain, S.G. Aylott, J.W. Chan, W.C. Garnett, M.C. Alexander, C.,2011. Thermoresponsive Polymer Colloids for Drug Delivery and Cancer Therapy, *Macromolecular Bioscience* 11:1722–1734.
- Ayano, E. Karki, T. Kanawaza, H. Okano, T.,2012.Poly (N-isopropylacrylamide)-PLA and PLA blend nanoparticles for temperature-controllable drug release and intracellular uptake, *Colloids and surfaces. B, Biointerfaces* 99:67-73.
- Banerjee, S. Chaurasia, G. Ghosh, A.,2010. smart polymers: around the cosmos, *Asian Journal of Pharmaceutical and Clinical Research*3(2):135-141.
- Bao, X. Wang, W. Wang, C. Wang, Y. Zhou, J. Din, Y Wang, X. Jin, Y.,2014. A chitosan-graft-PEI-candesartan conjugate for targeted co-delivery of drug and gene in anti-angiogenesis cancer therapy, *Biomaterials* 35:8450-8466.
- Bawa, P. Pillay, V. Choonara, Y.E. du Toit, L.C.,2009. Stimuli-responsive polymers and their applications in drug delivery, *Biomedical Materials* 4:1-15.
- Cammas, S. Suzuki, K. Sone, C. Sakurai, Y. Kataoka, K. Okano, T.,1997. Thermo-responsive polymer nanoparticles with a core-shell micelle structure as site-specific drug carriers, *Journal of Controlled Release* 48:157-164.
- Chaw, C.S. Chooi, K.W. Liu, X.M. Tan, C.W. Wang, L. Yang, Y.Y.,. 2004. Thermally responsive core-shell nanoparticles self-assembled from cholesteryl end-capped and grafted polyacrylamides: drug incorporation and in vitro release, *Biomaterials* 25:4297-4308.
- Chen, G. Chen, R. Zou, C. Yang, D. Chen, ZS.,2014. Fragmented polymer nanotubes from sonication induced scission with a thermo-responsive gating system for anti-cancer drug delivery, *Journal of materials of chemistry B* 2:1327–1334.
- Chen, N. Xiang, X. Heiden, P.A.,2013. Tuning thermoresponsive behavior of diblock copolymers and their gold core hybrids. Part 2. How properties change depending on block attachment to gold nanoparticles, *Journal of Colloid and Interface Science* 391:60-69

- Chen, W. Du, J.,2013. Ultrasound and pH Dually Responsive Polymer Vesicles for Anticancer Drug Delivery, *Scientific Reports* 3(2162)1-9.
- Chen, W. Meng , F. Cheng, R. Denga, C. Feijen , J. Zhong, Z.,2014. Advanced drug and gene delivery systems based on functional biodegradable polycarbonates and copolymers, *Journal of Controlled Release* 190(2014):398–414.
- Chen, YY. Wu, HC. Sun, JS. Dong, GC. Wang,TW.,2013. Injectable and Thermo-responsive Self-Assembled Nanocomposite Hydrogel for Long-Term Anticancer Drug Delivery, *American Royalty Society. Langmuir* 29:3721–3729.
- Cho, CS.,2012. Design and Development of Degradable Polyethylenimines for Delivery of DNA and Small Interfering RNA: An Updated Review, *Materials Science* 2012:1-24.
- Cheng, W. Gu, L. Ren, W. Liu, Y.,2014. Stimuli-responsive polymers for anti-cancer drug delivery, *Materials Science and Engineering C* 45:600–608.
- Chung, J.E. Yokoyama, M. Yamato, M. Aoyagi, T. Sakurai, Y. Okano, T., 1999. Thermo-responsive drug delivery from polymeric micelles constructed using block copolymers of poly(N-isopropylacrylamide) and poly(butylmethacrylate), *Journal of Controlled Release* 62:115-127.
- Ci, T. Chen, L. Yu, L. Ding, J.,2014. Tumor regression achieved by encapsulating a moderately soluble drug into a polymeric thermogel, *Scientific Reports*. (2014):1-13.
- Cochran, M.C. Emsbery, J. Ouma, R.O. Soulen, M. Wheatley, M.A.,2011. Doxorubicin and paclitaxel loaded microbubbles for ultrasound triggered drug delivery, *International Journal of Pharmaceutics* 414:161– 170.
- Cooperstein, MA. Canavan, HE.,2013. Assessment of cytotoxicity of (N-isopropyl acrylamide) and Poly(N-isopropyl acrylamide) coated surfaces, *Biointerphases*. 8(1):8-19.
- Couture. O, Foley.J, Kassell. N.F, LarratB., Aubry.J-F.,2014.Review of ultrasound mediated drug delivery for cancer treatment: updates from pre-clinical studies. *Translational Cancer Research*. 3(5):494-511.
- Curley, S.A. Palalon, F. Sanders, K.E. Koshkina, N.V.,2014. The Effects of Non-Invasive Radiofrequency Treatment and Hyperthermia on Malignant and Nonmalignant Cells, *Int. J. Environ. Res. Public Health* 11:9142-9153.
- Deckers, R., Moonen, C.T.W.,2010 Ultrasound triggered, image guided, local drug delivery, *Journal of Controlled Release*. 148 25–33.
- de Smet, M. Langereis, S. van den Bosck, S. Grüll, H.,2010. Temperature-sensitive liposomes for doxorubicin delivery under MRI guidance, *Journal of Controlled Release* 143:120-127.
- Dicheva, B.M. ten Hagen, T.L.M. Schipper, D. Seynhaeve, A.L.B. von Rhoon, G.C. Eggermont, A.M.M. Koning, G.A.,2014. Targeted heat-triggered doxorubicin delivery to tumors by dual targeted cationic thermosensitive liposomes. *Journal of Controlled Release*. 195:37–48.
- Dou, Y.N. Zheng, J. Foltz, W.D. Weersink, R. Chaudary, N. Jaffay, D.A. Allen, C.,2014. Heat-activated thermosensitive liposomal cisplatin (HTLC) results in effective growth delay of cervical carcinoma in mice, *Journal of Controlled Release* 178:69-78.

Einsbery, J.R. Burnstein, O.M. Kambhampati, R. Forsberg, F. Lui, J.B.,2010. Development and optimization of a doxorubicin loaded poly(lactic acid) contrast agent for ultrasound directed drug delivery, *Journal of Controlled Release* 143:38–44.

Fabiilli, M.L. Haworth, K.J. Sebastian, I.E. Kripfgans. O.D. Carson, P.L. Fowlkes, J.B.,2010. Delivery of Chlorambucil Using an Acoustically-Triggered, Perfluoropentane Emulsion, *Ultrasound Med Biol* 36(8):1364–1375.

Fan, C.H. Ting, C.Y. Lin, H.J. Wang, C.H. Liu, H.L. Yen, T.C. Yeh. C.K.,. 2103. Antiangiogenic-targeting drug-loaded microbubbles combined with focused ultrasound for glioma treatment, *Biomaterials* (34):2142-2155.

Fan, C.H. Ting, C.Y. Lin, H.J. Wang, C.H. Liu, H.L. Yen, T.C. Yeh, C.K.,2013. SPIO-conjugated, doxorubicin loaded microbubbles for concurrent MRI and focused-ultrasound enhanced brain-tumor drug delivery, *Biomaterials* (34):3706-3715.

Fuchise, K.,2014. Design and precise synthesis of thermoresponsive polyacrylamides, *Journal of polymer science*.

Gabizon, A. Catane, R. Uziely, B. Kaufman, B. Safra, T. Cohen, R. Martin, F. Huang, A. Barenholz, Y.,.1994. Prolonged circulation time and enhanced accumulation in malignant exudates of doxorubicin encapsulated in polyethylene-glycol coated liposomes, *Cancer Res*. 54(4):987– 992.

Galaev, I. Mattiasson, B.,. 2007. Smart Polymers: Applications in Biotechnology and Biomedicine, Second Edition, *CRC Press* 144-146.

Gandhi. A, Paul. A, Sen. SO, Sen. KK.,2015. Studies on thermoresponsive polymers: Phase behaviour, drug delivery and biomedical applications. *Asian journal of pharmaceutical sciences* 10:99 -107.

Gao, Z.G. Fain, H.D. Rapoport, N.,2005. Controlled and targeted tumor chemotherapy by micellar-encapsulated drug and ultrasound, *Journal of Controlled Release* 102:203–222.

Gao, Z. Kennedy, A.M. Christensen, D.A. Rapoport, N.Y.,. 2008. Dru-loaded nano/microbubbles for combining ultrasonography and targeted chemotherapy. *Ultrasonics*. 48(4):260–270.

Gao, Z. Zhang, L.,2012. Y. Sun, nanotechnology applied to overcome tumor drug resistance. *Journal of Controlled Release* 162:45–55.

Geers, B. Lentacker, I. Sanders, N.N. Demeester, J. Meairs, S. De Smedt, S.C.,2011. Self-assembled liposome-loaded microbubbles: The missing link for safe and efficient ultrasound triggered drug-delivery, *Journal of Controlled Release* 152:249–256.

Gourevich, D. Dogadkin, O. Volovick, A. Wang, L. Gnaïm, J. Cochran, S. Melzer, A.,2013. Ultrasound-mediated targeted drug delivery with a novel cyclodextrin-based drug carrier by mechanical and thermal mechanisms, *Journal of Controlled Release* 170:316–324.

Haidar, Z.S.,2010. Bio-Inspired/-Functional Colloidal Core-Shell Polymeric-Based NanoSystems: Technology Promise in Tissue Engineering, Bioimaging and NanoMedicine, *Polymers*. 2:323-352.

Hoare, T.R. Kohane, D.S.,2008. Hydrogels in drug delivery: Progress and challenges. *Polymer*. 49:1993-2007

- Howard, B. Gao, A. Lee, SW. Seo, MH. Rapoport, N.,. 2006. Nanobiotechnology: Inorganic nanoparticles versus Organic nanoparticles. *AMJ Drug Delivery* 4:97.
- Husseini, G.A. Pitt, W.G.,.2008. The Use of Ultrasound and Micelles in Cancer Treatment, *J Nanosci Nanotechnol.* 8(5):2205–2215.
- Iyer, A.K. Singh, A. Ganta, S. Amiji, M.M.,.2013. Role of integrated cancer nanomedicine in overcoming drug resistance, *Advanced Drug Delivery Reviews.* 65:1784–1802.
- James, H.P. John, R. Alex, A. Anoop, K.R.,.2014. Smart polymers for the controlled delivery of drugs – a concise overview, *Acta Pharmaceutica Sinica B* 4(2):120-127.
- Kikuchi, S. Chen, Y. Fuchise, K. Takada, K. Kitakado, J. Sato, S-I. Satoh, T. Kakuchi, T.,.2014. Thermoresponsive properties of 3-, 4-, 6-, and 12armed star-shaped poly[2-(dimethylamino)ethyl methacrylate]s prepared by core-first group transfer polymerization, *Polymer Chemistry, The Royal Society of Chemistry* 5:4701–4709.
- Kiminta, D.M.O. Braithwaite, G. Luckham, P.F.,. Colloid Dispersions.1999. Nanogels, in; J.C. Salamone (Eds). *Concise Polymeric materials encyclopedia . CRC Press LLC.* 259 -261.
- Kohori, F. Sakai, K. Aoyagi, T. Yokoyama, M. Yamato, M. Sakurai, Y. Pkano, T.,.1999. Control of Adriamycin cytotoxic activity using thermally responsive polymeric micelles composed of poly(N-isopropylacrylamide-co-N,N-dimethylacrylamide)b-poly\*D,L-lactide). *Colloids and Surfaces B: Biointerfaces* 16:195-205.
- Kokardekar, R.R. Sha, V.K. Mody, H.R. Hiranandani, L.H.,.2012. PNIPAM Poly (N-isopropylacrylamide): A Thermoresponsive “Smart”Polymer in Novel Drug Delivery Systems, *Internet Journal of Medical Update* 7(2):60-63.
- Kost, J. Langer, R. Responsive polymeric delivery systems.2012. *Advanced Drug Delivery Reviews* 64:327–341.
- Kudo, N. Okada, K. Yamamoto, K.,.2009. Sonoporation by Single-Shot Pulsed Ultrasound with Microbubbles Adjacent to Cells, *Biophysical Journal* 96:4866–4876.
- Lai, B.F.L. Zou, Y. Yang, X. Yu , X. Kizhakkedathu, J.N.,.2014. Abnormal blood clot formation induced by temperature responsive polymers by altered fibrin polymerization and platelet binding, *Biomaterials* 35:2518-2528.
- Lai, CY. Fite, B.Z. Ferrara, K.W.,.2013 Ultrasonic enhancement of drug penetration in solid tumours, *Frontiers in oncology* 3(204):71-78.
- Lee, H.J. Liu, Y. Zhao, J. Zhou, M. Bouchard, R.R. Mitchama, T. Wallace, M. Stafford, R.J. LI, C. Gupta, S. Melancon, M.P.,.2013. In vitro and vivo of mapping of drug release after laser ablation thermal therapy with doxorubicin-loaded hollow gold nanoshells using fluorescence and photoacoustic imaging, *Journal of Controlled Release* 172:152-158.
- Legay, M. Gondrexon, N. Person, SL. Boldo, A. Bontemps A.,.2011. Enhancement of Heat Transfer by Ultrasound: Review and Recent Advances, *International Journal of Chemical Engineering* 2011:1-17.
- Lepock. R.,.2003 Cellular effects of hyperthermia: relevance to the minimum dose for thermal damage, *Int. J. Hyperthermia* 19(2003):252–26 6.

- Li, L. Lim, L.H. Wang, Q. Jiang, S.P., 2008. Thermoreversible micellization and gelation of a blend of pluronic polymers, *Polymer* 49:1952-1960.
- Lin, H.Y. J.L., 2004. Thomas, Factors Affecting Responsivity of Unilamellar Liposomes to 20 kHz Ultrasound, *Langmuir*. 20:6100-6106.
- Lin, Z. Gao, W. Hu, H. Mac, K. He, B. Dai, W. Wang, X. Wang, J. Zhang, X. Zhang, Q., 2014. Novel thermo-sensitive hydrogel system with paclitaxel nanocrystals: High drug-loading, sustained drug release and extended local retention guaranteeing better efficacy and lower toxicity, *Journal of Controlled Release* 174:161-170.
- Li, P. Zheng, Y. Ran. H. Tan, J. Lin, Y. Zhang, Q. Ren, J. Wang, Z., 2012. Ultrasound triggered drug release from 10-hydroxycamptothecin-loaded phospholipid microbubbles for targeted tumor therapy in mice, *Journal of Controlled Release* 162:349–354.
- Liu, S.Q. Tong, Y.W. Yang, Y-Y., 2005. Incorporation and in vitro release of doxorubicin in thermally sensitive micelles made from poly(N-isopropylacrylamide-co-N,N-dimethylacrylamide)-b-poly(D,L-lactide-co-glycolide) with varying compositions. *Biomaterials* 26:5064–5074.
- Liu, W. Mackay, J.A. Dreher, M.R. Chen, M., McDaniel, J.R. Simnick, A.J. Callahan, D.J. Zalutsky, M.R. Chilkoti, A., 2010. Injectable intratumoral depot of thermally responsive polypeptide-radionuclide conjugates delays tumor progression in a mouse model. *Journal of Controlled Release* 144::2-9.
- Liu, S.Q. Tong, Y.W. Yang, Y.Y., 2005. Incorporation and in vitro release of doxorubicin in thermally sensitive micelles made from poly(N-isopropylacrylamide-co-N,N-dimethylacrylamide)-b-poly(D,L-lactide-co-glycolide) with varying compositions, *Biomaterials* 26:5064-5074.
- Lui, T.Y. Wu, M.Y. Lin, M.H. Yang, F.H., 2013. A novel ultrasound-triggered drug vehicle with multimodal imaging functionality. *Acta Biomaterialia* (9):5453–5463.
- Mah, E. Ghosh, R., 2013. Thermo-Responsive Hydrogels for Stimuli-Responsive Membranes, *Processes* 1(2013):238-262.
- Mao, Z. Maa, L. Yana, J. Yan, M. Gao, C. Shen, J., 2007. The gene transfection efficiency of thermoresponsive N,N,N-trimethyl chitosan chloride-g-poly(N-isopropylacrylamide) copolymer. *Biomaterials* 28:4488–4500.
- Meyer, D.E. Shin, B.C. Kong, G.A. Dewhirst, M.W. Chilkoti, A., 2001. Drug targeting using thermally responsive polymers and ocal hyperthermia, *Journal of Controlled Release* 74: 213-224.
- Miller, D.L. Smith, N.B. Bailey, M.R. Czarnota, G.J. Hynynen, K. Makin, I.R.S., 2012. Overview of Therapeutic Ultrasound Applications and Safety Considerations, *Journal of ultrasound in medicine* 31:623–634.
- Mishra, V. Jung, S-H. Jeonga, H.M. Lee, H-I., 2014. Thermoresponsive ureido-derivatized polymers: the effect of quaternization on UCST properties, *Polymer Chemistry* 5:2411–2416.
- Mura, S. Nicolas, J. Couvreur, P., 2013. Stimuli-responsive nanocarriers for drug delivery, *Nature Materials* 12:991-1003.

- Nakayama, M. Okano, T.,2005. Polymer Terminal Group Effects on Properties of Thermoresponsive Polymeric Micelles with Controlled Outer-Shell Chain Lengths, *Biomacromolecules* 6:2320-2327.
- Nakayama, M. Okano, T. Miyazaki, T. Kohori, K. Sakai, M. Yokoyama, M.,2006. Molecular design of biodegradable polymeric micelles for temperature-responsive drug release, *Journal of Controlled Release* 115(1)46-56.
- Nazar, H. 2013 Using “smart” biomaterials and systems for targeted drug delivery. *The Pharmaceutical Journal* 290:646.
- Ninomiya, K. Yamashita, T. Kawabata, S. Shimizu, N.,2014. Targeted and ultrasound-triggered drug delivery using liposomes co-modified with cancer cell-targeting aptamers and a thermosensitive polymer, *Ultrasonics Sonochemistry*. 21:1482–1488.
- Peteu, S.F. Oancea, F. Siciua, O.A. Constantinescu, F. Dinu, S.,2010. Responsive Polymers for Crop Protection, *Polymers* 2:229-251.
- Phenix, C.P. Togtema, M. Pichardo, S. Zehbe, I. Curiel, L.,2014. High Intensity Focused Ultrasound Technology, Its Scope and Applications in Therapy and Drug Delivery, *Journal of Pharmaceutical Sciences* 17(1):136-153.
- Pradhan, P. Giri, J. Rieken, F. Koch, C. Mykhaylyk, O. Döblinger, M. Banerjee, R. Bahadur, D. Plack, C.,2010. Targeted temperature sensitive magnetic liposomes for thermochemotherapy, *Journal of Controlled Release* 142:108-121.
- Pruitt, J.D. Pitt, W.D.,2002. Sequestration and Ultrasound-Induced Release of Doxorubicin from Stabilized Pluronic P105 Micelles, *Drug Delivery* 9:253–258.
- Purushotham, S. Chang, P.E.J. Rumpel, H. Kee, I.H.C. Ng, R.T.H. Chow, P.H.K. Tan, C.K. Ramanujan, R.V.,2015. Thermoresponsive core-shell magnetic nanoparticles for combined modalities of cancer therapy. *Nanotechnology* 20:1-11.
- Purushotham, S. Ramanujan, R.V.,2010. Thermoresponsive magnetic composite nanomaterials for multimodal cancer therapy. *Acta Biomaterialia* 6:502-510.
- Qiao, Z.Y. Zhang, R. Du, F.S. Liang, D.H. Li, Z.C.,2011. Multi-responsive nanogels containing motifs of ortho ester, oligo (ethylene glycol) and disulphide linkage as carriers of hydrophobic anti-cancer drugs, *Journal of Controlled Release* 152:57-66.
- Qui, Y. Park, K.,2012 Environment-sensitive hydrogels for drug delivery, *Advanced Drug Delivery Reviews* 64:49–60.
- Rao, W. Zhang, W. Poventud-Fuentes, I. Wang, Y. Lei, Y. Agarwal, P. Weekes, B. Li, C. Lu, X. Yu, J. He, X.,2004. Thermally responsive nanoparticle-encapsulated curcumin and its combination with mild hyperthermia for enhanced cancer cell destruction, *Acta Biomaterialia* 10:831-842.
- Rapoport, N.Y. Kennedy, A.M. Shea, J.E. Scaife, C.L. Nam, K.H.,2009. Controlled and targeted tumor chemotherapy by ultrasound-activated nanoemulsions/microbubbles, *Journal of Controlled Release* 138:268– 276.
- Rapoport, N.Y. Payne, A. Dillon, C. Shea, J. Scaife, C. Gupta, R.,2013. Focused ultrasound-mediated drug delivery to pancreatic cancer in a mouse model, *Journal of Therapeutic Ultrasound*. 1:11.



Ray, D. Mohapatra, D.K. Maohapatra, R.K. Mohanta, G.P. Sahoo, P.K.,2008.Synthesis and colon-specific drug delivery of a poly(acrylic acid-co-acrylamide)/MBA nanosized hydrogel. *J Biomater Sci Polym Ed.* 19(11):1487-1502.

Rezaeia, S.J.T. Nabida, M.R. Niknejadb, H. Entezami, A.A.,2012. Folate-decorated thermoresponsive micelles based on star-shaped amphiphilic block copolymers for efficient intracellular release of anticancer drugs, *International Journal of Pharmaceutics* 437:70– 79.

Rezaei , S.J.T. Nabid, M.R. Niknejad, H. Entezami, A.A.,2012. Multifunctional and thermoresponsive unimolecular micelles for tumor-targeted delivery and site-specifically release of anticancer drugs, *Polymer* 53:3485-3497.

Schmaljohann, D. Thermo- and pH-responsive polymers in drug delivery.2006. *Advanced Drug Delivery Reviews* 58:1655–1670.

Schroeder, A. Honen, R. Turjeman, K. Gabizon, A. Kost, J. Barenholz, Y.,2009. Ultrasound triggered release of cisplatin from liposomes in murine tumors, *Journal of Controlled Release* 137:63–68.

Shao, P. Wang, B. Wang, Y. Li, J. Zhang, Y.,2011. The Application of Thermosensitive Nanocarriers in Controlled Drug Delivery, *Journal of Nanomaterials* 2011:1-12.

Stover, T.C. Kim, Y.S. Lowe, T.L. Kester, M.,2008.Thermoresponsive and biodegradable linear-dendritic nanoparticles for targeted and sustained release of a pro-apoptotic drug, *Biomaterials* 29(3):359–369.

Strong, L.E. Dahorte, S.N. West, J.L.,2014. Hydrogel-nanoparticle composites for optically modulated cancer therapeutic delivery, *Journal of Controlled Release* 178:63-68.

Suzuki, R. Namai, E. Oda, Y. Nishiie, N. Otake, S. Koshima, R. Hirata, K. Taira, Y. Utoguchi, N. Negishi, Y. Nakagawa, S. Maruyama, K.,2010. Cancer gene therapy by IL-12 gene delivery using liposomal bubbles and tumoral ultrasound exposure, *Journal of Controlled Release* 142:245–250.

Suzuki, R. Oda, Y. Utoguchi, N. Namai, E. Taira, Y. Okada, N. Kadowaki, N. Kodama, T. Tachibana, K. Maruyama, K.,2009. A novel strategy utilizing ultrasound for antigen delivery in dendritic cell-based cancer immunotherapy, *Journal of Controlled Release*, 133:198–205.

Tagami, T. May, J.P. Ernsting, M.J. Li, S.D.,2012. A thermosensitive liposome prepared with a Cu 2+ gradient demonstrates improved pharmacokinetics, drug delivery and antitumor efficacy, *Journal of Controlled Release* 161(2012):142-149.

Ta, T. Bartolak-Suki, E. Park, E.J. Karrobi, K.M. McDannold, N.J. Porter,T.M.,2014. Localized delivery of doxorubicin in vivo from polymer-modified thermosensitive liposomes with MR-guided focused ultrasound-mediated heating, *Journal of Controlled Release* 194:71-81.

Tinkov, S. Winter, G. Coester, C. Bekeredjian, R.,2010. New doxorubicin-loaded phospholipid microbubbles for targeted tumor therapy: Part I— Formulation development and in-vitro characterization, *Journal of Controlled Release* 143(1)143–150.

Wadajkar, A.S. Menon, J.U. Tsai, Y.S. Gore, C. Dobin, T. Gandee, L. Kangashiemi, K. Takahashi, M. Manandhar, B Ahn, J.M. Hsieh, J.T. Nquyen, K.T.,2013 Prostate cancer-specific thermo-responsive polymer-coated iron oxide nanoparticles, *Biomaterials* 34:3618-3625.

- Wang, J. Pelletier, M. Zhang, H. Xia, H. Zhao, Y., 2009. High-Frequency Ultrasound-Responsive Block Copolymer Micelle, American Chemical Society. *Langmuir* 25(22):13201-13205.
- Ward, M.A. Georgiou, T.K., 2011. Thermoresponsive Polymers for Biomedical Applications, *Polymers*. 3:1215-1242.
- Xuan, J. Pelletier, M. Xia, H. Zhao, Y., 2011. Ultrasound-Induced Disruption of Amphiphilic Block Copolymer Micelles, *Macromolecular Chemistry and Physics* 212:498–506.
- Yahuafai, J. Asaia, T. Nakamura, G. Fukuta, T. Siripong, P. Hyodo, K. Ishihara, H. Kikuchi, H. Oku, N., 2014. Suppression of mice of immunosurveillance against PEGylated liposomes by encapsulated doxorubicin, *Journal of Controlled Release* 192:167-173.
- Yan, F. Li, L. Deng, Z. Jin, Q. Chen, J. Yang, W. Yeh, C. Wu, J. Shandas, R. Liu, X. Zheng, H., 2013. Paclitaxel-liposome– microbubble complexes as ultrasound-triggered therapeutic drug delivery carriers, *Journal of Controlled Release* 166:246–255.
- Yang, F.Y. Wong, T.T. Teng, M.C. Liu, R.S. Lu, M. Liang, H.F. Wei, M.C., 2012. Focused ultrasound and interleukin-4 receptor-targeted liposomal doxorubicin for enhanced targeted drug delivery and antitumor effect in glioblastoma multiforme, *Journal of Controlled Release* 160:652–658.
- Yang, M. Liu, C. Li, Z. Gao, G. Liu, F., 2010. Temperature-Responsive Properties of Poly(acrylic acid-co-acrylamide) Hydrophobic Association Hydrogels with High Mechanical Strength, *Macromolecules* 43:10645–10651.
- Yang, P. Li, D. Jin, S. Ding, J. Guo, J. Shi, W. Wang, C., 2014. Stimuli-responsive biodegradable poly(methacrylic acid) based nanocapsules for ultrasound traced and triggered drug delivery system, *Biomaterials* 35(6):2079-2088.
- Yang, Y. Mijalis, A.J. Fu, H. Agosto, C. Tan, K.J. Batteas, J.D. Bergbreiter, D.E., 2012. Reversible Changes in Solution pH Resulting from Changes in Thermoresponsive Polymer Solubility, *American Chemical Society* 134:7378–7383.
- Yang, Y. Wang, J.C. Zhang, X. Lu, W.L. Zhang, Q., 2009. A novel mixed micelle gel with thermo-sensitive property for the local delivery of docetaxel, *Journal of Controlled Release* 135:175-182.
- Yannic, B. Schuetz, Y.B. Gurny, R. Jordan, O., 2008. A novel thermoresponsive hydrogel based on chitosan, *European Journal of Pharmaceutics and Biopharmaceutics* 68:19–25.
- You, J-O. Almeda, D. Ye, G.J.C. Auguste, D.T., 2010. Bioresponsive matrices in drug delivery, *Journal of Biological Engineering*. 4(2010):15.
- Yudina, A. de Smet, M. Lepetit-Coiffé, M. Langereis, S. Van Ruijssevelt, L. Smirnov, P. Bouchaud, V. Voisin, P. Grüll, H. Moonen, C,T,W., 2011. Ultrasound-mediated intracellular drug delivery using microbubbles and temperature-sensitive liposomes, *Journal of Controlled Release* 155:442–448.
- Yudina, A. Lepetit-Coiffé, M. De Smet, M. Langereis, S. Grüll, H. Moonen, C., 2012. In vivo temperature controlled ultrasound-mediated intracellular delivery of cell-impermeable compounds, *Journal of Controlled Release* 161:90–97.

Yu, L. Hu, H. Chen, L. Bao, X. Li, Y. Chen, L. Xu, G. Yeb, X. Ding, J.,2014. Comparative studies of thermogels in preventing post-operative adhesions and corresponding mechanisms, *Biomaterials Science*. 2:1100-1109.

Zeng, Y. Pitt. W.G.,2006. A polymeric micelle system with a hydrolysable segment for drug delivery. *J Biomater Sci Polym Ed* 17(5):591-604.

Zhang, Z. Wang, J. Nie, X. Wen, T. Ji, Y. Wu, X. Zhao, Y. Chen, C.,2014. Near Infrared Laser-Induced Targeted Cancer Therapy Using Thermoresponsive Polymer Encapsulated Gold Nanorods, *American Chemical Society* 136:7317-7326.

Zhang, X. Zheng, Y. Wang, Z. Huang, S. Chen, Y. Jiang, W. Zhang, H. Ding, M. Li, Q. Xiao, X. Luo, X. Wang, Z. Qi, H.,2014. Methotrexate-loaded PLGA nanobubbles for ultrasound imaging and Synergistic Targeted therapy of residual tumor during HIFU ablation, *Biomaterials* 35:5148-5161.

Zhao, Y-Z. Du, L-N. Lu, C-T. Jin, Y-G Ge, S.P.,2013. Potential and problems in ultrasound-responsive drug delivery systems, *International Journal of Nanomedicine*. 8:1621-1633.

Zhou, Q-L. Chen, Z-Y. Wang, X-Y. Yang, F. Lin, Y. Liao, Y-Y.,2014. Ultrasound-Mediated Local Drug and Gene Delivery Using Nanocarriers. *BioMed Rearesrch International* (2014):1-13.

Zhu, L. Torchilin,V.P.,2013. Stimulus-responsive nanopreparations for tumor targeting, *Intergrative biology*. 5(1):1-20.

Zong, Y.J. Wan, J.J Qiao, Y-Z. Li, W.S. Zou, X.R. Wan, M.X.,. 2013.Cavitation Endothelium Damage of Large Artey Vessel : The Application to Animal Model of Atherosclerosis. *The International Conference on Health Informatics IFMBE Prceedings*,42(2014):63-66.

## CHAPTER 3

### FACILE GREEN SYNTHESIS OF THERMOSONIC INJECTABLE ORGANOGELS (TIO's)

---

#### 3.1 Introduction

Stimuli-responsive hydrogels has been an attraction in various biomedical applications including tissue engineering, biosensing wound healing and drug delivery (Tong *et al.* 2015; Zhao *et al.* 2013). Progressive research allowed the development of fourth generation biomimetic materials used for stimuli-responsive systems (Knipe & Peppas, 2014) to advance into multi-stimuli responsive systems such as dual or tri-responsive to enhance mimetic action of the body (Chejaraa *et al.* 2016; Yan *et al.* 2014;). By introducing multi-responsive systems drugs with a high toxic profile such as anticancer drugs can acquire an augmented control release of the drug. Understanding that cancerous tissue possesses changes in temperature and pH (Zhang, Lin & Gillies, 2010) compared to healthy body tissue a dually temp/pH responsive system can be applied to release specifically to those conditions.

Recent development of gels includes the incorporation of lipid to synthesize stimuli responsive lipogels. This is reported to improve drug encapsulation, extended payload retention and modulated drug administration (Lu *et al.* 2013). Since lipogels have these properties, it can be said that they are valuable in anticancer drug delivery and have been used to encapsulate antineoplastic agents such as 17 DMAPG, a geldanamycin derivative through active encapsulation (Wang *et al.* 2013). The ring opening method is one of three important methods of polymerization in the 21st century and is a well established skill for synthetic grafting cyclic monomers e.g. anhydrides and copolymerization of linear polymers, most of these reactions are made possible with catalysts under an inert environment with controlled temperature (Carlmark, Larsson & Malmstrom, 2012; Lerum, Chen, 2011; Nuyken & Pask, 2013)

Several methods used to undertake open ring polymerization is done under inert conditions with heat and stirring, these range in periods of hours (Samah & Heard 2013; Silvaa *et al.* 2013; Singh & Lyon 2008). Many researchers are moving away from using hazardous and toxic material and organic solvents, employing green chemistry techniques towards developing improved delivery systems with enhanced biocompatibility. Green chemistry follows 12 principles and focuses on replacing any harmful materials or methods with safer or alternative options or reducing these toxic materials to a minute concentration of the

formulation (Schulte *et al.* 2013). Furthermore green chemistry is an increasingly pursued concept in the pharmaceutical industry due to common errors such as material wastage, this includes determining the least quantity of drug that is needed to achieve the therapeutic objective working with the most potent compounds of which quantities one will need fewer to manufacture the drug that is most efficient and design formulations in a manner that will permit increase absorption and decreased excretion into the environment, this specifically pertains to chemotherapeutic drugs due to the large magnitude of side effects (Zhang & Cue 2012).

The use of DMSO is a controversial subject in drug delivery, its claimed to be carcinogenic while to researchers, it is known to be a penetration enhancer and is effective when used as 60% or more in a formulation, other researchers state that it is specifically used as skin penetrators in drug delivery (Touito, Williams & Barry 2011; Marren, 2011; Karande & Mitragotri 2009). Scheller *et al.* (2014) reported the use of 5% DMSO injectable microemulsion. It is also stated that according to the Australian Code of Practice for the Care and Use of Animals for Scientific Purposes a 0,5-5% of DMSO is a permissible concentration to use. Injectable in situ systems that employ the polymer precipitation strategy consists of water insoluble polymers dissolved in water miscible solvents i.e. N-methyl-2-pyrrolidone or DMSO. Injectable gels has captured the interest of many researchers for the past decade due to its advantages such as comfortable, effortless and decreased frequency of administration, it also promotes healthier patient compliance (Madhu, Shaila & Anwar, 2009).

In our study principles of green chemistry was applied through decreasing and exchanging organic solvents, open ring polymerization reaction times are decreased and decrease variety of chemicals used to formulate a TIO for delivery of biomedical materials.

## **3.2 Materials and methods**

### *3.2.1 Materials*

Ethylene Glycol (EG), Ethanol, Dimethyl Sulfoxide (DMSO), N-(Isopropyl Acrylamide) NIPAM, Sebacic Acid (SA), 1,3 4-(Carboxyphenoxy) propane (CPP), Sodium Dodecyl Sulfate (SDS), Methylene Bis-Acrylamide (MBA) and Ammonium Persulfate (APS). All chemicals were purchased from Sigma–Aldrich®Inc. (St. Louis, MO, USA).

## **Preparation of the TIO's**

### *3.2.2 N-isopropyl acrylamide and Sebacic Acid – TIO 1*

NIPAM (300mg) was dissolved in 5mL of Ethylene Glycol (EG). Sebacic Acid (SA) 25mg solution was separately prepared. The Sebacic Acid solution was added in a drop-wise manner to the NIPAM solution to form an emulsion. Sodium Dodecyl Sulfate (7mg) was added to the emulsion. Methylene Bis-Acrylamide (135mg) of an appropriate quantity was added to the solutions and allowed to dissolve. Within a sealed apparatus under inert and heating conditions, the solution (12:1:5:7/50) was stirred with the addition of APS (10%) to complete the reaction. Reaction gelling time was recorded. The TIO was then refrigerated at 5°C to stabilise.

### *3.2.3 N-isopropyl Acrylamide and 1,3 4-(Carboxyphenoxy) propane - TIO 2*

NIPAM (300mg) was dissolved in 5mL of EG while CPP (25mg) was separately dissolved in 0.25mL of DMSO under mild heating conditions. The CPP solution was added to the Nipam solution in a drop-wise manner to form a milky suspension. Sodium Dodecyl Sulfate (7mg) was added to the emulsion. Methylene Bis-Acrylamide (90mg) was added to the solution (12:1:1:3/10:7/50). Under similar conditions as mentioned above, TIO formation was achieved. Reaction gelling time was recorded. The TIO was then refrigerated at 5°C to stabilise.

### *3.2.4 N-isopropyl acrylamide, Sebacic acid and 1,3 4-(Carboxyphenoxy) propane - TIO 3*

NIPAM (300mg) was dissolved in 5mL of EG while SA (25mg) and CPP (25mg) solutions were prepared separately under mild heating conditions. The CPP solution was added drop-wise to the SA solution under mild heating conditions with the resultant of a cloudy emulsion. The resultant emulsion was added drop-wise to the Nipam solution. Sodium Dodecyl Sulfate (7mg) was added to the emulsion. Methylene Bis-Acrylamide (90mg) was added to the emulsion (12:1:3/10:7/50). TIO formation was achieved through similar conditions previously mentioned. Reaction gelling time was recorded. The TIO was then refrigerated at 5°C to stabilise.

## **3.2.5 Drying Protocol of the Thermosonic Injectable Organogels TIO's**

All samples were washed and dried using a specific method. The TIO's were washed in ethanol, twice the amount of TIO for 2 hours. Thereafter the washed TIO's were left to settle and separate from the organic solvent. The solvent was decanted and the same amount of ethanol was added to the TIO's and washed for a further 2 hours. After discarding the

supernatant, the washed resultant was left in the oven at 60°C until it formed a very thin layer of solid gel. The layers of TIO's were then transferred to a mortar and liquid nitrogen was added to the mortar to freeze the samples. During this reaction the TIO's were crushed to a fine powder. The powder was transferred to a petri dish and placed back into the oven at 60°C to ensure the powder was free of moisture. The resulting product was then collected and ready for characterization.

### **3.2.6 Thermo- and Ultrasound Response Analysis**

Images of the TIO's were captured against a black screen at different assimilated conditions to evaluate the efficiency of the dual mechanism. The TIO's were taken out of the fridge and left to stabilise at room temperature, after heating in an oven to 39°C (Tumoural temperate) and after exposure to ultrasound stimuli, the trigger release stimulus for the TIO's assimilated by the SCIENTECH ultrasound bath at set conditions temperature (°C) 25°C, T (min) = 5 min Intervals, Power = 005 and the frequency = Lo and the time was recorded.

### **3.2.7 Morphology Analysis of the TIO's**

The morphological structural analyses of the three dried TIO's were undertaken using the scanning electron microscope (FEI Phenom™, Hillsboro, Oregon, USA). The dried TIO samples were mounted on the SEM stubs using double sided adhesive carbon tape. The fixed samples were coated with gold for 2 minutes employing a gold sputter-coater (SPI Module TM Sputter Coater, SPI Supplies, PA, USA). The images obtained were on a 100 µm scale to analyse the surface morphology and the physical structure of the three TIO's. Two images of each TIO at different views were obtained.

### **3.2.8 Chemical Structure Integrety Analysis of the TIO's**

Identification of new bonds were established through fourier transform infrared spectroscopy employing the Perkin Elmar Spectrum 2000, Llantrisant, Wales, UK that utilizes a single reflection diamond MIRTGS detector (Perkin Elmar Spectrum 100, Lantrisant, Wales, UK) fixed with a universal ATR polarization accessory (Perkin Elmar Ltd.,Beaconsfield, UK) possessing a resolution of 4cm<sup>-1</sup>. The parent compounds were scanned to obtain the spectrum of each monomer and the complex of every TIO to detect the possible structural molecular transitions during the preparation of the combined formulations. The cone probe was used for all samples and each sample was set to scan 10 times. The resultant outcome was the average of all ten scans in the range of 1800-550cm<sup>-1</sup> at a set pressure of 120 psi. All three TIO's were analysed to obtain comparative results in the molecular transitions and these were reported.

### **3.2.9 Thermoanalytical Analysis of the TIO's**

Thermal analysis was carried out using differential scanning calorimetry (DSC) with the Mettler-Toledo, DSC1 STAR<sup>e</sup> system, Switzerland to obtain the thermal behaviour of all monomers and changes in phase transitions and melting points in the TIO complexes. All samples were measured at an average weight of  $10 \pm 1$  mg in 40- $\mu$ L aluminium crucible pans with a finished pinhole on the crucible lid and underwent thermal analysis of temperatures between 20°C-500°C at a rate of 10°C/min under a constant N<sub>2</sub> atmosphere. TIO complexes were analysed to observe new melting points which occurred that related to the results presented by the monomer.

### **3.2.10 Phase Identification of the TIO's**

The solid state of the TIO complexes in powder form and individual polymers were analysed through the employment of the Rigaku MiniFlex600 Benchtop X-Ray Diffractometer (Rigaku Corporation, Tokyo, Japan) equipped with a 600 W (40 Kv-15mA) X-ray generator, a high intensity D/tex ultra high speed 1D detector and a counter monochromator that cuts X-rays with the exception of Cu K $\alpha$  X-rays. The results of all parent monomers and all three TIO's were evaluated for the molecular arrangement of the compounds in terms of crystalline or amorphous arrangement. Observations between XRD and DSC results were compared for complimentary status of the molecular arrangements.

### **3.2.11 Rheological Analysis of the TIO's**

Rheological studies were performed on all TIO samples. Rheological assessments of the TIO's were undertaken using the Haake Mars (II) Modular Advanced Rheometer System using cone plate geometry (C35/1,  $D = 1$  mm, 1° Titan). The TIO's and a reference were prepared for comparison assessments. They were removed from the refrigerator and left to stabilize at room temperature. The following tests were performed for each TIO: a) Frequency sweeps b) dynamic viscosities at various shear rates and c) temperature ramp assessments. Oscillatory frequency sweeps were undertaken from 50 to 0.10 Rad.s<sup>-1</sup> at a continuous shear stress of 1Pa and a temperature of 25°C for all TIO's. Temperature ramp tests were performed from 20°C to 50°C at a constant frequency of 1 Hz and analysis of the graphs were reported.

### **3.2.12 Physicomechanical Behaviour of the TIO's**

The change in physicomechanical behaviour of the TIO's were evaluated using the Texture Analyser (TA.XT plus, Stable Microsystems, Surrey, UK) employing a 50mm circumference textural probe whilst increasing temperature from 25°C to 39°C was applied via a heating



chamber (Peltier Cabinet). Compression strength (CS), gel resilience (GR) to evaluate the energy of the TIO's, recognized through elastic deformation and, rigidity gradient (RG) and the deformation energy (DE) were investigated under heating conditions to test the increasing strength of the TIO's under thermal stimuli. The parameters were set as follows: Pre-test speed=0.20 mm/sec, test speed=0.2mm/sec, post test speed=5mm/sec, target mode=distance, distance=8mm, trigger type auto (force), trigger force=100g, break mode=off, stop plot at =start position, tare mode=auto, advanced options=on.

### **3.2.13 Cell Culture and Fibroblast Proliferation Studies**

A cell proliferation study was undertaken for a period of 5 days. The fibroblast HeLa cell line was purchased from Sigma Aldrich. The cells were transferred into a T25 flask containing 5% FBS media solution that had been pre incubated (CO<sub>2</sub> 5%, 37°C). The cells were washed and nurtured every two days using DPBS and replacement of media. Once the cells reached confluency, they were transferred to a T75 flask to culture a sufficient number of cells. Once confluency was reached the cells were counted by means of a new bar chamber and a microscope. The cell count (CC) was calculated at 1000 cells in 100µL using the following equation:

$$[\text{The number of cells (in the 4 corner quadrants)/ 4}] \times \text{Dilution factor (4)} \quad \text{Equation 3.1}$$

The cell proliferation was performed using an MTT assay Kit purchased from Sigma Aldrich. A 96 plate well was used to undertake the proliferation of the cells. In each well plate 100µL was instilled and the well plate was incubated for 24 hours. Concentrations of washed TIO to media of 10mg/mL, 5mg/mL, 2.5mg/mL and 1.25mg/mL were tested in wells containing 1000cells/cm<sup>2</sup>. Once the dilutions were prepared the well-plate was incubated for 5 days. The cell proliferation for day 1, day 3 and day 5 were determined using a plate reader and bar graphs were plotted to represent the proliferation of fibroblasts. The method was adapted from Lin Zhang and co-workers (2014).

### 3.3 Results and Discussion

#### 3.3.1 Assessment of the gelation rate of the TIO's

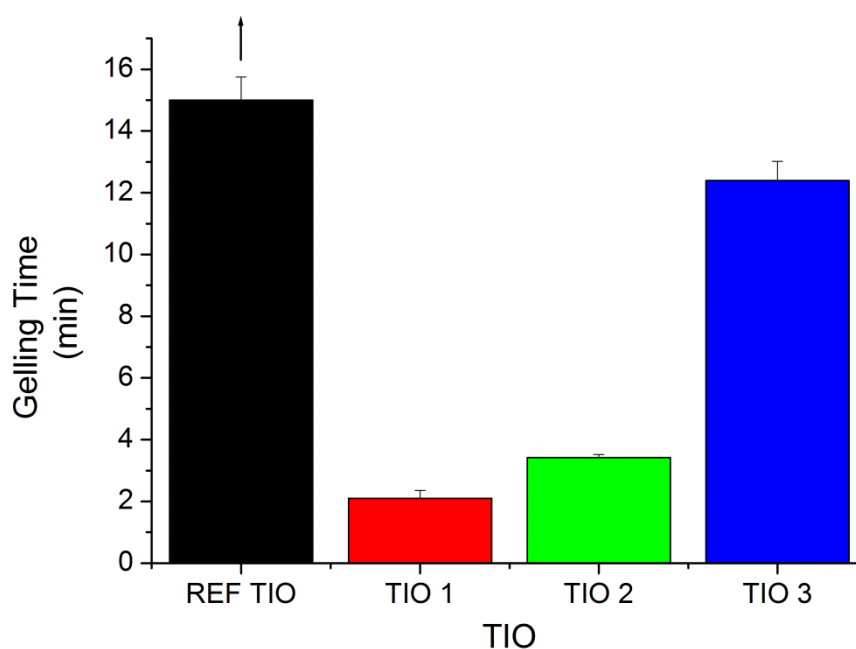


**Figure 3.1** Bar Graph comparing the gelling time during preparation of TIO 1 TIO 2 and TIO 3. Standard deviation < 0.75 (N=3)

#### 3.3.1 Assessment of the Gelation Rate of the TIO's

In this study three TIO's and a reference TIO were prepared and the times taken for these TIO's to form were recorded. The reference TIO reaction was allowed to stir for twelve hours in the absence of heat and  $N_2$ , whereas the other three gels were exposed to both conditions. The reference resulted in no TIO formation over a twelve hour period. This confirms that without heat and an inert environment the reaction cannot take place, possibly due to the inability for the APS to be initiated and the formulation exposed to the external environment respectively. Considering the three TIO's, TIO 1 (12:1:5:7/50) presents with the fastest gelation time of 2 minutes and 8 seconds compared to TIO 2 (12:1:3/10:7/50) 3 minutes and 25 seconds and TIO 3 (12:1:3/10:7/50) 12 minutes and 40 seconds. Kabiri et al. (2003) reports that the higher the crosslinker concentration, the shorter the gelation time; particularly with MBA.

TIO 2 (12:1:3/10:7/50) had a slightly longer gelation time than TIO 1 (12:1:5:7/50) but shorter time than TIO 3 (12:1:1:3/10:7/50). This can be accounted for due to the lower crosslinker concentration to TIO 1 (12:1:5:7/50) and the presence of SA in TIO 3 (12:1:1:3/10:7/50)

respectively. SA also provides gelation properties when reacted with polymers that lack the ability to gel on its own such as CPP. TIO 3 (12:1:1:3/10:7/50) presented with the longest gelation time compared to TIO 1 (12:1:5:7/50) and TIO 2 (12:1:3/10:7/50) this relates to the lower crosslinker and the absence of SA in TIO 3's (12:1:1:3/10:7/50) formulation and may also be related to the double concentration of DMSO (Shikanov & Domb, 2005).

### **3.3.2 Evaluation of the Stimuli-Responsiveness of the TIO's**

Analysing figure 3.2 a) TIO 1 consisting of Nipam and SA, it can be observed that at room temperature the TIO tilted at a 135° angle presents a low physical degree of flowability due to its high viscosity. Once a) was exposed to a 39°C temperature (Tumoural temperature) the viscosity was increased to become a stronger TIO, when rotated to a 270° angle the TIO maintains its status by holding its weight against gravity. After confirming that the TIO has thermosensitive properties it was placed directly from the oven and placed in the ultrasound bath for measured periods with low frequencies at 40°C. TIO 1 took 110 minutes to lose its integrity to ultrasound stimuli and it can therefore be deduced that the thermoresponsive properties of the TIO are strong as it holds its own weight and ultrasound responsiveness is present. This is owing to the formulation as it consists of Nipam and SA with no CPP decreasing the ultrasound responsive sensitivity and once responded it moves in bulk.

Assessing figure 3.2 b) TIO 2 under the same conditions as a) the flowability of the TIO is increased at room temperature studying the smooth gradient of the TIO tilted at a 135° angle. After exposed to tumoural temperature and rotated to a 270° angle, the TIO maintains its status as a stronger TIO holding its weight against gravitational force, demonstrating thermoresponsive properties. The sample was directly transferred from the oven to the ultrasound bath. Thereafter the application of 15 minutes of ultrasound at a rotation just above 180° and the rate of flowability was increased. The bulk flow was not as much as a) TIO 1.

Assessment of c) TIO 3, showed a similar behaviour to a) and b) when exposed to heat and ultrasound (30 minutes), however physical changes to the TIO state was very minor when exposed to the stimuli. After heating, at a 270° rotation there is a slight increase in the viscosity of the TIO and presents with a bulk flow above 180° rotation respectively. Even though TIO 2 and 3's responsive times to ultrasound are shorter compared to TIO 1, it can be concluded that further studies should be undertaken on all three TIO's to evaluate the efficacy of each TIO's response to both stimuli.

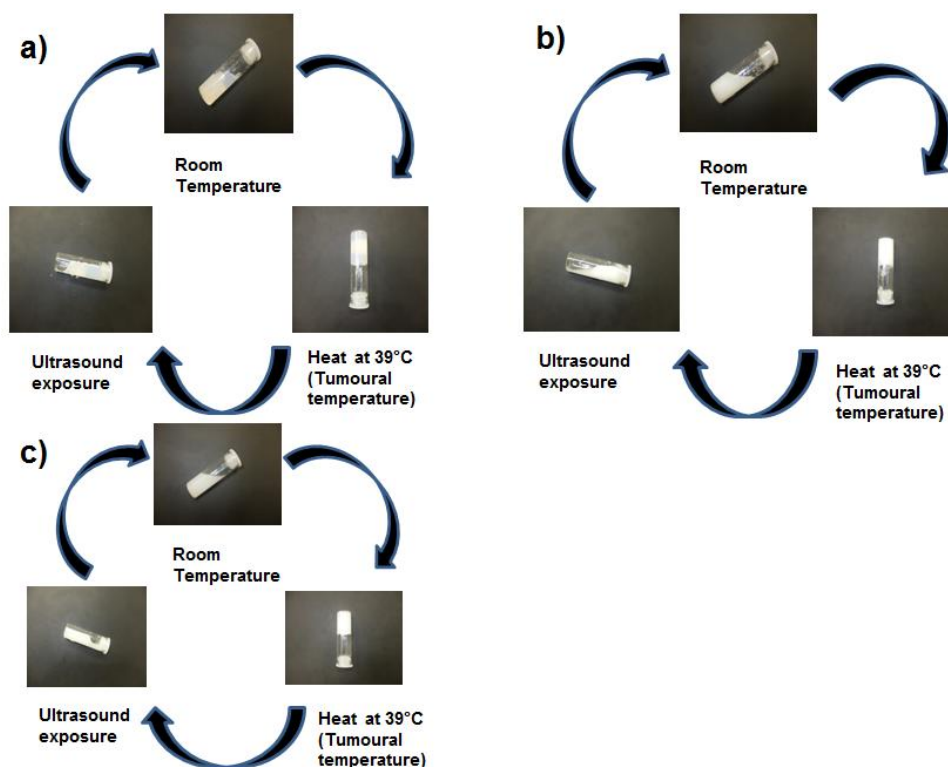


**Figure 3.2** Figures illustrating the mechanism cycle of response to thermal and ultrasonic stimuli a) TIO 1 b) TIO 2 c) TIO 3.

### 3.3.3 Evaluation of the TIO's Morphological Structure

The general morphology of the TIO's was all very similarly structured in formation. It can be observed from the images below that the TIO's structure contains striations and pores along the surfaces. The pores of image 3.3a) are of similar diameter and widely dispersed although inconsistently arranged. The pores presented in image 3.3a) illustrates a lower quantity and can be related to the increased MBA concentration that possibly decreases pore quantity and porosity, this was also reported by Chavda and Patel, 2011. Concentrations of MBA were increased from 7.37% to 14.36% resulted in a decrease in porosity (Chavada & Patel, 2011). Capturing a magnified view of the gels appearance in 3.3.b) the detail of the TIO's formation of its pores and striated appearance can be observed. The striated appearance is presented by a bundle of threadlike formations clumping to form the TIO and pores are created in the process.

The observed distribution of the pores in 3.3.c) complements even and increased loading of any substance whether it being the active or the vectors encapsulating the active for augmentation of drug release. The increase in pores compared to TIO 1 is due to a lower concentration of MBA. The cracks seen in this image and the latter, is caused by the drying process of the TIO's. A pattern that can be observed when analysing 3.3.d); the pores are concentrated greatly along the striations as previously noted in the enlarged area of image 3.3.b) pores are highly visible compared to the smooth surface.

Comparing 3.3.e) with the former image, a similarity of pores along the striations can be seen but they prove to be equally dispersed on the smooth surface of the TIO. It can also be noted in image 3.3.f) that the smooth surface contains pores although randomly dispersed. Although the surface morphology of all 3 TIO's are similar, the general structure of the gels provided by the images below suggests a randomly arranged molecular configuration due to the inconsistent forms that are present in the images. Amorphous gel systems are used as a strategy to increase the solubility of hydrophobic compounds or drugs to enhance drug loading and release by preventing re-crystallisation when exposed to the dissolution medium.

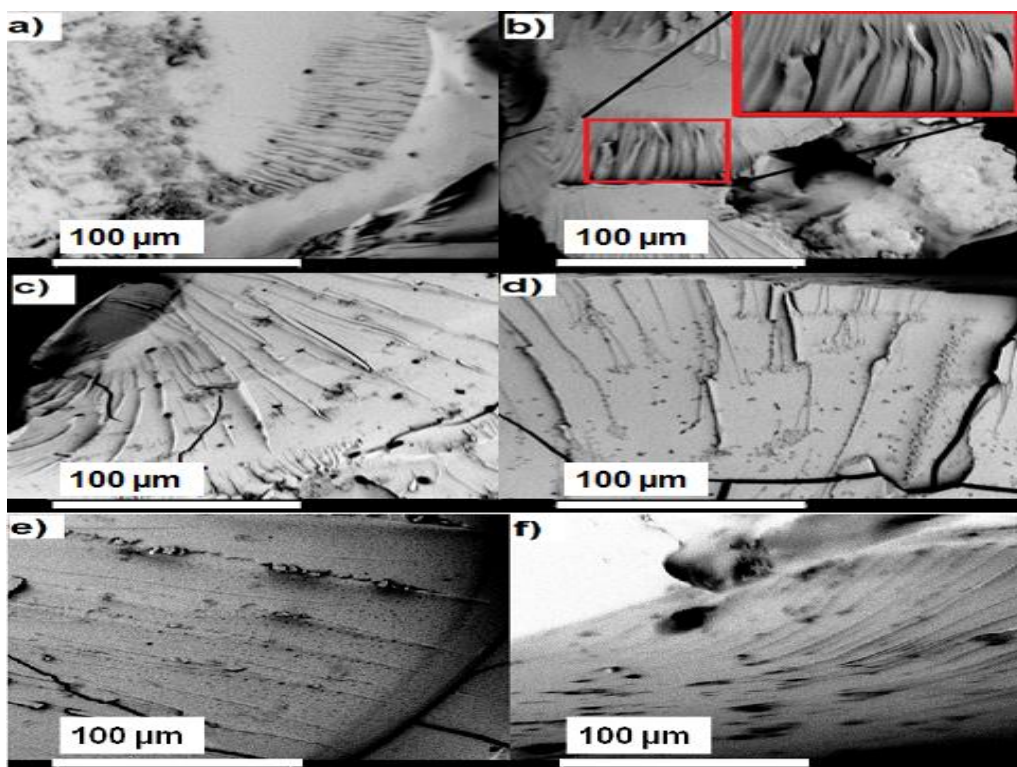


**Figure 3.3** SEM Images TIO 1, a) and b), TIO 2 c) and d) and TIO 3 e) and f). Illustrating the general surface morphology of the TIO's.

### 3.3.4 Chemical Structure Identification of the TIO's

FTIR was undertaken for TIO 1, 2 and 3 and its individual constituents. Studying the graphs below, it can be seen how each constituent presents itself in these TIO's by either forming new bands or shifting bands. From the noted bands of the monomers it can be deduced that there is the presence of a C=O stretch carbonyl group at  $1645\text{cm}^{-1}$  and following this; the most important band is the -NH band at  $1546\text{cm}^{-1}$  which represents the presence of the amide in the structure (Thoing *et al.* 2013; Xue *et al.* 2014). Another significant band may be noted at  $1243\text{cm}^{-1}$  suggesting a -NH amide III band (Dharmesh *et al.* 2016).

Analyzing CPP structure the most important bands to find are the following, a carbonyl group C=O stretching can be seen prominently by wavenumber  $1690\text{cm}^{-1}$  (Jung, Park & Han, 2010). This illustrates a hydrogen bonded carboxylic acid attached to an aromatic ring. C-O stretch can be seen at  $1242\text{cm}^{-1}$ , and may represent ether which is present in the structure of CPP. The area demarcated 2 expresses newly formed bands, this is due to CPP, TIO 1 does not contain CPP and will not present with these new bands. Furthermore bands at  $847\text{cm}^{-1}$  and  $770\text{cm}^{-1}$  accounting for aromatic ring presence in TIO 2 and TIO 3 due to the presence of CPP can be noted (Mayet *et al.* 2014). Studying SA, although not aromatically bound, the most prominent band peaks at  $1691\text{cm}^{-1}$  falling within very close proximity of CPP's significant band representing a hydrogen - bonded carboxylic acid bonded to a C=C depicted by SA's structure.

Having established the main peaks of each monomer, a concise interpretation was made. TIO 1, having no CPP does not present with bands that represent aromatic rings as there are no aromatic rings in NIPAM nor SA. TIO 2 and 3 contain CPP and therefore present with bands that correspond to aromatic bands found in the CPP spectra. The low intensity that the band presents is due to the concentration of CPP in the total formulation. Furthermore the spectra for TIO 2 and 3 illustrates a new but low intensity band at  $1249\text{cm}^{-1}$  which is not present in TIO 1, confirming that this band is caused by crosslinking of the CPP monomers with the other monomers.

The greatest changes are the additional bands that are formed in all three TIO's spectra outlined in demarcation 1 between  $821$  and  $1171\text{cm}^{-1}$ . This suggests the formation of new bonds in all three TIO's as these bands do not exist in either of the monomers. The formation of a band at  $1037\text{cm}^{-1}$  indicates -CH deformation vibrations and a band presented at  $1080\text{cm}^{-1}$ , representing a C=O carbonyl functional group bound to an aromatic ring structure (Mabrouk *et al.* 2015). A shift of the prominent band expressed in the NIPAM spectra from  $1546$  to  $1643\text{cm}^{-1}$  in all three synthesised TIO spectra and could be a result of C-N stretching related to the degree of crosslinking (Hoosain *et al.* 2014). In demarcation 2

there is a prominent band present in TIO 2 and TIO 3 at  $1244\text{cm}^{-1}$  and is absent in TIO 1. Since TIO 1 contains no CPP it can be assume that this C-C stretch bond is formed by the addition of CPP. The decrease in the intensity of the peak may be due to the concentration ratio within the formulation (Bijukumar *et al.* 2015).

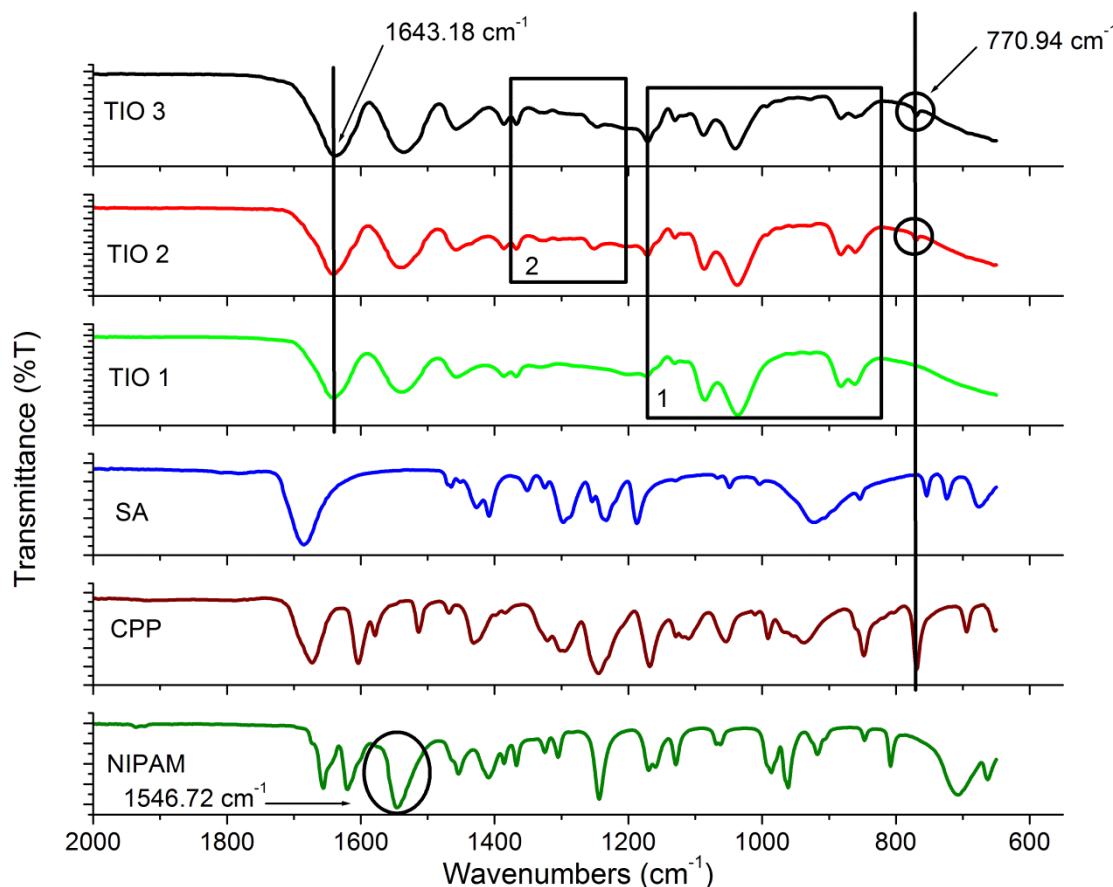


**Figure 3.4** FTIR Spectra illustrating the chemical transformations of the monomers to the TIO formulations

### 3.3.5 Thermoanalytical Assessment of the TIO's

Thermal analyses were elucidated by DSC graphs produced by the DSC. All three monomers and TIO's thermograms are presented in figure 3.5. A detailed analysis of the thermal behaviour was done on the TIO's. Each monomer illustrates a relatively sharp specific endothermic peak relating to their individual melting point. The melting points of NIPAM, CPP and SA are  $60\text{-}63^\circ\text{C}$ ,  $310^\circ\text{C}$  and  $135^\circ\text{C}$  respectively (Sailakshmi, Mitra & Gnanamani, 2013). NIPAM conveys a peak at  $64.09^\circ\text{C}$ , CPP at  $310.84^\circ\text{C}$  and SA at  $136.34^\circ\text{C}$ .

Considering the properties and thermal behaviour of the 3 TIO's, the glass transition ( $T_g$ ) temperatures of all three TIO's are  $34.81^\circ\text{C}$ , this is the temperature by which an amorphous systems changes from the glassy to the rubbery state (Abbas, 2010). The thermal behaviour of the TIO's, presents with higher thermal activity as thermograms depicts additional endothermic and exothermic peaks that are broader. This relates to the molecular arrangement of the TIO's. TIO 1 and TIO 3 presents with a broad exothermic peak at  $125.24^\circ\text{C}$  as well as a broad endothermic peak at  $181.48^\circ\text{C}$  representing thermal activity in line with SA and suggests the decrease in crystallinity by an extensive degree and is not seen in TIO 2 as it is absent (Choonara *et al.* 2015). This endothermic peak represents the crystalline melting point of the gels and is more pronounced in these gels containing SA.

NIPAM has the highest concentrated solid monomer in all three formulations, NIPAM endothermic peak shifts to a higher temperature of about  $184.41^\circ\text{C}$ , but forms a broader peak suggesting a decrease in the crystallinity phase of the TIO from the parent monomer. TIO 2 and TIO 3 containing CPP presents with broader endothermic peaks compared to TIO 1 which depicts a greater intensity peak. This accounts for the presence of CPP in TIO 2 and TIO 3. Amorphous delivery systems possess enhanced molecular mobility and increased thermodynamic properties (Tejaa *et al.* 2013).

The presence of CCP suggests a decrease in the intensity of the shifted NIPAM peak. TIO 1 containing no CPP, presented with an endothermic peak of greater intensity than TIO 2 and TIO 3 that contain CPP. The broad endothermic peak presented by TIO 1 and TIO 3 at approximately  $125.24^\circ\text{C}$  is due to the SA content in the two formulations of which TIO 2 does not contain and hence does not convey. It could be said that the presence of SA is responsible for the increase in intensity of the NIPAMs' peak and also a decrease in thermal behaviour from approximately  $300^\circ\text{C}$ .

Proceeding the crystalline melting peaks, the thermograms depicts crystallisation of TIO 1 and TIO 3 before the melting points are reached. Endothermic peaks signify that the melting points of the gels which are  $270.99^\circ\text{C}$ ,  $278.26^\circ\text{C}$  and  $251.73^\circ\text{C}$  which correspond to TIO 1, TIO 2 and TIO 3 respectively. Following the melting point in TIO 1 and TIO 2 the endothermic peaks present itself at  $368.05^\circ\text{C}$  and  $358.04^\circ\text{C}$ , at these temperatures the process of crosslinking takes place also known as the curing process, the presence of this crosslinking peak is dependent on the concentration of the crosslinker (Hoosain *et al.* 2014).



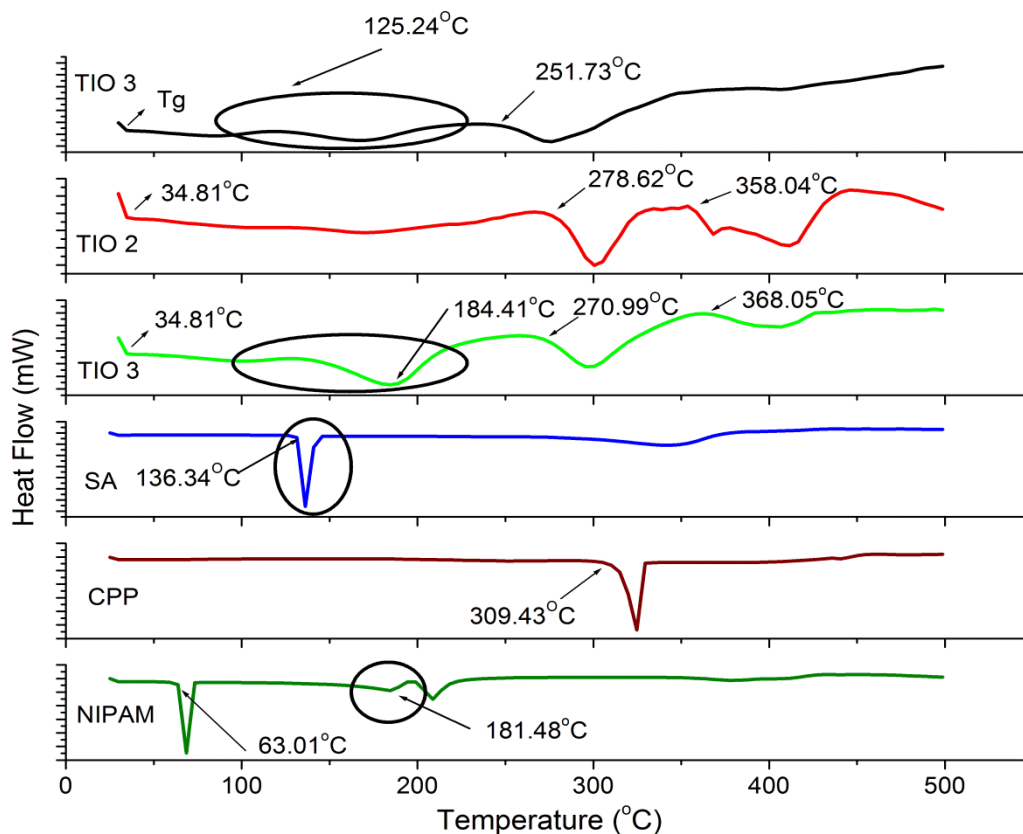


**Figure 3.5** Thermal behaviour of the TIO formulations and their parent monomers

### 3.3.6 Physicochemical Integrity of the TIO's

The key focus of this characterization test was to observe the changes in state between crystallinity and amorphous arrangement of molecules from the monomers to the TIO's. Through general overview of the graphs presented in figure 3.6, all three monomers are in the crystalline form and all three TIO's are in amorphous form. NIPAM shows one main peak that has intensity of 5103.75 a.u. at 14,23° and less intense peaks at 12.92°,21.58°,22.54° with intensities of 439.76°, 866.13° and 439.76° respectively.CPP also has one main intensity peak based at 16.85° with an intensity of 945.78 a.u. SA shows 3 major peaks at 18.95°, 21.23° and 39.58° at intensities of 170.85, 97.22 and 202.87 a.u.

When analysing the gels it can be noted that all three TIO's have transformed from crystalline phase to amorphous phase, they formed a broad peak at an average intensity of 960.92 a.u. at 21° from sharp intense crystalline peaks demarcated on the graph. This can be due to the physical interaction between the monomer during crosslinking.

A correlation between the transformations from the monomer state to the TIO state can be observed when comparing the results of the outcomes provided by the DSC and XRD graphs. All three monomers give sharp peaks for DSC and XRD and for the TIO's the peaks become broad, the difference is TIO's obtained greater thermal activity given by the increase in the number of peaks due to merging properties of the monomers and the crystalline structure of all the monomers become a consistent amorphous gel.

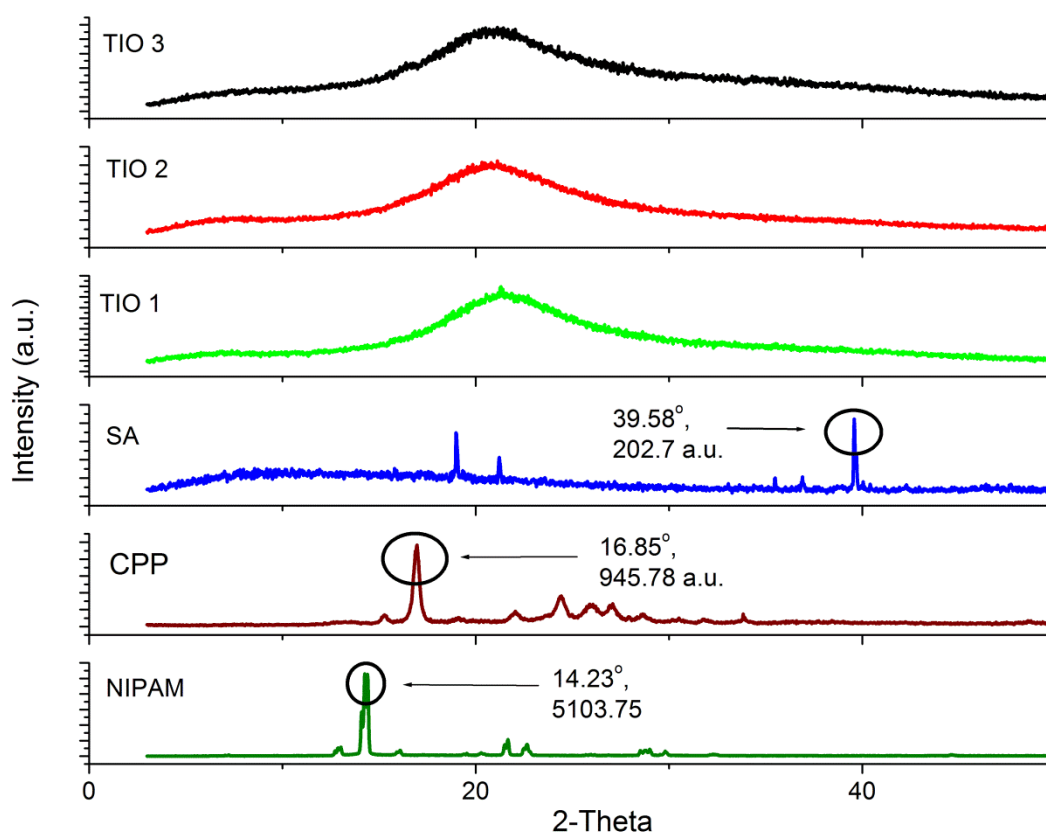


**Figure 3.6.** X-ray Diffraction depicting the physicomechanical nature of TIO 1, TIO 2, TIO 3 and the parent monomers of the gel

### 3.3.7 Rheological Evaluation of the TIO's

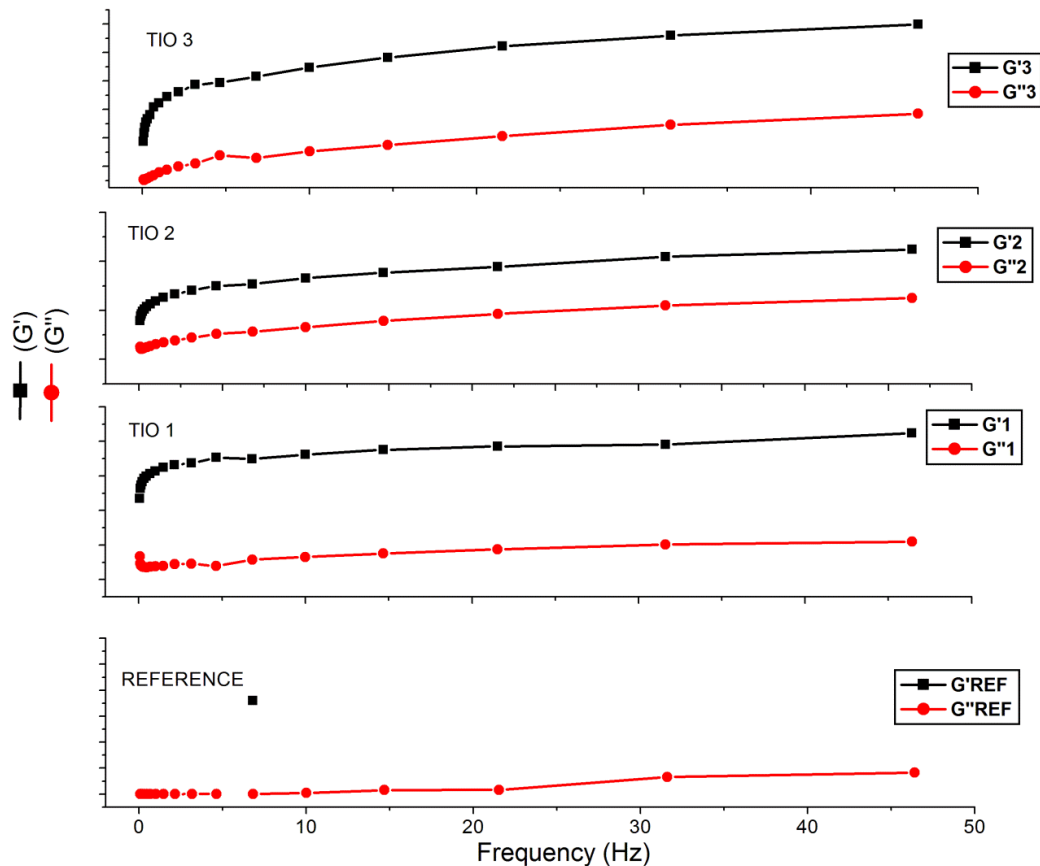


**Figure 3.7** Frequency sweep of TIO 1, TIO 2, TIO 3 and a Reference.

A frequency sweep test was conducted for all three TIO's and a reference formulation. The graphs for TIO 1, TIO 2 and TIO 3 convey that these gels have a greater elastic modulus/ storage modulus, depicted by  $G'$ , than its viscosity modulus/ loss modulus  $G''$  whereas the reference this behaviour is not present. This suggests that all three TIO's have a strong structure. TIO 3 has the highest increase in elastic modulus ( $G'$ ) from 741.23 Pa to 2426.06 Pa whereas TIO 2 and TIO 1 increase from 62.50 Pa to 455.1 Pa and 451.60 Pa to 847.13 Pa respectively. From this observation it can be said that TIO 3 has the greatest mechanical strength. Considering the linear viscoelastic region (LVR), it can also be noted that TIO 3 has the largest LVR with a substantially higher  $G'$  value of 2426.06 Pa and  $G''$  value of 1135.86 Pa compared to TIO 2 with a storage modulus  $G'$  value of 455.17 Pa and a loss modulus  $G''$  value of 245.80 Pa and TIO 1 possess a  $G'$  of 847.13 Pa and loss modulus  $G''$  value of 235.67 Pa (Bairi *et al.* 2014). These results can be directly correlated with the compression strength outcomes of all three TIO's confirming the strength of each TIO.

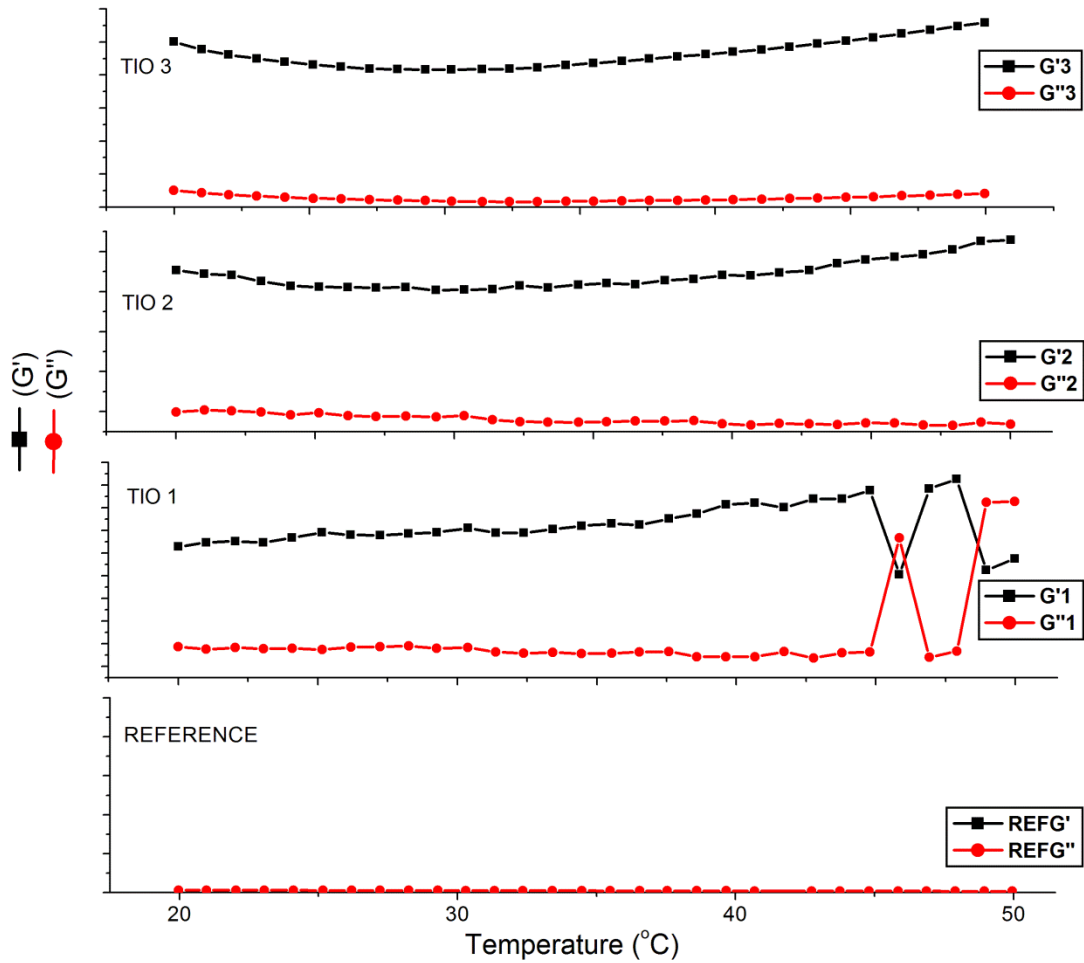


**Figure 3.8** Temp ramp rheological characterization for TIO 1, TIO 2, TIO 3 and a Reference

Temp ramp tests between 20°C and 50°C were performed on all three TIO's and the reference formulation in order to observe the thermal gelling behaviour of each TIO. In sol-gel formulations loss modulus  $G''$  initially dominates storage modulus  $G'$ , which represents the formulation as a liquid state as the temperature increases, a rapid increase in  $G'$  occurs compared to  $G''$  and results in the intersection of  $G'$  and  $G''$ . At this point  $G'$  supersedes  $G''$  and the solutions transforms into a gel (Li *et al.* 2014). Figure 3.8 depicts  $G'$  as initial dominance suggesting that the natural state of the formulation is already in a gel state. In all three gels  $G'$  has a drastic increase compared to  $G''$  representing a change in gel state to a stronger gel confirming successful response to thermal stimuli. It can be noted that TIO 1 has the most drastic change in storage modulus ( $G'$ ) compared to TIO 2 and TIO 3. According to this analysis TIO 1 has the strongest response to thermal stimuli. The reference formulation presented with no storage modulus ( $G'$ ) results and therefore no gellation occurred during heating of the formulation.

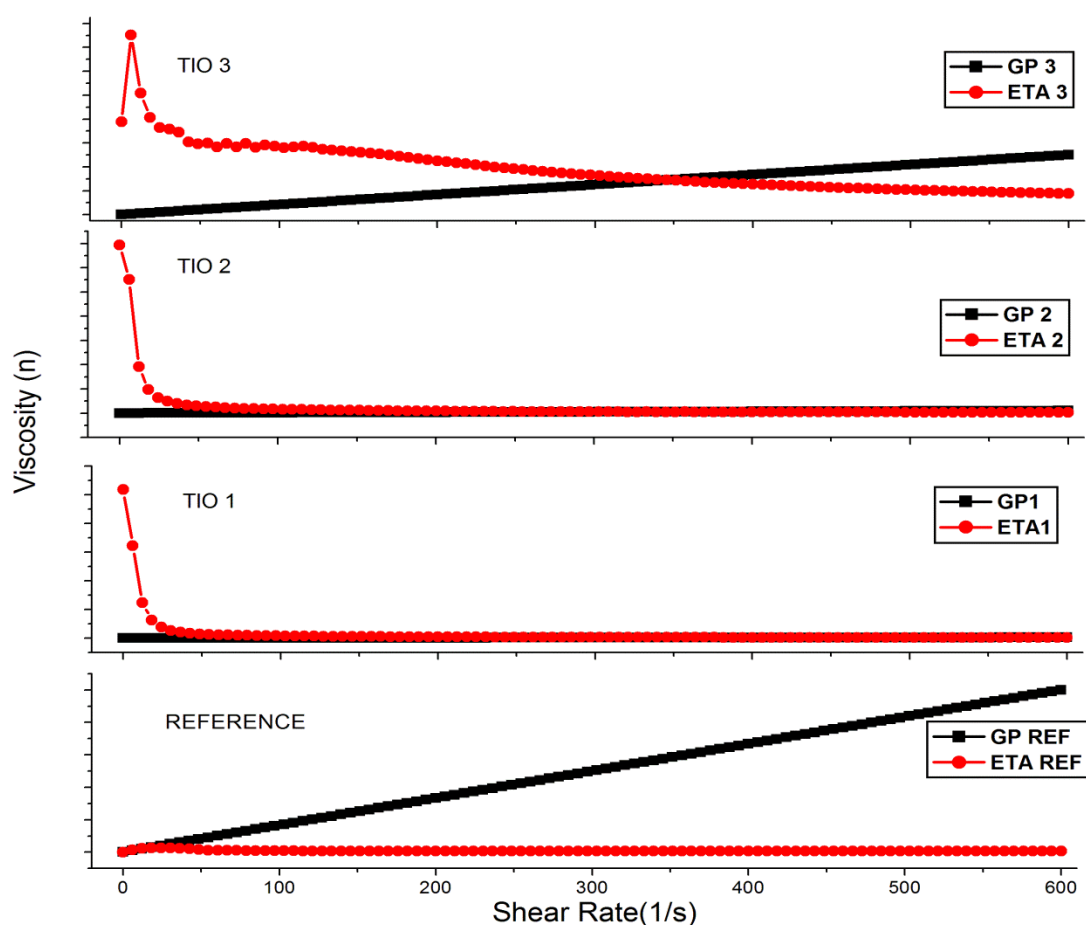


**Figure 3.9** Graphs illustrating the shear viscosity for TIO 1, TIO 2 and TIO 3.

The shear viscosity results of all three TIO's and the reference TIO are presented in figure 3.9. In all three TIO's it can be observed that with an increase in the shear rate ( $\dot{\gamma}$ ) yield there is a decrease in the viscosity of the TIO. This portrays that all three TIO's have shear thinning properties. As the shear rate increases in consistent intervals it can be noted that TIO 3 has an initial increase in viscosity from 776.50 to 1513.87 in the first interval but follows the general decrease in viscosity as in TIO 1 and TIO 2. TIO 1 has the highest viscosity results at every increase in shear rate compared to TIO 2 and TIO 3 with an initial viscosity of 102855.66, 34823.78 and 776.50 respectively. A higher crosslinker concentration would result in an increase in hydrogen bonding of the functional groups of the monomers and lead to stronger networks of the TIO which could be the basis of higher viscosity results as seen in TIO 1.

### 3.3.8 Textural Analysis of the TIO's

Compression Strength, Deformation Energy and % Resilience on TIO 1, TIO 2 and TIO 3 at increasing temperature 25°C- 39°C (tumoural temperature) using a Peliter cabinet heating chamber.

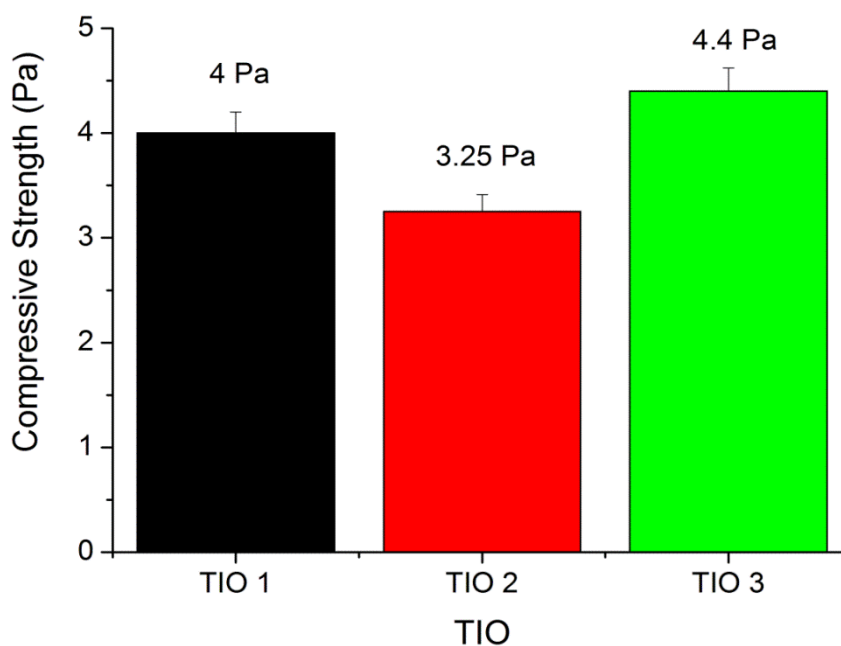


**Figure 3.10** Compressive strength demonstrated by TIO 1, TIO 2 and TIO 3. Standard deviation <math><0.25</math> (N=3).

The compressive strengths of all three gels were determined to evaluate the maximum force that the gels endure before losing the ability of resistance towards compression; also known as crush loading (Jaikumar *et al.* 2015). It can be noted from figure 11, that TIO 1 4Pa and TIO 3 4.4 Pa possessing sebacic acid presents with a higher compressive strength than TIO 2 3.25 Pa. Although TIO 1 contains a higher concentration of crosslinker compared to TIO 2 and 3; the compressive strength of TIO 1 is lower than TIO 3. This suggests that the sebacic acid and crosslinker concentration plays a significant role in the resultant compressive strength of the gel.

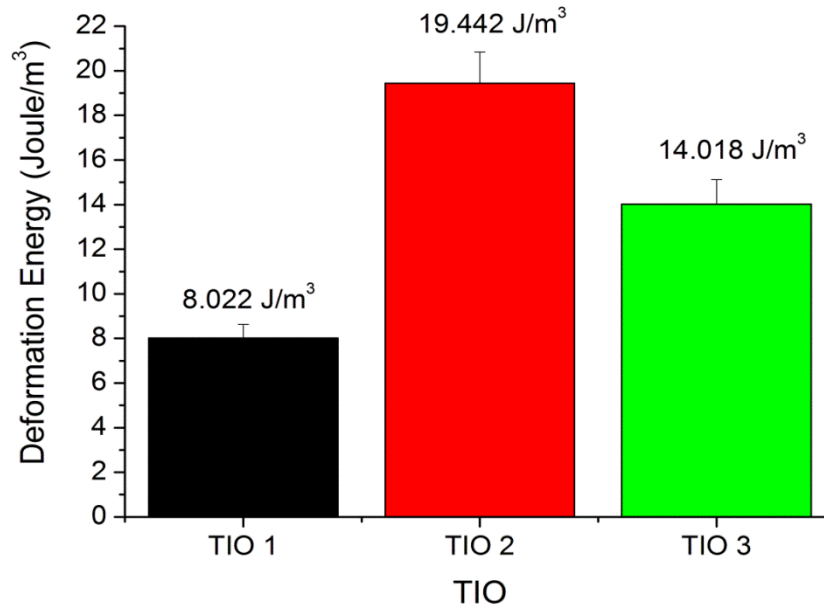


**Figure 3.11** Deformation energy demonstrated by TIO 1, TIO 2 and TIO 3. Standard deviation <0.15 (N=3).

Deformation energy is known as the energy that is absorbed by the gel that would result in the deformity of the gels nature (Indermun *et al.* 2014). The deformation Energy graph depicts that the concentration of the materials and crosslinker in the gels are indirectly proportional to the deformation energy and to the matrix resilience.

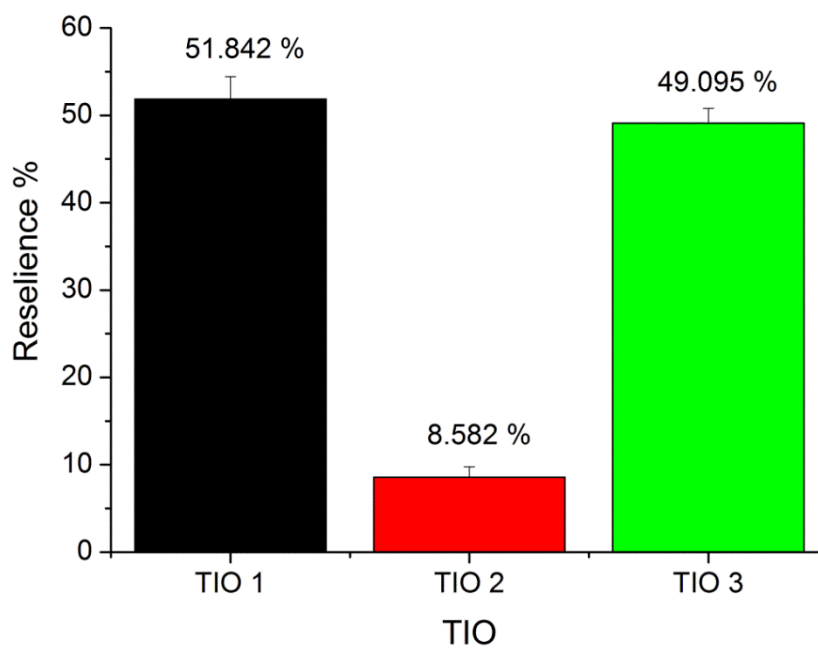


**Figure 3.12** Gel Resilience % given by TIO 1, TIO 2 and TIO 3. Standard deviation <3 (N=3).

Textural analytical resilience were undertaken on all three TIO's to establish the ability for them to adapt to the change in stress applied, whereby a gel undergoes elastic deformation and energy is released thereafter (Inderman *et al.* 2014; Mabrouk *et al.* 2015). The resilience of the TIO's was determined through the ratio percentage that links the area under the curve from the peak to the base line (subsequent to the removal of the force) and the area under the curve linking the peak to the base line (prior to the removal of the force) from a force-time profile (Hibbins *et al.* 2014). It can be deduced from Figure 3.11 that TIO 1 has the highest resilience of 51.42%. This is followed by TIO 3 (49.01%) and TIO 2 (5.58%). The high resilience of TIO 1 can be accounted for due to the increased concentration of crosslinker within the TIO compared to TIO 2 and TIO 3 (Tierneya *et al.* 2009). The high resilience of TIO 3 is fairly similar to TIO 1 and this may be due to the presence of SA that possesses gelling properties.

### 3.3.9 Fibroblasts Cell Proliferation Studies

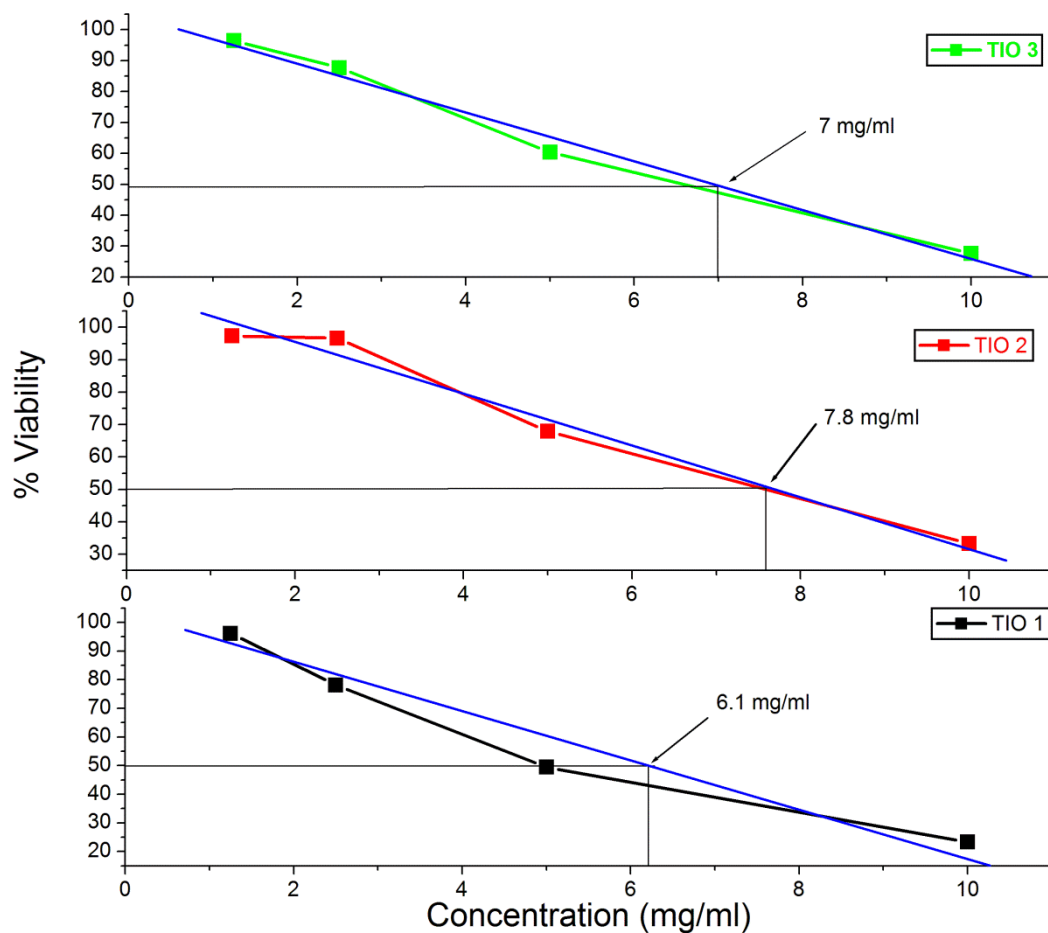


**Figure 3.13** Graph Illustrating the EC 50 of TIO 1 TIO 2 and TIO 3



The EC<sub>50</sub> of all three TIO's were analysed to determine the inhibitory concentration of each. Numerous concentrations 10mg/mL, 5mg/mL, 2.5mg/mL and 1.25mg/mL were analysed over a period of 24 hours. The inhibitory concentration is the concentration at which 50% of cells are surviving. The % cell viability for all four concentrations was calculated. Each TIO has four points of reference used to plot a scatter graph to observe the trend in nature as the concentration of the TIO decreases. The general trend suggests that there is an indirect correlation of the concentration of the TIO to the survival of the cells. A line of best fit was inserted to obtain the EC<sub>50</sub> of each gel, observations were made and results were noted. In Figure 3.12, a line of best fit was used to establish the inhibitory concentration by locating the point of intersection whereby 50% viability and the concentration meet on the line.

TIO 1 has the lowest EC<sub>50</sub> of 6.1mg/mL, TIO 2 possesses the highest EC<sub>50</sub> of 7.8mg/mL and TIO 3 possesses an EC<sub>50</sub> of 7mg/mL. This proposes that the use of these TIO's over their derived EC<sub>50</sub> concentrations would eradicate the cells and therefore it is essential to note that at 10mg/mL, all three TIO's are cytotoxic. Concentrations of 5mg/mL, 2.5mg/mL and 1.25mg/mL were employed to expand the study to determine the cell proliferation at an extended period of time in order to assess the gels biocompatibility at all three concentrations. 10mg/mL was not included in cell proliferation studies due to its cytotoxic properties. An interesting fact that can be noted is that the gels containing DMSO contains a higher EC<sub>50</sub> concentration than the TIO containing no DMSO.

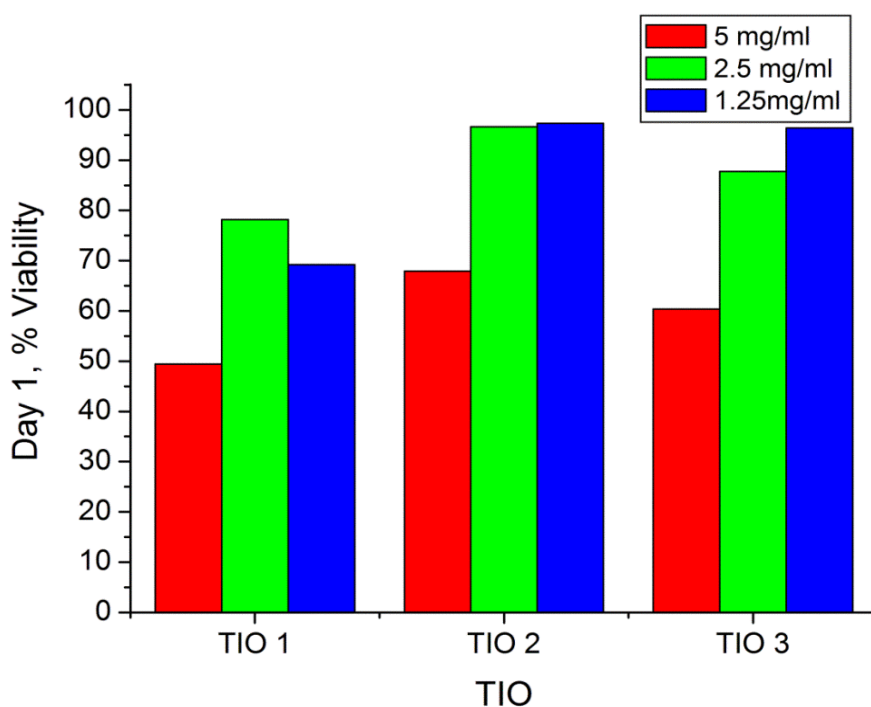


**Figure 3.14** Graph illustrating the % cell viability on day 1 for TIO 1 TIO 2 and TIO 3. Standard deviation <21 in all cases (N=3).

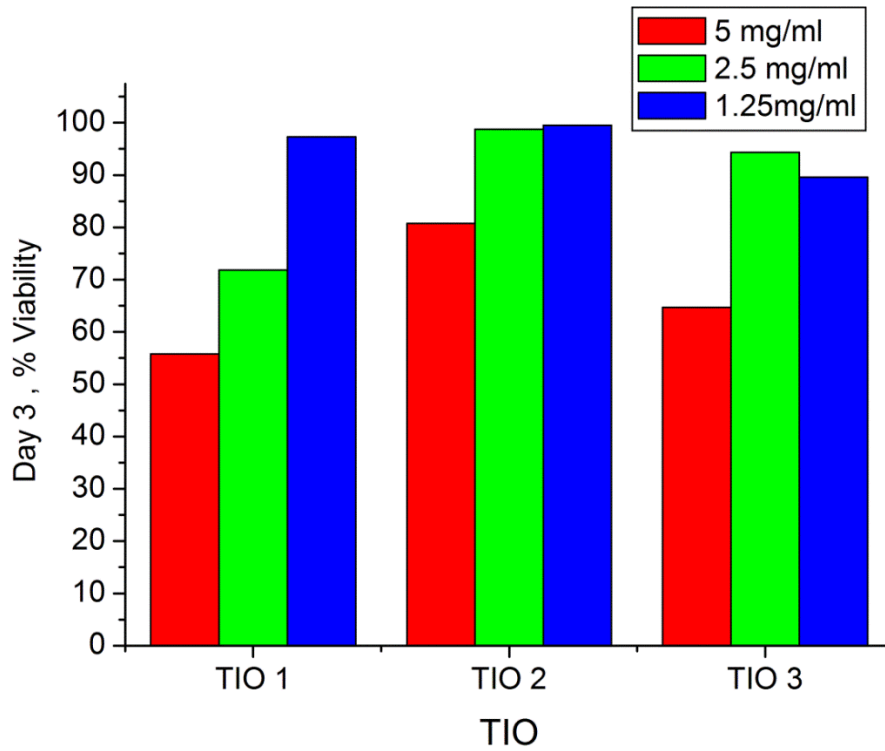


**Figure 3.15** Graph illustrating the % cell viability on day 3 for TIO 1 TIO 2 and TIO 3. Standard deviation <20 in all cases (N=3).

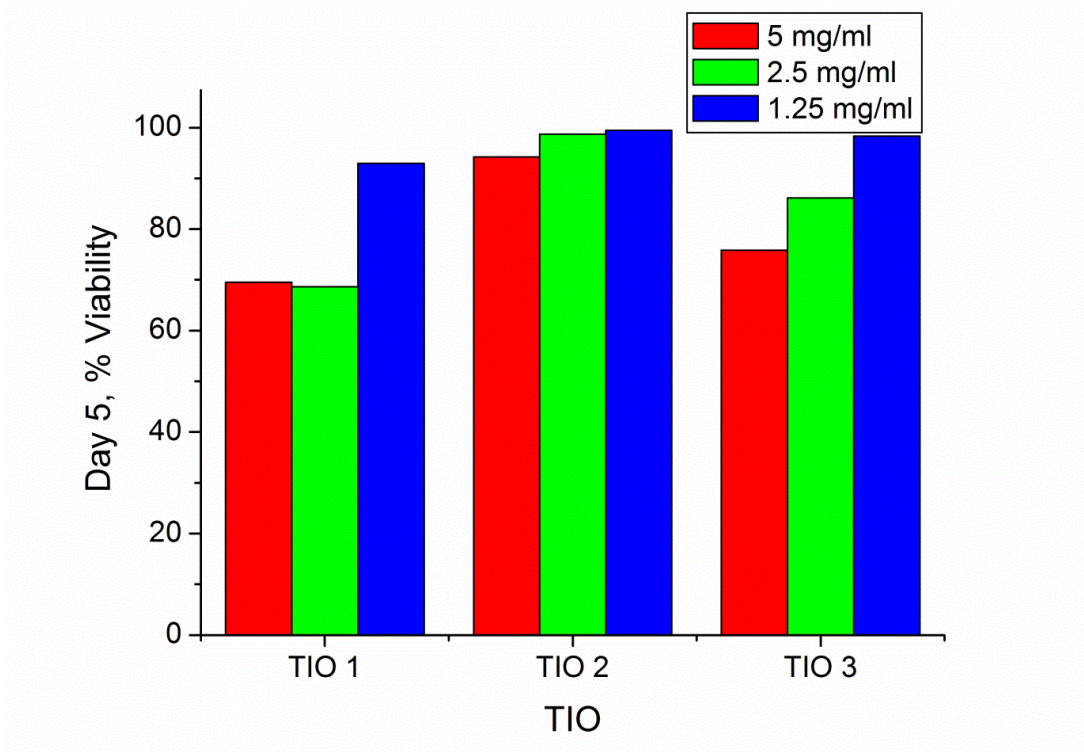


**Figure 3.16** Graph illustrating the % cell viability on day 5 for TIO 1 TIO 2 and TIO 3. Standard deviation <20 in all cases (N=3).

Cell proliferation studies were undertaken over an interval of 5 days. The cell % viability was examined on days 1, 3 and 5. The plate reader was set at 570nm for each read. After each read, the average was taken for all samples including the blank sample also known as the control. The % cell viability was calculated by dividing the average absorbance of the sample by the average absorbance of the control sample multiplied by 100.

$$\% \text{ cell viability} = \text{Absorbance of sample} / \text{Absorbance of control} \times 100 \quad \text{Equation 3.2}$$

The % cell viability was recorded for each day and bar graphs were constructed to present the trends of proliferation at each concentration of each TIO on days 1, 3 and 5. It can be noted that the concentration of the TIO has an indirect proportion to the % viability of the cells. There is an increase in cell proliferation with progression of time, the formulation forms a three-dimensional platform by where the cells can attach and multiply. All % viability results presents itself with a % viability  $50\% \leq$  and increases to  $70\% \pm 1 \leq$ , this suggests that all three TIO's formulations promote cell proliferation and are not cytotoxic within a 5 day interval. The  $EC_{50}$  results can be correlated to the % viability, TIO 2 with the highest  $EC_{50}$  concentration has the highest % cell viability with the progression of the proliferation study. TIO 1 and TIO 3's  $EC_{50}$  concentration can also be correlated to their results of the proliferation study.

### 3.4 Conclusions

Thermosonic Injectable Organogel's (TIO's) was successfully designed via a facile process by incorporating green chemistry principals such as decreasing concentration and exchanging harmful organic substances to less toxic substances. The length of time taken to form the TIO's was directly related to the concentration of crosslinker and is also noted with increasing DMSO concentration. Each TIO had its own degree of responsiveness to heat and ultrasound, primarily tested via an oven and ultrasound bath. All three formulations are readily in gel state and increase gellation as it is exposed to increased heat. TIO 1 has the greatest gelling effect in response to heat in accordance with rheological temp ramp tests as compared to TIO 2 and TIO 3. The TIO'ss proved to be amorphously structured through X-ray diffractive measurements which is augmentative for enhanced drug delivery. Furthermore all three TIO's with a concentration of 5mg/mL presented with proliferative properties towards fibroblast cells over a period of 5 days and can be said to be non toxic with concentrations of  $\geq 5\text{mg/mL}$ .

### 3.6 References

Abbas, K.,2010. The Significance of Glass Transition Temperature in Processing of Selected Fried Food Products: A Review. *Modern Applied Science* (4) 5:3-21.

Bairi, P., Chakraborty, P., Mondal, S., Roy,B., Nandi, A.K.,2014. A thixotropic supramolecular hydrogel of adenine and riboflavin-50-phosphate sodium salt showing enhanced fluorescence properties. *Royal Society of Chemistry. Soft Matter* 10:5114–5120.

Bijukumar, D., Choonara, Y.E., Murugan, K., Choonara, B.F., Kumar, P., du Toit, L.C., Pillay, V.,2015. Design of an Inflammation-Sensitive Polyelectrolyte-Based Topical Drug Delivery System for Arthritis. *AAPS PharmSciTech* 1-11

Carlmark, A., Larsson, E., Malmström,E.,2012. Grafting of cellulose by ring-opening polymerisation – A review. *European Polymer Journal* 48(2012):1646–1659.

Chavda, H.V., Patel,C.N.,2011. Effect of crosslinker concentration on characteristics of superporous hydrogel. *Int J Pharm Investig* 1(1):17–21.

Chejaraa, D.R., Mabrouk, M., Badhea, R.V., Mulla,J.A.S., Kumara,P., Y Choonaraa, Y.E., du Toit, L.C., Pillay, V.,2016. A bio-injectable algin-aminocaproic acid thixogel with tri-stimuli responsiveness. *Carbohydrate Polymers* 135(2016):324–333

Choonara, B.F., Choonara, Y.E., Kumar, P., du Toit, L.C., Tomar, L.K., Tyagi, C., Pillay, V.,2015. A Menthol-Based Solid Dispersion Technique for Enhanced Solubility and Dissolution of Sulfamethoxazole from an Oral Tablet Matrix. *AAPS PharmSciTech* 16(4):72-786.

Dharmesh R.C., Mabrouk, M., Badhea,R.V., Mulla,J.A.S., Pradeep Kumara,P., Choonaraa,Y.E., du Toita, L.C., Pillay,V.,2016. A bio-injectable algin-aminocaproic acid thixogel with tri-stimuli responsiveness. *Carbohydrate Polymers* (135):324–333.

Hibbins, A.R., Choonara, Y.E., Kumar, P., du Toit, L.C., Pillay, V.,2013. Physicomechanical Characterization and Optimization of EDTA–mPEG and Avicel ®–EDTA–mPEGInSitu Melt Dispersion Mini-Pellets. *AAPS PharmSciTech* 14:935-949.

Hoosain, F.G., Choonara, Y.E., Kumar, P., Tomar, L., Tyagi, C., du Toit, L.C. Pillay, V., 2014. An Epichlorohydrin-Crosslinked Semi-Interpenetrating GG-PEO Network as a Xerogel Matrix for Sustained Release of Sulpiride. *AAPS PharmSciTech* 15(5):1293-1305.

Indermun, S., Choonara, Y.E., Kumar, P., du Toit, L.C., Modi, G., Luttge, R., et al. 2014. An interfacially plasticized electro-responsive hydrogel for transdermal electro-activated and modulated (TEAM) drug delivery. *Int J Pharm.* 2014 462:52–65.

Jaikumar, D., K.M, Sajesh., Soumya, S., Nimal, T.R, Chennazhi., K.P., Nair, S.V., Jayakumar, R.,. 2015. Injectable alginate-O-carboxymethyl chitosan/nano fibrin composite hydrogels for adipose tissue engineering. *International Journal of Biological Macromolecules* 74:318–326.

Jung, H.H., Park, K., Han, D.K.,. 2010. Preparation of TGF- $\beta$ 1-conjugated biodegradable pluronic F127 hydrogel and its application with adipose-derived stem cells. 2010. *Journal of Controlled Release* 147(2010):84–91.

Kabiri, K., Omidian, A., Hashemi, S.A., Zohuriaan-Mehr, M.J. Synthesis of fast-swelling superabsorbent hydrogels: effect of crosslinker type and concentration on porosity and absorption rate. *European Polymer Journal* 39 (2003) 1341–1348.

Karande, P., Mitragotri, S.,. 2009. Enhancement of transdermal drug delivery via synergistic action of chemicals. *Biochimica et Biophysica Acta* 1788(2009):2362–2373.

Knipe, J.M., Peppas, N.A.,. 2014. Multi-responsive hydrogels for drug delivery and tissue engineering applications. *Regenerative Biomaterials* 2014:57–65

Lerum, M.F., Chen, W., . 2011. Surface-initiated Ring-opening Metathesis Polymerization in the Vapor Phase: An Efficient Method for Grafting Cyclic Olefins of Low Strain Energies. *langmuir* 3 27(9):5403–5409.

Li, C., Han, Q., Guan, Y., Zhang, Y.,. 2014. Thermal gelation of chitosan in an aqueous alkali–urea solution. *Soft Matter* 10:8245–8253.

Lu, N., Yang, K., Li, J., Weng, Y., Yuan, B., Ma, Y., 2013. Controlled Drug Loading and Release of a Stimuli-Responsive Lipogel Consisting of Poly(N-isopropylacrylamide) Particles and Lipids. *J Phys Chem B*. 117(33):9677-9682.

Mabrouk, M., Mulla, J.A.S., Kumar, P., Chejara, D.R., Badhe, R.V., Choonara, Y.E., du Toit, L.C., Pillay, V., 2015. Intestinal Targeting of Ganciclovir Release Employing a Novel HEC-PAA Blended Lyomatrix. *AAPS PharmSciTech*. 1-11.

Madhu, M., Shaila, L., Anwar, B.J., 2009. Biodegradable injectable implant systems for sustained delivery using poly (lactide-co-glycolide) copolymers. *International Journal of Pharmacy and Pharmaceutical Sciences* 1(1):103-107.

Marren, K., 2011. Dimethyl sulfoxide: an effective penetration enhancer for topical administration of NSAIDs. *Phys Sportsmed*. 2011 39(3):75-82.

Mayet, N., Kumar, P., Choonara, Y.E., Tomar, L.K., Tyagi, C., du Toit, L.C., Pillay, V., 2014. Synthesis of a Semi-Interpenetrating Polymer Network as a Bioactive Curcumin Film. *AAPS PharmSciTech*, 15(6):176-1489.

Nuyken, O., Pask, S.D., 2013. Ring-Opening Polymerization—An Introductory Review. *Polymers* 2013 5:361-403.

Sailakshmi, G., Mitra, T., Gnanamani, A., 2013. Engineering Of chitosan and collagen macromolecules using sebacic acid for clinical applications. *Progress in Biomaterials* 2013 2:11.

Samah, N.H.A., Heard, C.M., 2013. Enhanced in vitro transdermal delivery of caffeine using a temperature- and pH-sensitive nanogel, poly(NIPAM-co-AAc). *International Journal of Pharmaceutics* 453(2013):630– 640.

Scheller, K.J., Williams, S.J., Lawrence, A.J., Jarrott, B., Djouma, E., 2014. An Improved method to prepare an injectable microemulsion of the galanin-receptor 3 Selective antagonist, SNAP 37889, Using Kolliphor 1HS15. *MethodsX* 1(2014):212–216.

Schulte, P.A., McKernan, L.T., Heidel, D.S., Okun, A.H., Dotson, G.S., Lentz, T.J., Geraci, C.L., Heckel, P.E., Branche, C.M., 2013. Occupational safety and health, green

chemistry, and sustainability: a review of areas of convergence. *Environmental Health* 2013 12:31

Shikanov, A., Domb, A.J., 2005. Poly(sebacic acid-co-ricinoleic acid) Biodegradable Injectable in Situ Gelling Polymer. *Biomacromolecules*, 2006 7 (1):288–296.

Silvaa, C.S.O., Lansalotb, M., Garciaa, J.Q., M. Taipaa, A., Martinho, J.M.G., 2013. Synthesis and characterization of biomimetic nanogels for immunorecognition. *Colloids and Surfaces B: Biointerfaces* 112 (2013):264–271.

Singh, N., Lyon.L.A., 2008. Synthesis of Multifunctional Nanogels Using a Protected Macromonomer Approach. *Colloid Polymer Science* 286(8-9):1061–1069.

Tejaa, S.B., Patila, S.P. Shetea, G., Patelb, S., Arvind Kumar Bansal, A.K., 2013. Drug-excipient behavior in polymeric amorphous solid dispersions. *Journal of excipients and food chemicals* 4(3):70-94.

Tierneya, C.M., Haugh, M.G., Liedla, J., Mulcahya, F., Hayesa, B., O'Brien, F.J., 2009. The effects of collagen concentration and crosslink density on the biological, structural and mechanical properties of collagen-GAG scaffolds for bone tissue engineering. *Second International Conference on the Mechanics of Biomaterials and Tissues* 2(2):202-209.

Thoing, C., Pfeifer, A., Kakorin, S., Tilman Kottke, T., 2013. Protonated Triplet-Excited Flavin Resolved by Step-Scan FTIR Spectroscopy: Implications for Photosensory LOV Domains. *Phys. Chem. Chem. Phys.*, 2013 15:5916-5926.

Tong, R., Wang, L., Yu, H., Zain-ul-Abdin., Khalid, H., Akram, A., Chen, Y., 2015. Redox and Temperature Dual Responsive Gel Based on Host–Guest Assembly. *J Inorg Organomet Polym* 25:1053–1059.

Touito, E., Williams, A.C., Barry, B.W., 2011. Enhancement in drug delivery. 12 chemical permeation in drug delivery 233-251.

Wang, Y., Tu, S., Pinchuk, A.N., Xiong, M.P., 2013. Active drug encapsulation and release kinetics from hydrogel-in-liposome nanoparticles. *Journal Of Colloid And Interface Science* 406(2013):247–255.

Xiao, L., Wang, B., Yang, G., Gauthier, M., 2012. Poly(Lactic Acid)-Based Biomaterials: Synthesis, Modification and Applications. *Biomedical Science, Engineering and Technology*. 11:248-282.

Xue, Y., Wang, L., Shao, Y., Yan, J., Chen, X., Lei, B., . 2014. Facile and green fabrication of biomimetic gelatin–siloxane hybrid hydrogel with highly elastic properties for biomedical applications. 2014. *Chemical Engineering Journal* 251(2014):158–164.

Yan, L., Li, G., Ye, Z., Tian, F., Zhang, S., . 2014. Dual-responsive two-component supramolecular gels for self-healing materials and oil spill recovery†. *The Royal Society of Chemistry. Chem. Commun., 2014*, 50(1):4839-4842.

Zhang, L., Wang, L., Guo, B., Ma, P.X., 2014. Cytocompatible injectable carboxymethylchitosan/N-isopropylacrylamide hydrogels for localized drug delivery. *Carbohydrate Polymers* 103(2014):110-118.

Zhang, W., Cue, B.W., 2012. Green Techniques for Organic Synthesis and Medicinal Chemistry. *Wiley* 23:612-630.

Zhang, X., Lin, Y., Gillies, R.J., 2010. Tumor pH and Its Measurement. *The Journal of Nuclear Medicine* 51(8):1167-1170.

Zhao, L., Xiao, C., Ding, J., He, P., Tang, Z., Pang, X., Zhuang, X., Chen, X., . 2013. Facile one-pot synthesis of glucose-sensitive nanogel via thiol-ene click chemistry for self-regulated drug delivery. *Acta Biomaterialia* 9(2013):6535–6543.



## CHAPTER 4

### SYNTHESIS, CHARACTERIZATION AND ASSEMBLY OF SOLID LIPID NANOSPHERES INTO THE THERMOSONIC INJECTABLE ORGANOGELS (TINO's)

---

---

#### 4.1 Introduction

The establishment of nanotechnology has transformed the depth of medicine and participated in the essential revolution of oncology advancement (Coccia & Wang, 2015). Branching into drug delivery nanotechnology continues to progress in efficient therapy and exist in various structures such as nanoparticles, micelles, liposomes etc (Safari & Zarnegar, 2014; Yuan *et al.* 2015). Nanoparticles can constitute biodegradable or non-biodegradable polymers. It does not need to be polymer based but requires at least 1 submicronic dimension and therefore must be  $<1\mu\text{m}$  (Safari & Zarnegar, 2014; Brigger, Dubernet & Couvreur, 2012). Despite 5-Flourouracil being known as an adjunct drug to cervical cancer therapy recent research has shown that this drug applied topically serves as efficient medical therapy for women who are diagnosed with cervical intraepithelial neoplasia 2 (CIN II) (Mountzious *et al.* 2013; Rahangdale *et al.* 2014). Local chemotherapy is known to be very effective and decreases the chances of tumour recurrences and may increase the extent to which the drug penetrates through the tumour tissue (Wolinsky, Colson & Grinstaff, 2012). 5-Fluorouracil is a broad spectrum antineoplastic agent and has been incorporated into lipid nanostructures due to its excellent properties of lipid to enhance drug loading and controlled release (Andalib, 2012).

Solid lipid nanoparticles (SLN's) has reported to have increased in popularity due to its capability to site-specific drug delivery and decreased both, short and long term toxicity (Kakadia & Conway, 2014). SLN's have proved to be efficient in the prevention of chemoresistance, could be employed as a vehicle in chemotherapeutic delivery and has an advantage in cancers which are chemotherapy resistant (Kang *et al.* 2010). SLN's have proven dominance over other colloidal systems in many ways as they are capable of surface modification and are small in size but have a large surface area (Patel *et al.* 2014). There are two noteworthy advantages that SLN's offer, one of which is during the process of formulating the SLN's; due to an augmented drug encapsulating capacity, the process of drug loading less activity i.e. dispersing the drug within the nanoparticle solution. The other advantage surfaces during drug release whereby desirable outcomes of the drug are enhanced and this can be accounted for by its manufacturing process (Dolatabadi *et al.* 2015). A superior structural stability profile exists in SLN's owing to arrangement of the lipophilic core and the singular phospholipid layer bordering the nanoparticle (Thakor & Gambhir, 2013).

In most cases the drug release from SLN's is biphasic which includes an initial burst and thereafter a controlled release of drug (Kumar & Sawant, 2013). SLN's is known to have a rapid clearance from the body, incorporating these SLN's into a vehicle such as a gel to sustain the release of nanoparticles for a longer period of time has been proven positive (Dorraj & Moghimi, 2015). The structure of the polymer used in the gel determines the behaviour of the SLN:gel system and is also worth noting that elastic properties present itself with the addition of solid lipid material and that SLN:gel formulations possess a prominent prolonged release in comparison to SLN's alone (Bhaskar *et al.* 2009).

Ultrasound is an influential approach in drug delivery through its ability of surmounting the physiological challenges faced in effective drug delivery such as high molecular weight, poor solubility etc (Patel *et al.* 2014). Ultrasonic energy is used as therapeutic means within many medical conditions including tumoural ablation. Ultrasound mediated therapy has shown to increase the safety and efficacy of chemotherapeutic drug delivery through cavitation and drug diffusion into tumoural tissue (Miller *et al.* 2012; Rapoport *et al.* 2013). The use of ultrasound assists and augments the drug release leading to higher release profiles into the desired tissue, promoting focused therapy. This is due to the combination thermal and mechanical properties that ultrasound possesses, drug delivery can be achieved without microbubbles, this is possible through vapourization of gas-precursors (Couture *et al.* 2014).

This paper focuses on a recent method in the formation of Solid Lipid Nanospheres (SLN's) through physical mixing of the formulation that is fed through the nanospray dryer and the incorporation of the SLN's into Thermosonic Injectable Organogels (TIO's) to form Thermosonic Injectable Nano-Organogels (TINO's) . The physical analysis of SLN's and the SLN:TIO (TINO's) system were undertaken including drug release profiles of 5-fluorouracil from the TINO at different ratios of SLN to TIO formulation.

## **4.2 Materials and Methods**

### 4.2.1 Materials

Poly-L- Lactic Acid (PLA) , Palmitic Acid (PA), Poly Vinyl Alcohol (PVA), Dichloromethane (DCM), Methanol, 5-Fluoro Uracil (5-FU). Sigma–Aldrich®Inc. (St. Louis, MO, USA).

### 4.2.2 Preparation of the SLN's

#### *1:1 and 2:1 SLN's with Drug*

Two concentrations of SLN's PA:PLA were prepared 1:1 and 2:1. PA (25mg) and PLA (25mg) were weighed and simultaneously dissolved in 10mL of DCM. 5-FU (25mg) was

weighed out and dissolved in 2mL of methanol with mild heat. Once the 5-FU was dissolved, it was added to the stirring PA:PLA polymer solution. At the same time, 1g of PVA was measured and dissolved in 100mL of distilled water with mild heating until completely dissolved to form a 1% PVA solution. Once dissolved, the PVA solution was allowed to cool down while covered to prevent precipitation. The PA:PLA solution was then added to the 1% PVA solution during rapid stirring through a thin stream technique and allowed to stir until minimal precipitation was achieved in order to coat these SLN's. Thereafter the mixture was filtered with a 0.8 $\mu$ m pore, 50mm filter paper and collected in a cylinder. The resultant solution was then fed through the Nanospray dryer using a 5 $\mu$ m nozzle. The settings of the Nanospray dryer were set at the following. Gas flow = 112L/min, Inlet Temperature = 50°C, Outlet temperature = 36°C, Head temperature = 63°C, spray = 85%, Pressure = 34mBar and the pump = 2. These settings were applied to both concentrations, feeding it through the Nanospray dryer resulted in an off white powder which was obtained from the collecting chamber of the Nanospray dryer. The powder was collected for both concentrations and analytical tests were performed. The best ratio concentration SLN's were chosen by size, morphology and drug entrapment.

#### **4.2.3 Incorporation of SLN's into Thermosonic Injectable Organogels (TIO's)**

The incorporation of the SLN's was prepared by direct addition of the spheres into the formulation. Three TIO formulations were used and three concentrations of SLN's to TIO; 1:5, 2:5, 3:5 thus 9 samples of the combined system was prepared. The SLN's were dispersed within the original TIO formulation via mechanical stirring of the mixture until dispersion occurred before initiating the open ring reaction of the gel. The mixture was then reacted in a sealed vessel under N<sub>2</sub> atmosphere kept at a 50°C temperature to form a Thermosonic Injectable Nano-Organogel (TINO)

#### **4.2.4 Probing the Molecular Status of the SLN's**

Fourier Transform Infrared spectroscopy was undertaken on the individual polymers and the newly formed compounds to detect any newly arranged bonds or status changes from the individual polymers. This status was established by using the Perkin Elmer Spectrum 2000, Llantrisant, Wales, UK fitted with a universal ATR polarization accessory (Perkin Elmer Ltd., Beaconsfield, UK) which possesses a 4cm<sup>-1</sup> resolution. The cone shaped probe was attached for the reading of all samples. All readings were set at 10 scans to which the average was determined and presented and the force gauge was set at a psi of 120. All readings were scanned in the range of 4000cm<sup>-1</sup> to 600cm<sup>-1</sup> and were analysed and recorded.

#### **4.2.5 Analysis of the Thermal Behaviour of the SLN's**

The analyses of thermal activity of the SLNs were performed through the employment of the Mettler-Toledo, DSC1 STAR<sup>e</sup> system, Switzerland differential scanning calorimeter to observe the thermal processes through increasing temperature and attain the activity that the SLN's possess. The individual and compound polymers were weighed into the appropriate aluminium crucible pans which were sealed with pinhole crucible lids, approximately 10mg and 5mg respectively. The powder filled, sealed crucibles were positioned and calibrated individually according to their weights and had undergone a temperature rate increase of 10°C/min with a temperature range of 20°C-500°C under a constant N<sub>2</sub> atmosphere. Final outcomes of the possessed thermal activity by each powder were presented by thermograms produced by the differential scanning calorimeter. The alteration in thermal activity points that were notified signified modification of the parent polymers.

#### **4.2.6 Determination of the Molecular Phase Classification of the SLN's**

The molecular arrangement of the parent polymers and the SLN complex compounds were determined using the Rigaku Benchtop X-Ray Diffractometer MiniFlex600 (Rigaku Corporation, Tokyo, Japan) incorporated with a high intensity D/tex ultra high speed 1D detector, a 600 W x-ray generator and a counter monochromator which cuts X-rays with the exception of Cu K $\alpha$  X-rays. The XRD graphs of each material generated by the X-Ray diffractor was analysed and the phase of each parent polymer and SLN compound complex was determined and correlated to the intensity of the peaks presented in the DSC thermograms.

#### **4.2.7 Investigation of the Structural Morphology of the SLN's**

The structural morphology of the SLN's were analysed and confirmed using the CARL ZEISS SIGMA Field Emission SEM equipped with oxford x-act EDS detector-England. The samples were prepared by attaching a double sided carbon tape to stub holders and lightly applying SLN powder samples across the surface area of the free side. These samples were then coated with palladium-gold and loaded into the SEM to be analysed.

#### **4.2.8 Drug Entrapment Efficient Analysis within the SLN's**

The wavenumber of the drug was set in the UV and a series of dilutions of the drug in PBS were prepared. The dilutions were transferred to quartz cuvettes and scanned by the UV spectroscopy. A calibration curve was constructed from the UV results obtained from the UV. Drug loaded spheres 1:1 and 2:1 was dissolved in methanol with heat and scanned at 5-

FU's wavenumber and the UV results were recorded. The drug entrapment was calculated from the UV results that were obtained.

#### **4.2.9 Determination of the Size and the Zeta Potential of the SLN's**

The size of the spheres were analysed using the Zeta Sizer Nano-2s, nanoseries, Malvern instruments equipped with a MPT-2 multipurpose tirtrater Malvern Innstruments, This system works via dynamic light scattering to determine the size of submicron particles between 0.3 - 10 microns with a sensitivity of 0.1mg/mL. A small amount of approximately 2mg was diluted in 5mL of distilled water and ultrasonicated with the ultrasonicator Vibracell for 30 seconds to disperse the spheres in the water. The resultant dispersion for each sample was then filtered into plastic disposable cuvettes which were then inserted to analyse the size of the sphere and give a PDI for the spheres. On average 30 scans were taken before the graphs were produced. Samples from the stock dilutions used for zeta sizing were used for zeta potential which was loaded carefully into a folded capillary cell by means of a syringe. The air bubbles were removed from the folded capillary cell which contained electrodes that allow the measurement for zeta potential.

#### **4.2.10 Evaluation of Erosive and Swelling Dynamics of the SLN's Incorporated into the Thermosonic Injectable Organogel (TINO's)**

Degradation trials were undertaken with the TINO's. A total of 12 samples were prepared and its initial weights were recorded. The samples were suspended in acetate buffer pH 4.3 BP 100mL jars and placed in a shaker bath at 50 rpm at 37°C. The weights of these samples were recorded at day 1, day 3 and day 7. At each recording the additional residue was cleared off the sample before it was weighed. Graphs were constructed according to the results to understand the swelling and erosive behaviour.

#### **4.2.11 Drug release studies from the SLN's and the TINO's**

A total of 20 samples two groups of 10 were prepared for the dissolution. The first group was thermal tested. The second group was thermal and ultrasound exposed. Each group contained the 9 samples with TINO's and a control consisting of the SLN's only. The samples were sealed in dialysis tubing and suspended in acetate phosphate buffer solution (100mL jars) and placed in the shaker bath at 25 rpm, 37°C. At each interval, a withdrawal of 5 mL of acetate buffer saline from each jar sample. The second group of samples were exposed to ultrasound before the sample was withdrawn. The withdrawn sample was replenished with fresh acetate buffer saline. The samples were scanned through the UV and the UV results were used to calculate the drug release at each interval for both groups. Drug

release profiles were constructed from the results calculated and the pattern of drug release were studied.

### 4.3 Results and Discussion

#### 4.3.1 Assessment of SLN's Molecular Status

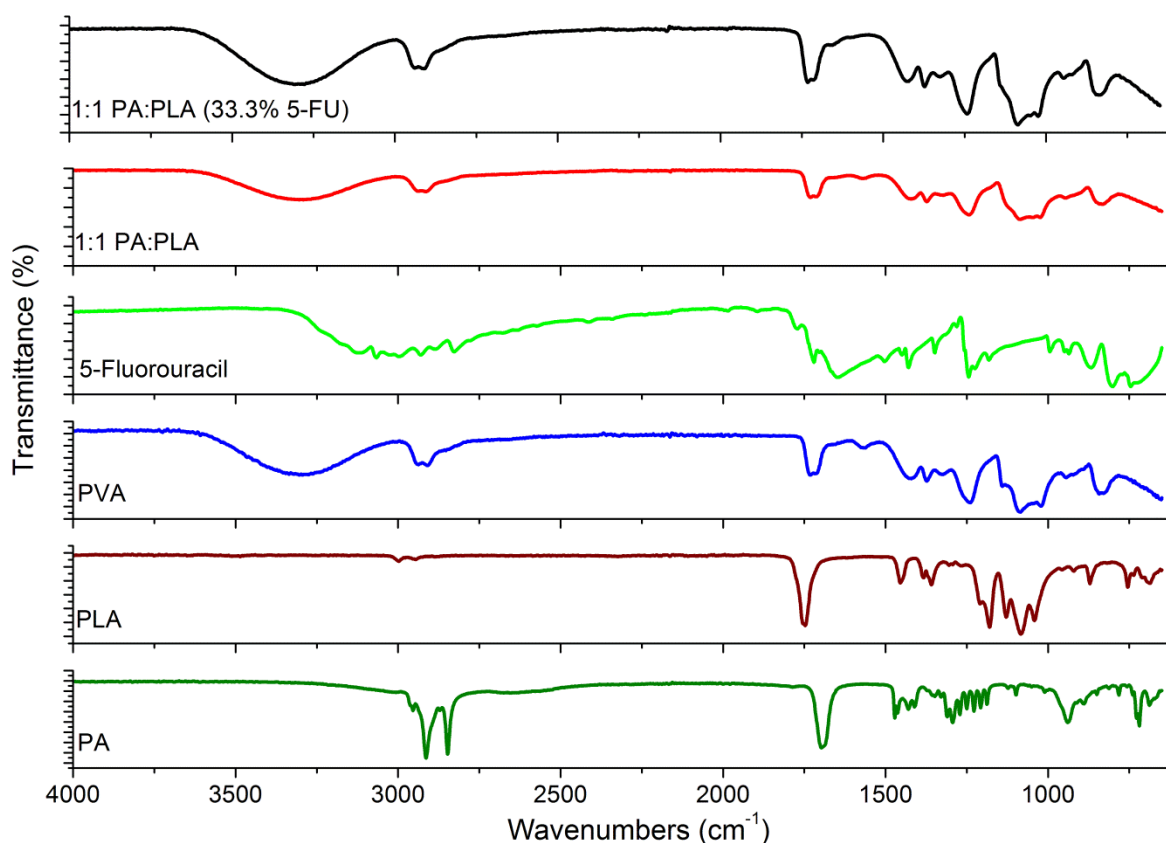


**Figure 4.1** Graph illustrating the surface molecular status of 1:1 PA:PLA plain and 1:1 PA:PLA drug encapsulated

Infra-red spectroscopy was undertaken for the pure materials and the SLN; plain and encapsulated with drug (5-Fluorouracil) to determine the molecular status of the SLN's. Analysing Figure 4.1, palmitic acid (PA) contains C-H stretch bands that occur between 2937cm<sup>-1</sup> and 2940cm<sup>-1</sup> (Garland *et al.* 2005), furthermore a prominent band at 1695cm<sup>-1</sup> COOH confirming the presence of the carboxylic acid functional group in PA. Poly-l-lactic acid (PLA) comprises of various prominent peaks, one of which 1 peak is very decisive 1752cm<sup>-1</sup> C=O carbonyl group that represents the strong ester backbone of PLA (Xu *et al.* 2011), other peaks 1085cm<sup>-1</sup> and 1182cm<sup>-1</sup> also suggests C-O ester groups. Poly vinyl alcohol was used to coat the SLN's, hence a higher concentration of PVA was used in formulating the SLN's. Analysing the IR spectra for PVA in Figure (4.1and 4.2), a broad band

can be noted between  $3027\text{-}3614\text{cm}^{-1}$  which proposes hydrogen bonded alcohols (OH). A C-H stretch band can be noted at  $2942\text{cm}^{-1}$  and further down the spectrum a strong carbonyl band presents itself as it peaks at  $1729\text{cm}^{-1}$ . Additionally, a small intensity peak at  $1376\text{cm}^{-1}$  and a larger, more visible band at  $840\text{cm}^{-1}$  can be observed these bands are reported to be C-H wagging and C-H rocking bands respectively (Ahad, 2012).

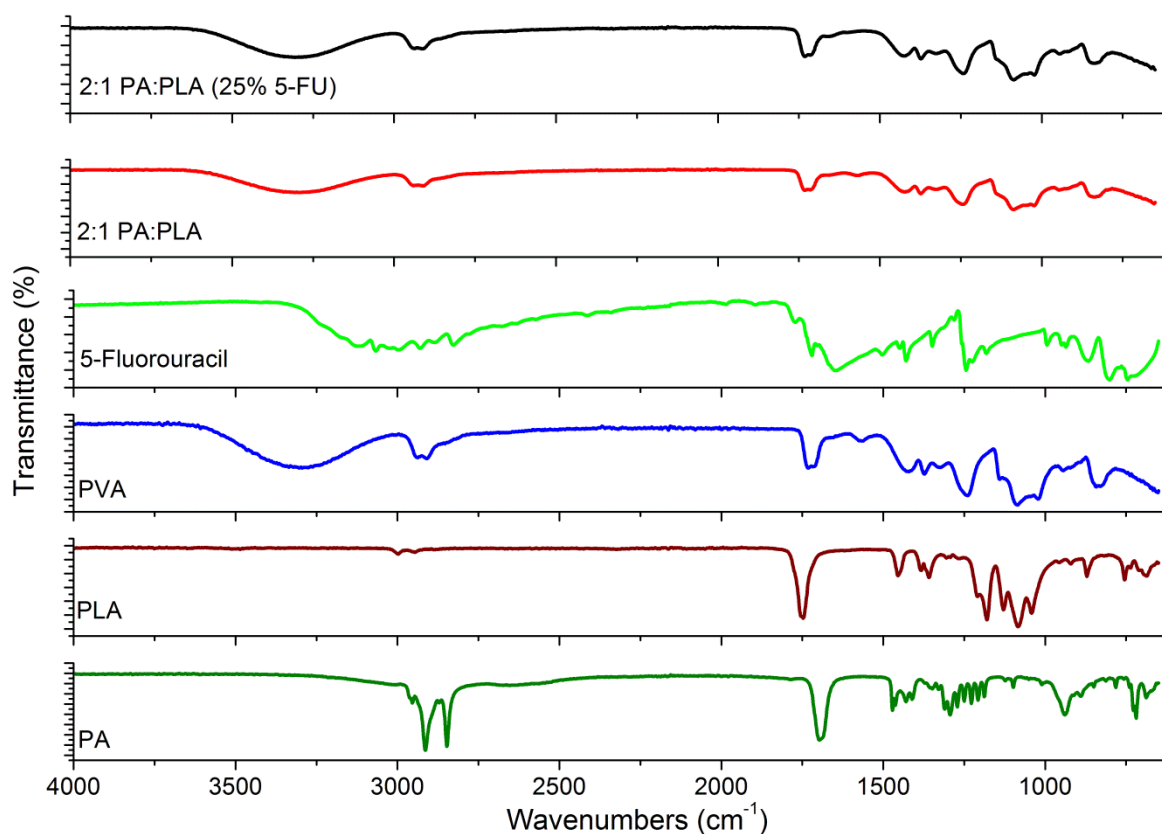


**Figure 4.2** Graph illustrating the surface molecular status of 2:1 PA:PLA (plain) and 2:1 PA:PLA (drug encapsulated)

A broad band can be seen between  $2750\text{cm}^{-1}$  and  $3250\text{cm}^{-1}$ , this confirms the presence of the amine as stretching bands around  $3000\text{-}3500\text{cm}^{-1}$  are usually attributed to the  $\nu\text{NH}$  stretching vibrations in the spectrum of 5-Fluorouracil. A band at  $1250\text{cm}^{-1}$  indicates a CF stretch band that represents a carbon-flouride bond in 5-FU (Olukman, Sanli & Solak, 2012). When analysing the IR spectra of the SLN's in both Figure 1. and 2. , it can be noted that the spectrum is almost identical to that of PVA with the exception of the intensity of the peaks, substantiating that PVA coated the SLN's.

#### 4.3.2 Analysis of the Thermal beaviour of the SLN's

Differential scanning calirometry was performed on the pure polymers and the SLN's, the thermal behaviour of all of these compounds was determined by the thermographs produced

by the DSC instrument. In figure 4.3 PA has a melting point of 68.59°C falling within a similar range reported by Latibari *et al.* (2014) thereafter no thermal activity can be seen until a visible exothermic peak is produced this could represent the oxidative degradation. When observing PLA, the first activity can be noted at approximately 184.89°C and soon after at 190.25°C which signifies the glass transition of PLA. At 358.86°C a broad exothermic peak which could possibly represent the melting point of PLA and that PLA is amorphous in nature can be observed. PVA undergoes glass transition at 57.04°C and crystallization at 276.32°C before presenting a broad exothermic peak signifying its melting point at 323.39°C.

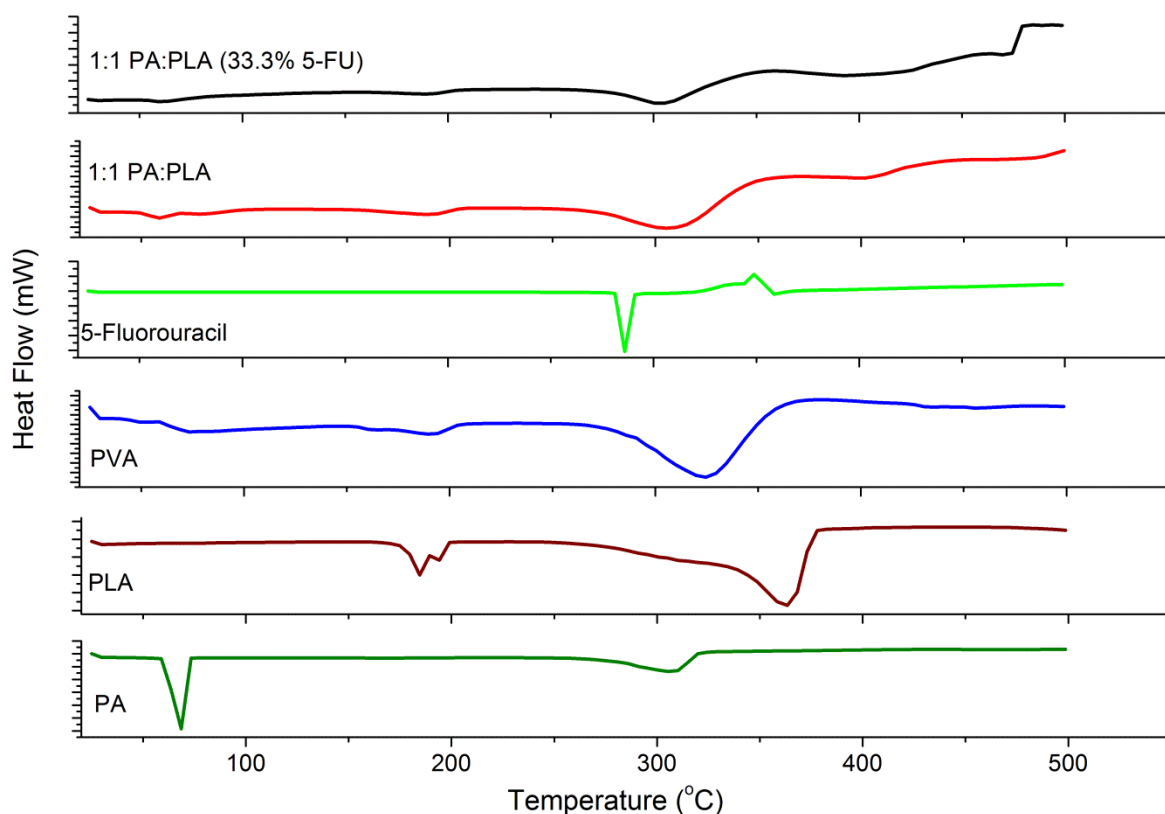


**Figure 4.3** Graph illustrating the thermal behaviour for 1:1 PA:PLA (plain) and 1:1 PA:PLA (drug encapsulated).

When analysing 5-Fluorouracil, a sharp peak can be noted at 278.09°C which is the melting point for 5-Fluorouracil (Olukman *et al.* 2012). At approximately 349.14°C 5-FU undergoes a process known as cold crystallization. When analysing the SLN's a very similar thermal activity to plain PVA can be seen, this could be due to the higher concentration that is used to coat the SLN's. The thermograms representing the SLN's show a lower melting point than pure PVA. With regards to the thermal activities of the SLN's, it can be noted that the drug encapsulated formulation has a slightly lower melting point and less intense peak than the formulation with no drug. Furthermore, the encapsulated SLN's expresses thermal activity at



472.45°C and 479.64°C for 1:1 PA:PLA (25% 5-FU) and 2:1 PA:PLA (33.3% 5-FU) respectively.

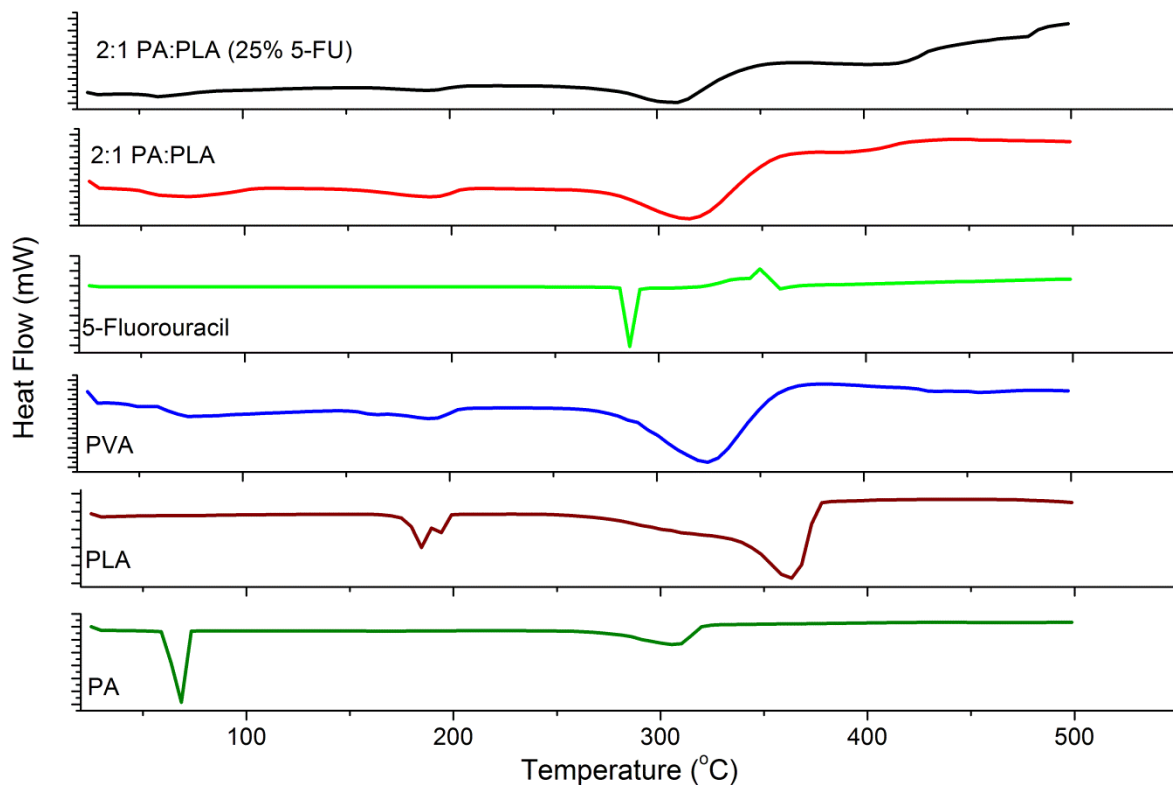


**Figure 4.4** Graph illustrating the thermal behaviour for 2:1 PA:PLA (plain) and 2:1 PA:PLA (drug encapsulated).

#### 4.3.3 Classification of the Molecular Phase of the SLN's

The molecular phase classification was determined by the graphs provided by the XRD instrument and the molecular phase of each polymer was resolved by the results obtained and confirmed by comparing the results of the XRD to that of the DSC. Studying the XRD graphs from Figure 4.5 and 4.6, PA has three peaks, the first peak occurs at 2.42° with an intensity of 3809.80a.u. The second peak presents a sharp more intense peak of 9824.67a.u. at 21.74° and another occurs at 24.62° with an intensity of 1997.55a.u, with the position reported by Latibari *et al.* (2014). These sharp intense peaks suggest that PA has a crystalline lattice structure, when comparing the peaks of PA for the DSC and XRD, a correlation of the sharp intense peaks can be noted. PLA possesses a broad peak that occurs at 16.99° with a low intensity of 56.06a.u proposing an amorphous molecular structure that can be confirmed by the broad peak present in the DSC thermogram of PLA. A broad peak occurs at 19° with a low intensity of 45.63a.u. for PVA which indicates that PVA an amorphous molecular arrangement and be confirmed by the presence of the broad peak in

the thermogram of PVA (Manjunath *et al.* 2015). Evaluating the XRD graph for 5-Fluorouracil a very sharp intense peak of 1086.79a.u. at 28° is observed, indicating the crystallinity of the drug and can also be confirmed by the sharp intense peaks of the thermogram of 5-Fluorouracil (Nair, Jaqadeeshan & Kumar, 2011).

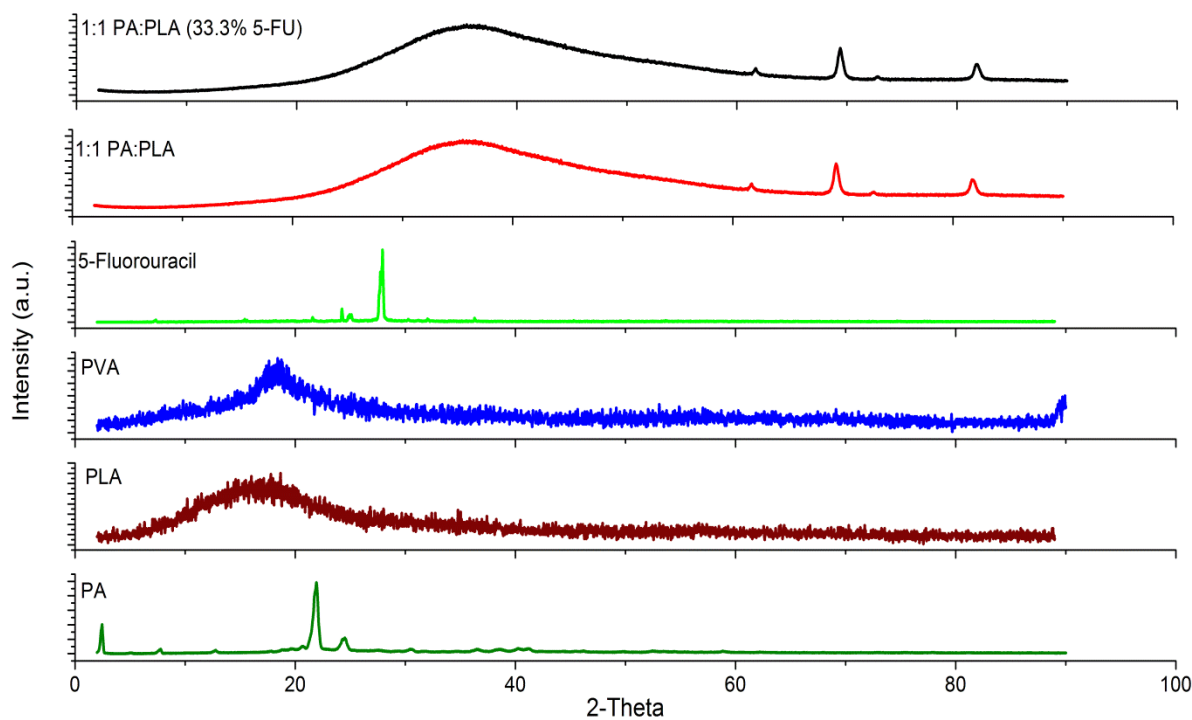


**Figure 4.5** Molecular phase classification of 1:1 PA:PLA (plain) and 1:1 PA:PLA (drug encapsulated).

An interesting observation can be noted when analysing the XRD graphs for the SLN formulations. As seen in Figure 5. there is a broad intense peak of 5562.86a.u. at 35.63°. for the plain SLN's and an intensity peak of 5493.78a.u. at 35.29°, furthermore sharp peaks are present 69.36° and 81.73° which indicates that this formulation could be semi crystalline. In Figure 6. It can be noted that the SLN's XRD graphs presents with a broad band at a low intensity of 61.35a.u at 17.67° and 58.89a.u at 18.35° for the encapsulated SLN's and the plain SLN's respectively. The broad band confirms the amorphous nature for the SLN's of this ratio.

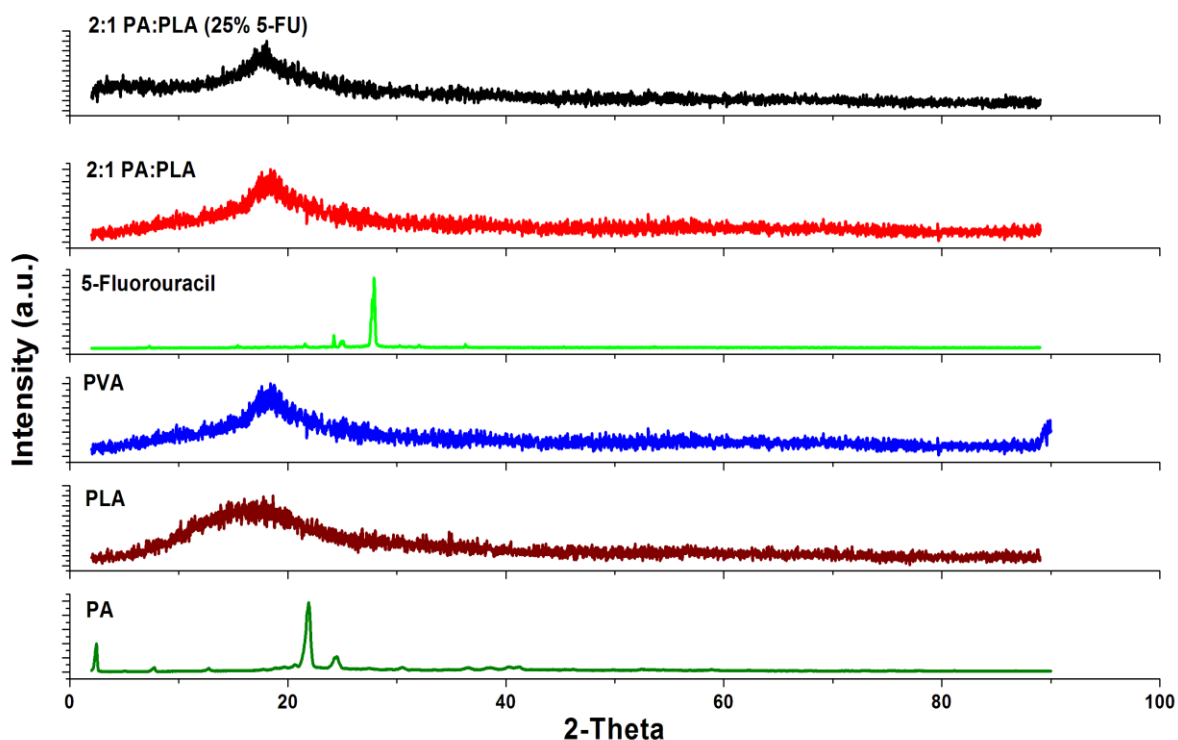


**Figure 4.6** Molecular phase classification of 2:1 PA:PLA (plain) and 2:1 PA:PLA (drug encapsulated).

#### 4.3.4 Elucidation of the Structural Morphology of the SLN's

The morphology, shape and the size range of the particles were determined by the CARL ZEISS SIGMA Field Emmission SEM equipped with oxford x-act EDS detector-England. The images in Figure 4.7, depicts the two formulations i.e. 1:1PA:PLA and 2:1PA:PLA with and without drug loading. Analysing the shape of the particles it can be confirmed that these are spherical in shape and by a greater percentage nanoscale spheres. The morphology of the spheres can be described as smooth surfaced spheres which possess contours. The scanning electron microscope used to capture these images, was used to demarcate (Da x) and measure (nm) spherical dimensions. In Figure 4.7a) two SLN's can be seen Da1=279.2nm and Da2=509.1nm among others, from these it can be seen that there is more than one size range. With an increase in surfactant such as tween or span the particle size can be decreased and controlled (Shi *et al.* 2011). In comparison to a) containing drug, it can be noted in image b) that smaller particles are present b) Da2=181.6nm. The increased sized spheres could be due to the encapsulation of drug. Abbaspour et al. (2013) reports that particle size increases when ionic complexed chemotherapeutic drugs are encapsulated in the SLN's and the amount of polymer. When analysing image c) a clear difference in the size range can be seen in comparison to a), SLN's measured possess sizes of Da1=666.3nm and Da2=450.7nm. This may indicate an increase in polymer concentration

promotes an increase in the size of the SLN's formed. The average sizes of the SLN's annotated and visible in image d) i.e. Da1=450.9nm and Da2=545.3nm depicts smaller size SLN's in relation to the visible size range seen in image c).

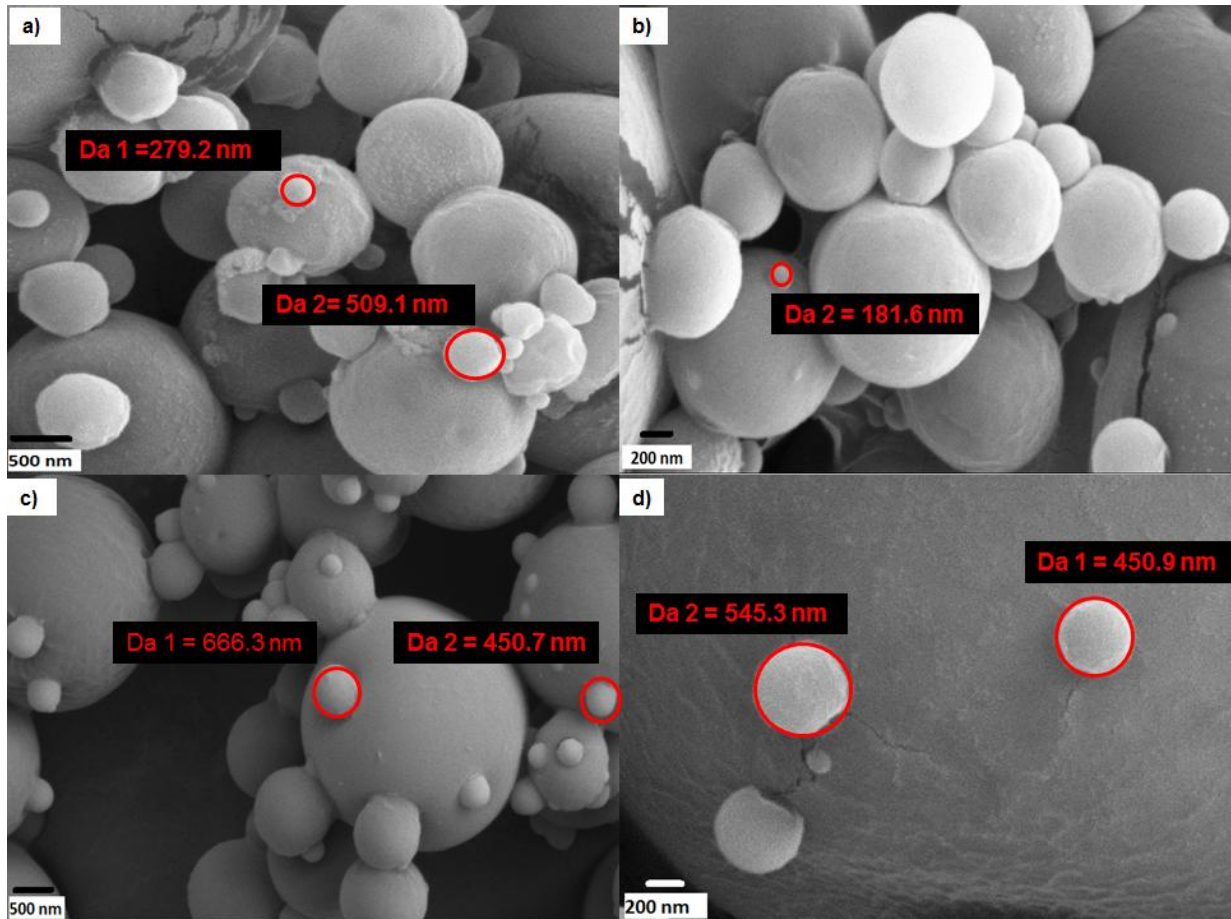


**Figure 4.7** Scanning electron microscope images for a) 1:1 PA:PLA (drug encapsulated), b) 1:1 PA:PLA (plain), c) 2:1 PA:PLA (drug encapsulated), d) 2:1 PA:PLA (plain).

#### 4.3.5 Drug Loading and Encapsulated Efficiency within the SLN's

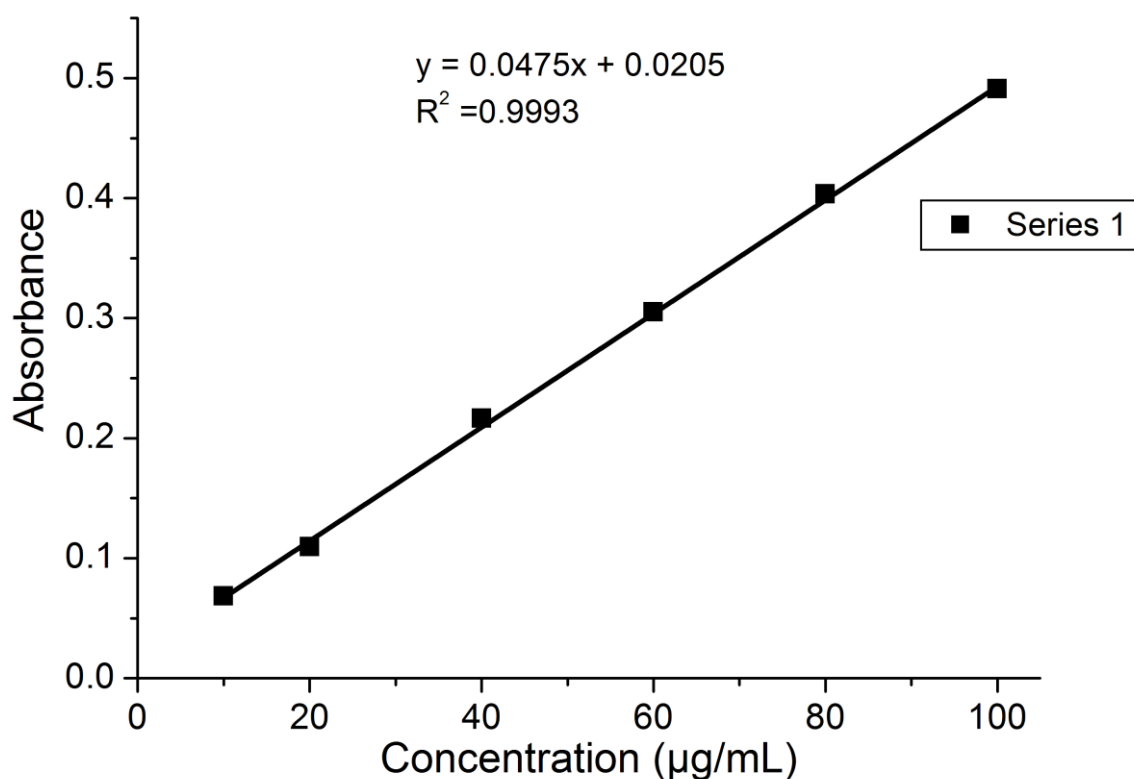


**Figure 4.8** A calibration curve for 5-FU in methanol.

The percentage drug loading (DL) for each formulation was calculated with the following equation (Maji & Dey, 2014):

$$\% \text{ DL} = \text{Weight of the drug in the formulation} / \text{Weight of total formulation} \times 100$$

Equation 4.1

The drug loading of the two formulations were determined and the % drug load for 1:1 PA:PLA and 2:1 PA:PLA were 33% and 25% respectively. The drug entrapment efficiency of 1:1 PA:PLA and 2:1 PA:PLA was calculated after dissolving 10mg of each formulation by mechanical stirring at rapid speed in methanol under heat ( $\pm 40^{\circ}\text{C}$ ). The concentrations of the two formulations were 17.49mg and 8.53mg. The following equation was used to calculate the encapsulated drug (ED) efficiency (Awotwe-Otoo *et al*, 2012):

$$\% \text{ ED} = \text{Actual drug loaded} / \text{Theoretical drug Loaded} \times 100$$

Equation 4.2

Once dissolved, the samples were transferred to a cuvette for UV spectroscopy. The calibration curve above was used to obtain the drug entrapment for these two formulations. The drug efficiencies of 1:1 PA:PLA and 2:1 PA:PLA is 58.29% and 34.11% respectively.

#### 4.3.6 Determination of the Size and Zeta Potential of the SLN's

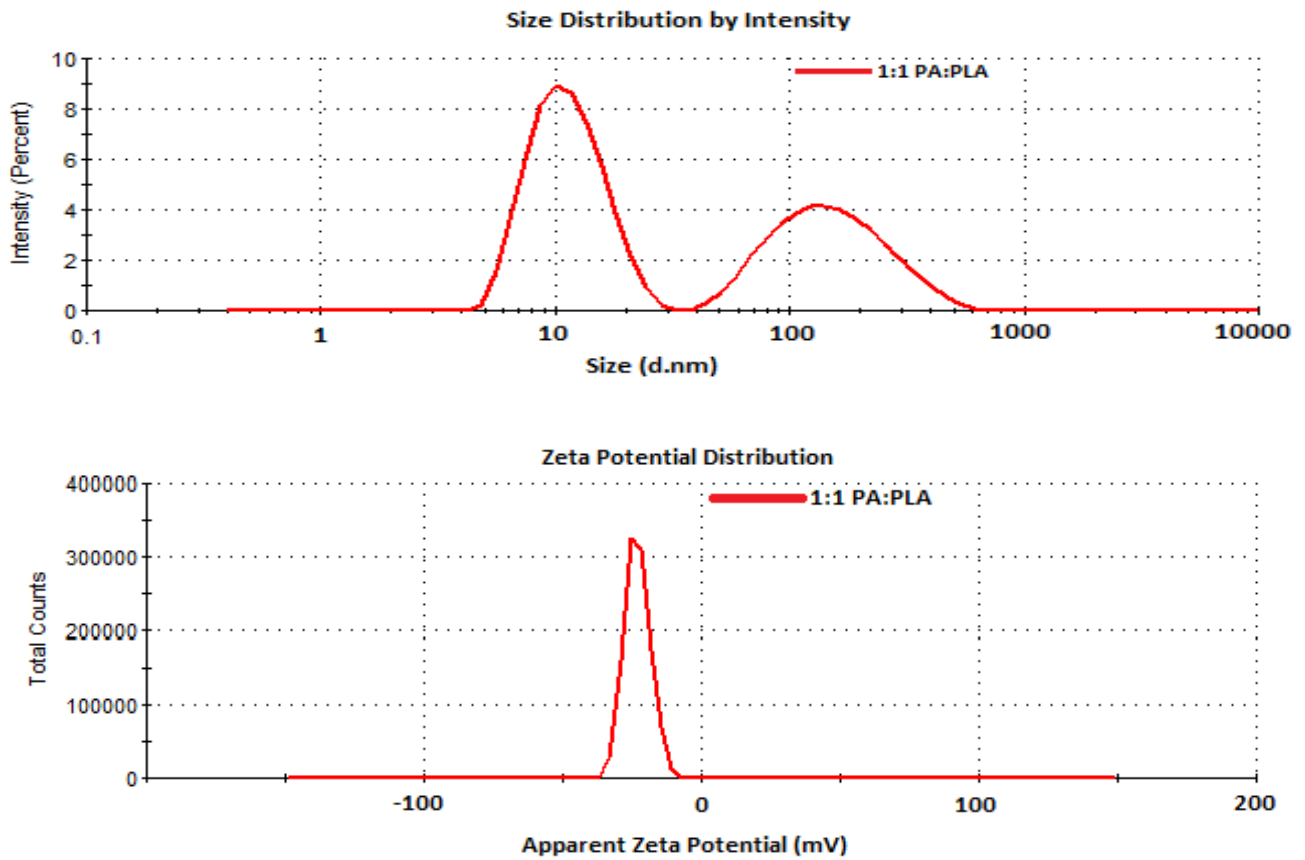


**Figure 4.9** Graphs depicting zeta size and zeta potential for 1:1 PA:PLA (plain).

Zeta sizing was undertaken to determine the size of the SLN's that are present in the different ratio formulations. The size range, Poly-dispersed index (PDI) and the average size of the SLN's present are reported. The PDI gives the size ranges of the SLN's that are present within a formulation, the greater the index the broader size distribution and a PDI below 0.7 suggests stability and possess an acceptable size distribution (Sharma *et al.* 2014; Abdellatif & Abou-Taleb, 2016). Figure 4.9 illustrates the percentage of SLN's that fall within a size range. The first peak occurs at 11.72d.nm (size) and has an intensity of 58.1% and the second peak, an intensity of 41.9% with a size of 167.4d.nm. The 1:1 PA:PLA has a PDI of 0.541 . The highest quantity of SLN's occurs in the first peak. The zeta potential for this formulation reads at -23.2mV indicating that the SLN's possess fair stability.

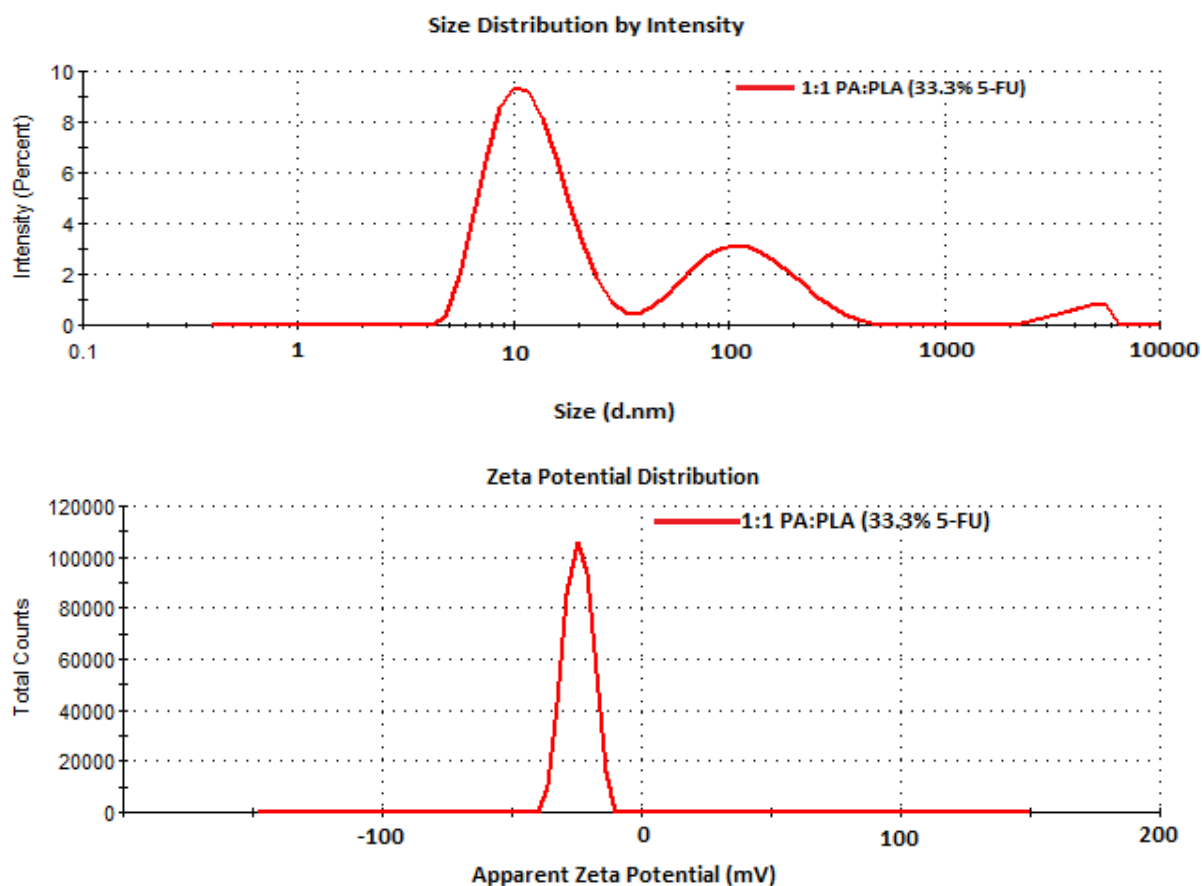


**Figure 4.10** Graphs depicting zeta size and zeta potential for 1:1 PA:PLA (drug encapsulated).

The drug loaded SLN's showed a greater size range than the plain SLN's, this could be due to the encapsulated drug. Three peaks are presented in Figure 4.10. The first peak occurs at 11.99d.nm with an intensity of 60.9%, with the following peak at 155d.nm with an intensity of 36%. Peak three occurs at 5233d.nm with an intensity of 3.1%.The PDI of the 1:1 PA:PLA is 0.151 indicating a low size distribution of SLN's. The zeta potential reading in Figure 10. is -24.6mV indicating fair stability of the nanoparticles. According to Honary & Zahir (2013), positively charged chitosan-modified-paclitaxil-PLGA nanoparticles (C-NP's) promotes an electrostatic interaction with cancerous cells due to a negatively charged surface area of tumour tissue, hence a greater accumulation of C-NP's at the tumour site for passive intracellular uptake. However it was reported by Grainger *et al.* (2010) that anionic (negatively charged) nanoparticles may be ideal for cancerous tissue as they move rapidly through the interstitium due to repulsive forces and settles between the matrix of the cell walls. Additionally, pulsed ultrasound may enhance the penetration process.

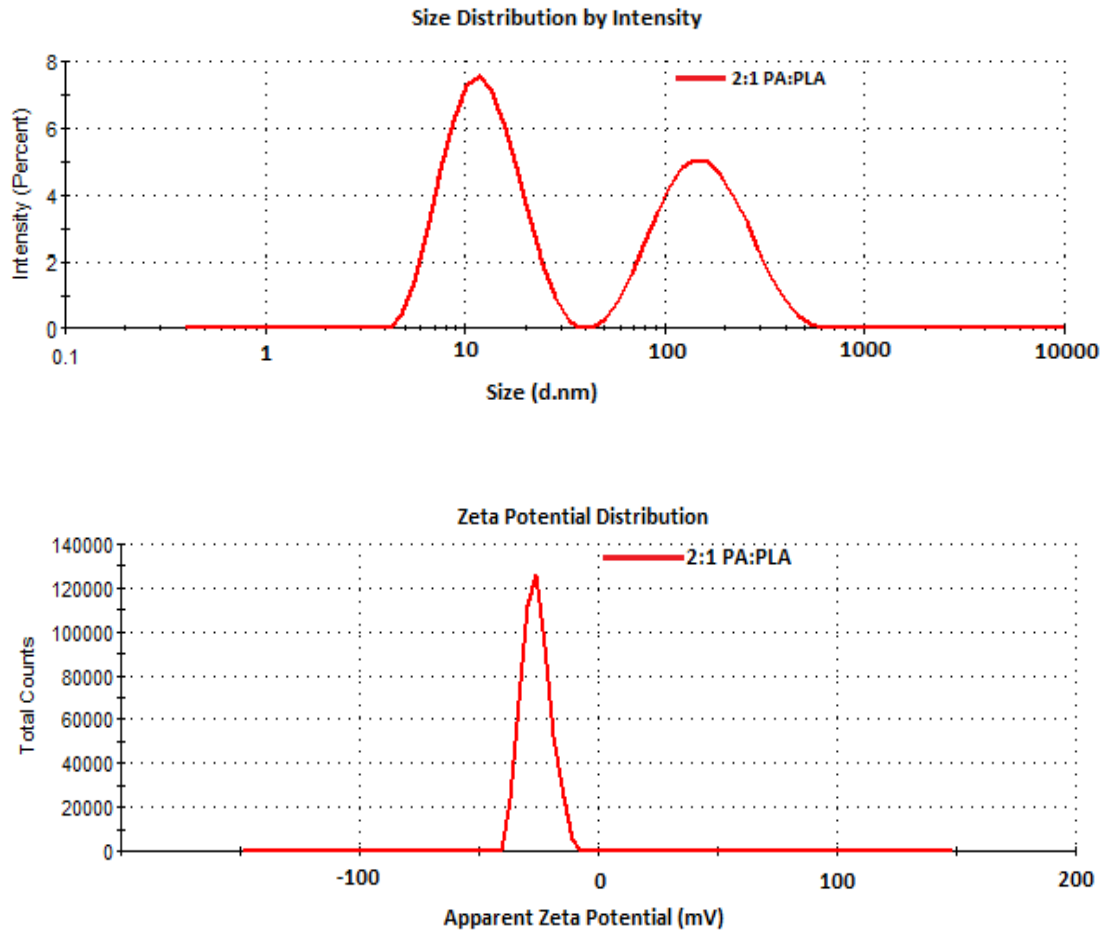


**Figure 4.11** Graphs depicting zeta size and zeta potential for 2:1 PA:PLA (plain).

In Figure 4.11, two size ranges of SLN's exists. The first peak occurs at 12.92d.nm with an intensity of 55% and the second peak occurs at 169.9d.nm with an intensity of 45%. The SLN's have an average size of 19.60d.nm with a PDI of 0.597. This suggests that the higher the polymer concentration, the bigger the size particles as this can be seen when comparing the two concentrations of SLN formulations. Zeta potentials greater than  $\pm 30$ mV are known to retain good stability properties and zeta potentials approaching  $\pm 60$ mV is considered to have outstanding stability (Lopez-Garcia & Ganem-Rondero, 2015). It can be noted that the zeta potential for 2:1 PA:PLA (plain) is -26.2mV and therefore could be described as reasonably stable.



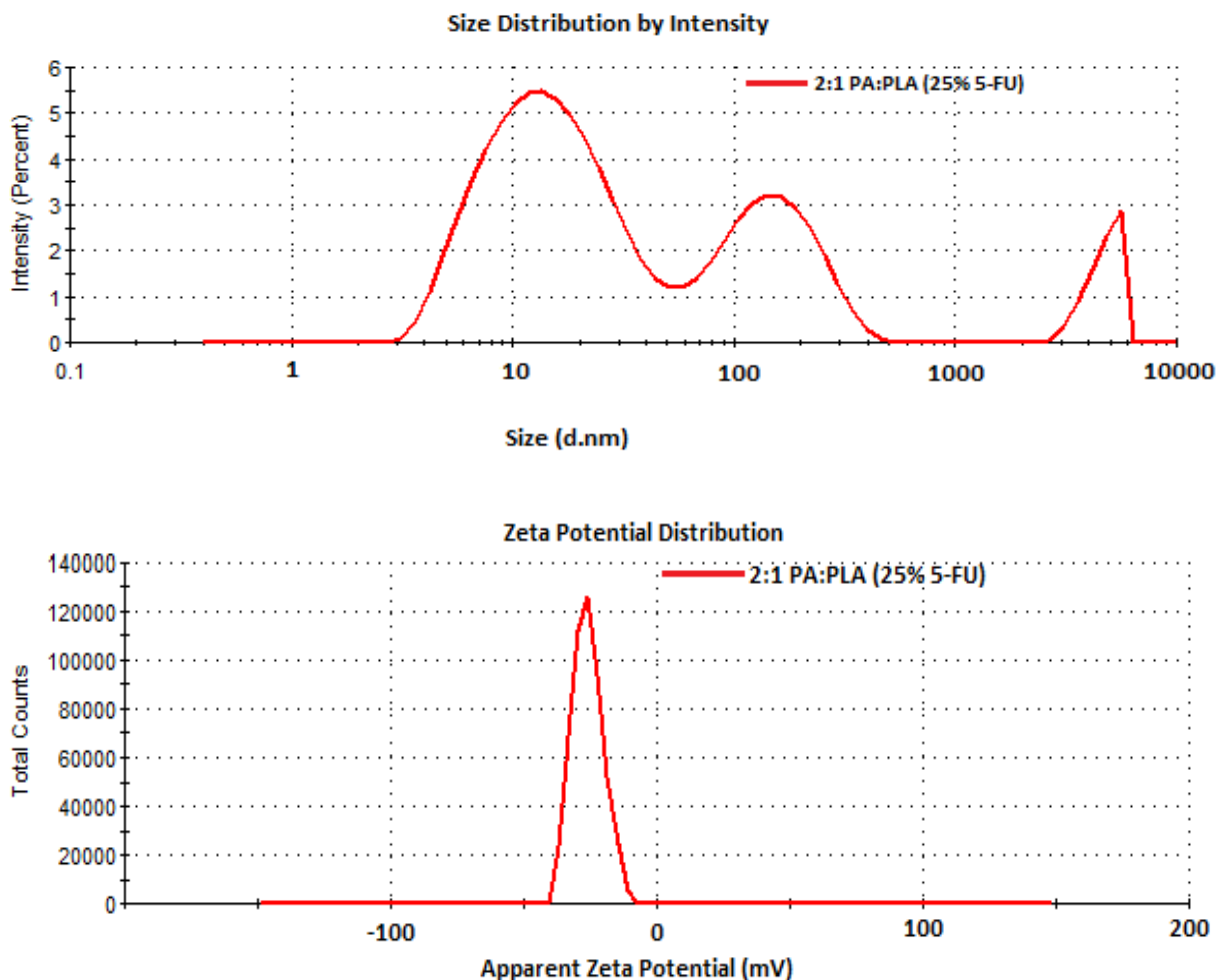


**Figure 4.12** Graphs depicting zeta size and zeta potential for 2:1 PA:PLA (drug encapsulated).

In Figure 4.12, it can be noted that as with 1:1 PA:PLA (33.3% 5-FU) loaded, 2:1 PA:PLA (25% 5-FU) presents with three peaks and the ranges are higher than 1:1 PA:PLA loaded SLN's. This could be due to the higher concentration of the polymer in these SLN's. In the above figure, the first peak arises at 16d.nm with an intensity of 62.6%. The second peak occurs at 153.8d.nm with an intensity of 29.4% and the third peak occurs at 472d.nm. The PDI is 0.307 that suggests the ideal size distributions for colloidal systems with a zeta potential of -25.2mV. Even though SLN's experience challenges with stability, improvements can be made via the addition of an appropriate surfactant or stabilizer to the formulation (Khadka *et al.* 2014; Narala & Veerabrahma, 2013).

#### 4.3.7 Evaluation of the Erosive and Swelling Dynamics of the TINO's.

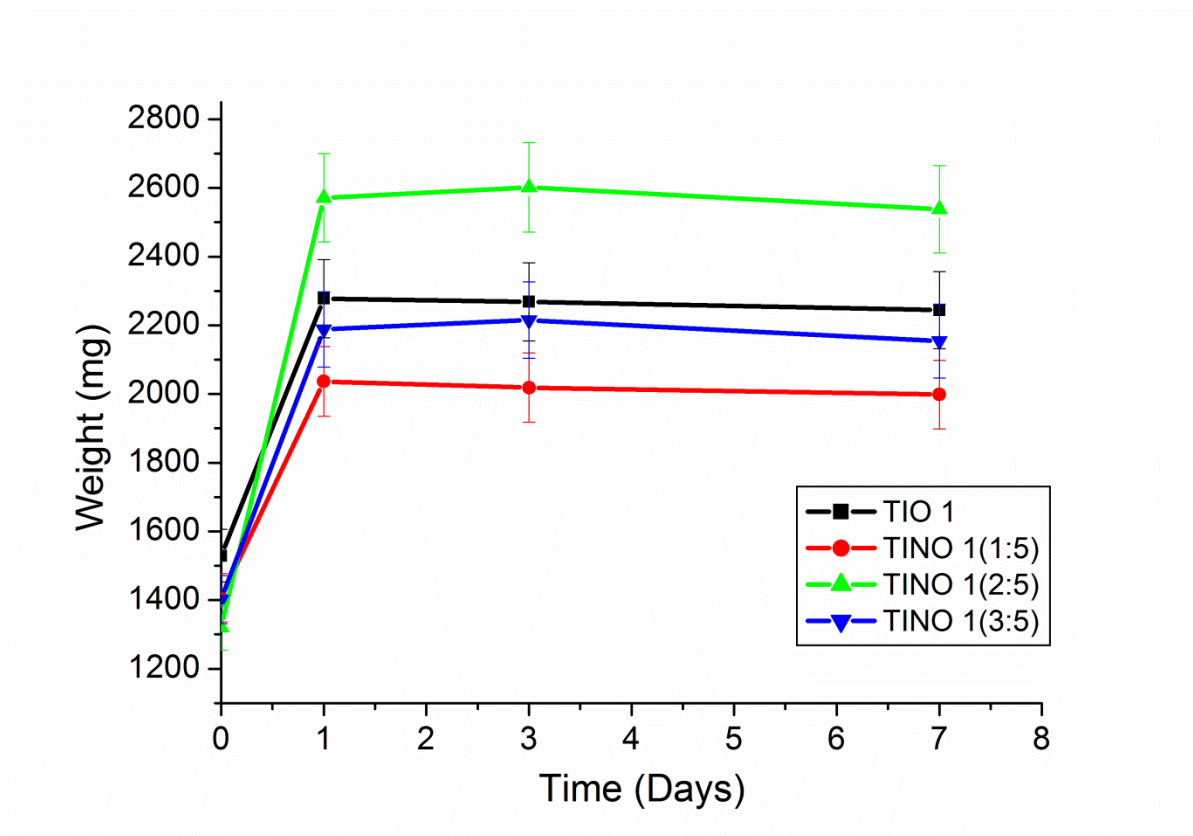


**Figure 4.13** Degradation and swelling profile for TIO 1, SLN: TINO 1 (1:5), (2:5) and (3:5). Standard deviation <131 in all cases (N=3).

Through analysis of Figure 4.13, on day 1 of the degradation study, an increase of weight was observed suggesting that TIO 1 is swelling. TINO 1 (2:5) and TINO 1 (3:5) continues to increase until day 3, TINO 1 (2:5) reaches a maximum weight of 2565.69mg and TINO 1 (3:5) reaches a maximum of 2189.50mg, thereafter a decrease in weight is noticeable and a further decrease is observed. This proposes degradation of the system. Analysing TIO 1 and TINO 1 (1:5), a peak in their weight can be noted, this could be due to water absorption between day 1 and day 3, slight degradation can be observed. Between Day 3 and day 7 a slight increase in weight can be noticed. Degradation by day 7 reveals that the weight of the TIO and TINO' does not reach its initial mass and can be correlating with the drug release profiles. On day 7, TINO 1 (1:5) released the highest concentration (46.8%) of drug and is closer to its initial weight faster than the other TINO's containing 5-FU loaded SLN's whereas TINO 1 (2:5) and TINO 1 (3:5) show a lower drug release profile, (23.8%) and (21.8%) respectively. This suggests a slower degradation rate than TINO 1 (1:5). Figure 4.13

indicates that with a higher concentration of SLN's in this TIO, the swellability of the TINO increases.

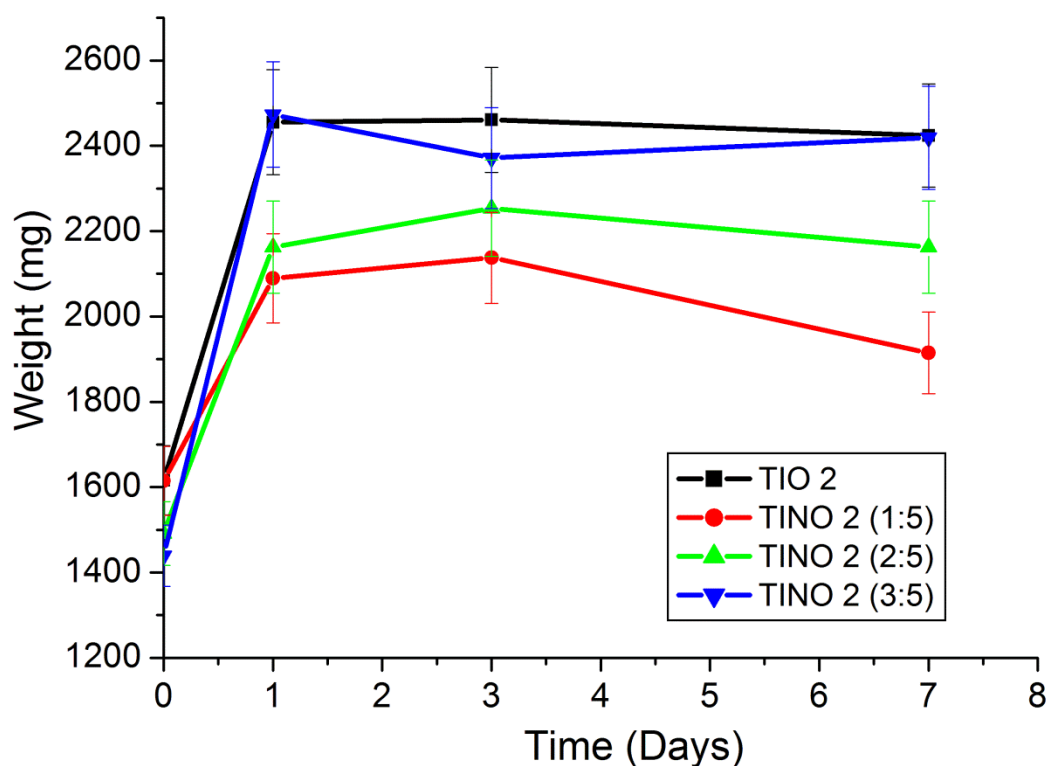


**Figure 4.14** Degradation and swelling profile for TIO 2, SLN: TINO 2 (1:5), (2:5) and (3:5). Standard deviation <124 in all cases (N=3).

When loading the SLN's in TIO 2 (TINO 2), degradation study patterns differed to those of TINO 1. In Figure 15, it can be noted that with an increase of SLN to TIO ratio, a significant weight increase of TIO 2 and TINO 2 samples after the first day of the study. Furthermore the rate of swelling of the TIO and TINO's on the first day also depicts an increase in weight which is proportional to SLN to TIO ratio. Subsequently to day three a decrease in the weight of TIO 2 and TINO 2 samples can be observed; the general pattern of activity for TINO 2 proposes degradation of the samples. TINO 2 (1:5) possesses the lowest weight of 1918.02mg, TINO 2 (2:5) has a final weight of 2159.27mg and TINO 2 (3:5) has a final weight of 2417.29mg. This again suggests that the higher the ratio of SLNs to TIO undergoes slower degradation. These degradation results can be correlated to the drug release profiles for TINO 2 (1:5), (2:5) and (3:5) which is 67.30%, 43.5% and 41.76% respectively on day seven.

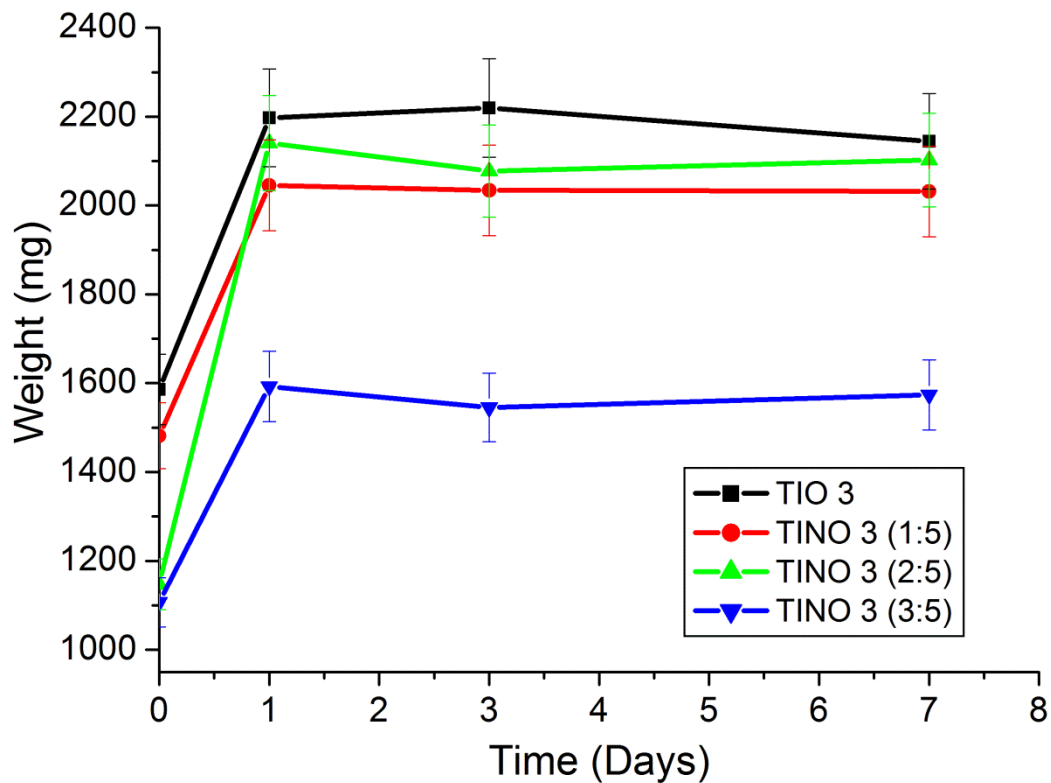


**Figure 4.15** Degradation and swelling profile for TIO 3, SLN: TINO 3 (1:5), (2:5) and (3:5). Standard deviation <111 in all cases (N=3).

The degradation study of TINO 3 conforms to a similar pattern as TINO 1 with regard to degradation rate of the TINO's i.e. the degradation TINO 3 (2:5) has the slowest degradation with TINO 3 (1:5) and TINO 3 (3:5) following subsequently. This can be noted with TINO 1's degradation profile. It can be observed, as seen in the two previous degradation figures, there is a substantial increase in the weight of all TIO three samples on the first day. Thereafter a decrease in weight following an increase can be observed. The pattern of the TINO's suggests an oscillating action between degradation and swelling. However, TIO 3, illustrates no oscillation but rather an increase upto day three, followed by a decrease in weight. This suggests a prolonged degradation with incorporation of SLN's (Dorraj & Moghimi, 2015). Furthermore, a higher concentration of incorporated SLN's in the TIO seem to decrease the swelling ability of this TIO this could be due to the SLN's occupying spaces within the gels network that fluid would in a plain gel.

#### 4.3.8 Drug Release Studies from the SLN's and the TINO's

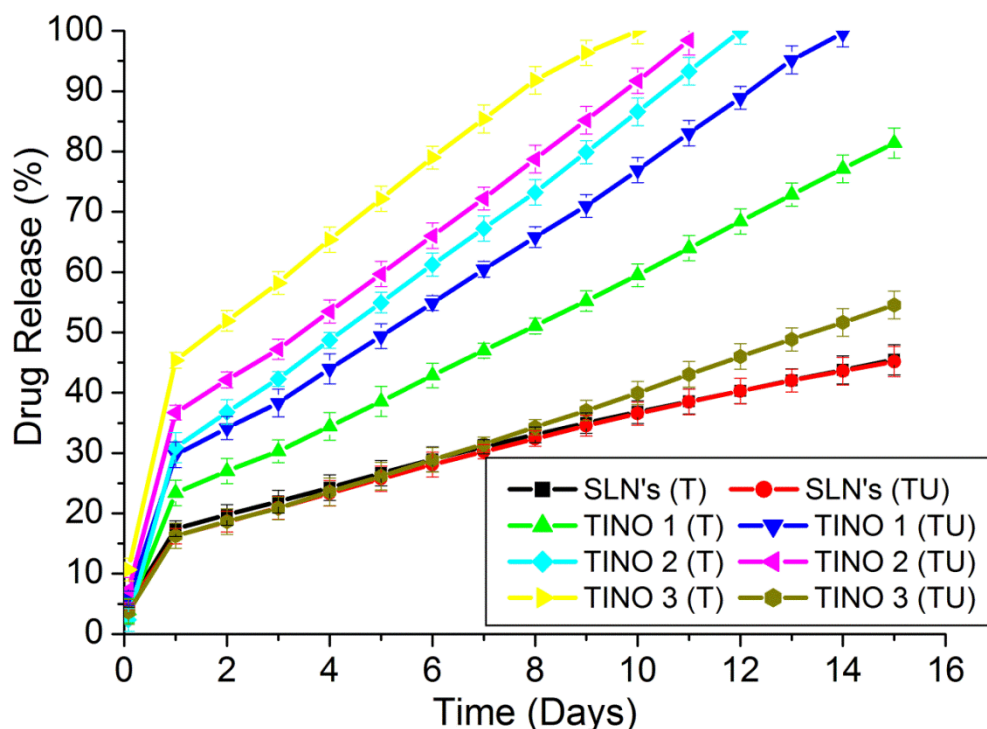


**Figure 4.16** Drug release profiles for 1:5 SLN: TIO ratio for TINO 1, TINO 2 and TINO 3. (T= Thermal ; TU = Thermal + Ultrasound). Standard deviation < 2.5 in all cases (N=3).

The general behaviour of all three drug release profiles shows an initial burst of drug on the first day and an overall sustained release for the next 14 days. In the drug release profile above, The SLN's presents with the lowest drug release profile in comparison to the SLN's incorporated into the TIO and shows no difference in the drug release when comparing the SLN'S exposed to thermal stimulation and the SLN'S exposed to a combination of thermal and ultrasound stimulation. This could be due to the gelation phenomenon discussed by Yadav et al.(2013), when the SLN's disperse they undergo rapid crystallization. This may have been the reason for the drug profile that is presented (Yadav *et al.* 2013). Incorporating the SLN's into the TIO increased the % release profiles therefore overcoming the problem of SLN gelation. In Figure 4.16, TINO 1 and TINO 2 respond to single and combined stimuli, and the TINO's exposed to the combined stimuli proves to have a release profile higher than that of the TINO's exposed to the single stimuli. TINO 3's behaviour contradicts the behaviour of TINO 1 and TINO 2. TINO 3 exposed to the combined stimuli, responds a lot less than the TINO 3 exposed to the single stimuli. It is worth mentioning that TINO 3 exposed to the single stimuli has the highest drug release and the TINO 3 exposed to the combined stimuli has the lowest release of the TINO formulations. From Figure 4.16, it can

be concluded that incorporating the SLN'S into the TIO formulation assisted with the promotion of drug release.

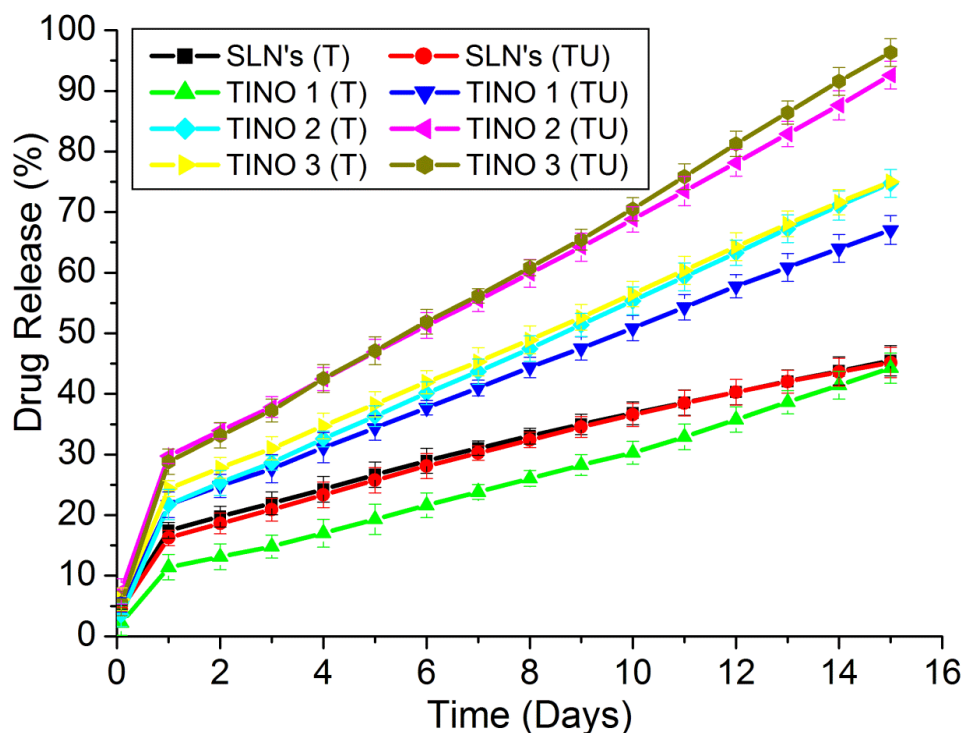


**Figure 4.17** Drug release profiles for 2:5 SLN: TIO ratio for TINO 1, TINO 2 and TINO 3. Standard deviation < 2.5 in all cases (N=3).

In the graph above, it can be noted that the SLN'S presents with the same behaviour as the figure before and all dissolution samples has an initial burst on the first day, thereafter has a steady drug release up to day 15. When analysing all the groups of TINO's it can be seen that all TINO samples release in a similar manner with regards to the groups of stimuli i.e. the TINO's exposed to the combined stimuli release was higher than that of the single stimuli. It can be noted that TINO 1 has the lowest release in a 15 day period suggesting that it has the highest sustained release profile of all three TINO's, with a drug release of 44.29% for the thermal stimuli and a drug release of 67.13% for TINO 1 with the combined stimuli. TINO 2 has a drug release profile of 74.38% and 92.54% for a single and combined stimulus at day 15. In this ratio of SLN:TIO; TINO 3 supersedes the drug release of TINO 1 and TINO 2 releasing 75.16% with thermal stimuli and 96.43% with combined stimuli by the 15<sup>th</sup> day. When comparing the overall drug release of Figure 4.16. Figure 4.17 shows a more sustained release with most formulations, this suggests that with an increase of SLN loading a greater sustained release is achieved.

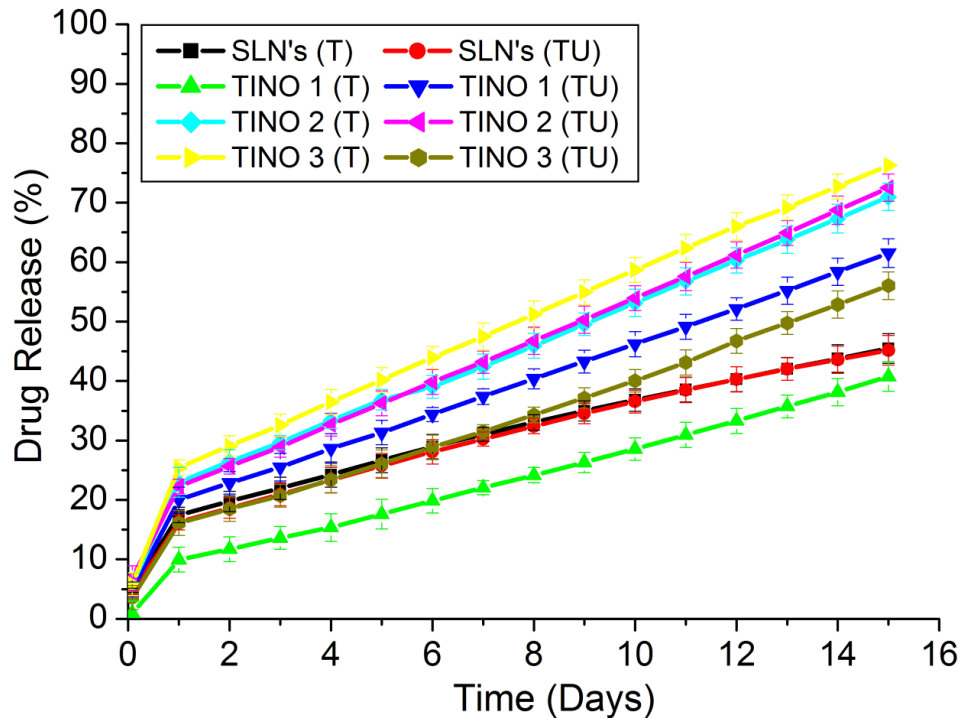


**Figure 4.18** Drug release profiles for 3:5 SLN: TIO ratio for TINO 1, TINO 2 and TINO 3. Standard deviation < 2.5 in all cases (N=3).

Observations of drug release patterns in the above Figure 4.18 can be very closely correlated to that of Figure 4.16, the SLN samples release 45.32% of the drug by day 15 as in the 2 previous figures. TINO 1 and TINO 2 demonstrates the behaviour desired while TINO 3 demonstrates an adverse behaviour as the TINO 3 under thermal (single) stimulation presents with a 20.38% higher difference by day 15 as compared to the TINO 3 under thermal and ultrasound (combined) stimuli. These release patterns can be seen in the above Figure. TINO 1 illustrates a vast difference between the single (40.66%) and combined (61.35%) stimuli of approximately 20% difference by day 15 whereas TINO 2 demonstrates a 2.27% difference between the single (70.67%) and dually (72.4%) stimulated TINO. It can be noted that the % drug release of Figure 4.18 decreased significantly in comparison to Figure 4.16 and Figure 4.17. It can be seen that the TINO release curves move towards the SLN release curves. This observation substantiates the suggestion made with regard to increasing the ratio of SLN's to TIO formulation. Another observation is that the TINO release profiles progresses to a steady linear state release rate as the SLN concentration in the formulation increases.



#### 4.4 Conclusions

TINO's were designed with the intention of in-situ application to the cervix as a potential treatment for cervical cancer to which would be augmented through ultrasound application as adjunctive therapy with increased drug release to the site. Solid Lipid Nanospheres were successfully designed with encapsulated 5-FU. Drug encapsulation increased the size of the SLN's but showed a fair stability and good size distribution. Drug release profiles were undertaken for the SLN's alone and for the TINO's. The drug release profiles for the SLN's displayed a prolonged release profile but when combined into a TIO it showed an easier controlled drug release with the concentration increase of SLN's in the system. TINO 1 and TINO 2 presented with desired results for drug release when comparing the single stimulus to the added ultrasound as this is better for local treatment in cancerous tissue.

#### 4.6 References

- Abbaspour, M., Makhmalzadeh, B.S., Arastoo, Z., Jahangiri, A., Shiralipour, R., 2013. Effect of Anionic Polymers on Drug Loading and Release from Clindamycin Phosphate Solid Lipid Nanoparticles. *Tropical Journal of Pharmaceutical Research*. 12(4):477-482.
- Abdellatif, A.A.H., Abou-Taleb, H.A., 2016. Transfersomal Nanoparticles of Keratolytic and Antibacterial Agents for Enhanced Transdermal Delivery. *Journal of Nanotechnology & Advanced Materials* 4(1):19-23.
- Ahad, N., Saion, E., Gharibshahi, E., 2012. Structural, Thermal, and Electrical Properties of PVA-Sodium Salicylate Solid Composite Polymer Electrolyte. *Journal of Nanomaterials* 2012(94):1-8.
- Andalib, S., Varshosaz, J., Hassanzadeh, F., Sadeghi, H., 2012. Optimization of LDL targeted nanostructured lipid carriers of 5-FU by a full factorial design. *Advanced Biomedical Research* 1(3):1-7.
- Awotwe-Otoo, D., Zidan, A.S., Rahman, Z., Habib, M.J., 2012. Evaluation of Anticancer Drug-Loaded Nanoparticle Characteristics by Nondestructive Methodologies. *AAPS PharmSciTech* 13:611-622.
- Bhaskar, K., Anbu, J., Ravichandiran, V., Venkateswarlu, V., Rao, Y.M., 2009. Lipid nanoparticles for transdermal delivery of flurbiprofen: formulation, *in vitro*, *ex vivo* and *in vivo* studies. *Lipids in Health and Disease* 8(6).



- Brigger, I., Dubernet, C., Couvreur, P., 2012. Nanoparticles in cancer therapy and diagnosis. *Advanced Drug Delivery Reviews* 64: 24–36.
- Coccia, M. Wang, L., 2015. Path-breaking directions of nanotechnology-based chemotherapy and molecular cancer therapy. *Technological Forecasting & Social Change* 94:155–169.
- Couture, C., Foley, J., Kassell, N.F., Larrat, B., Aubry, J-N. 2014. Review of ultrasound mediated drug delivery for cancer treatment: updates from pre-clinical studies. *Transl Cancer Res* 2014 3(5):494-511.
- Dolatabadi, J.E.N, Valizadeh, H., Hamishehkar H., 2015. Solid Lipid Nanoparticles as Efficient Drug and Gene Delivery Systems: Recent Breakthroughs. *Advanced Pharmaceutical Bulletin*. 5(2):151-159.
- Dorraj, G., Moghimi, H.R., 2015. Preparation of SLN-containing Thermoresponsive In-situ Forming Gel as a Controlled Nanoparticle Delivery System and Investigating its Rheological, Thermal and Erosion Behavior. *Iranian Journal of Pharmaceutical Research*. 14(2):347-358.
- Garland, R.M. Wise, M.E. Beaver, M.R., DeWitt, H.L., Aiken, A.C., Jimenez, J.L., Tolbert, M.A., 2005. Impact of palmitic acid coating on the water uptake and loss of ammonium sulfate particles. *Atmospheric Chemistry and Physics*. 5:1951-1961.
- Grainger, S.J., Serna, J.V., Sunny, S., Zhou, Y., Deng, C.X., El-Sayed. M.E.H., 2010. Pulsed Ultrasound Enhances Nanoparticle Penetration into Breast Cancer Spheroids. *Mol Pharm* 7(6): 2006–2019.
- Honary, S.H., Zahir, F., 2013. Effect of Zeta Potential on the Properties of Nano-Drug Delivery Systems - A Review (Part 1). *Tropical Journal of Pharmaceutical Research* 12(2):255-264.
- Kakadia, P.G., Conway, B.R., 2014. Solid Lipid Nanoparticles: A Potential Approach for Dermal Drug Delivery. *American Journal of Pharmacological Sciences* 2(5):1-7.
- Kang, K.W., Chun, M-K., Kim, O., Subedi, R.K., Ahn, S-G., Yoon, J-H., Choi, H-K., 2010. Doxorubicin-loaded solid lipid nanoparticles to overcome multidrug resistance in cancer therapy. *Nanomedicine: Nanotechnology, Biology, and Medicine* 6:210–213.
- Khadka, P., Ro, J., Kim, H., Kim, I., Kim, J.T., Kim, H., Cho, J.M., Yun, G., Lee, J., 2014. Pharmaceutical particle technologies: An approach to improve drug solubility, dissolution and bioavailability. *Asian journal of pharmaceutical sciences* 9: 304-316.

Kumar, A., Sawant, K.K.,2013. Solid lipid nanoparticle-incorporated gel: the future treatment for skin infections?.*Nanomedicine*. 8:1901-1903.

Latibari, S.T., Mehrali, M., Mehrali, M., Mahlia, T.M.I., Metselaar, H.S.C.,2014. Facile Preparation of Carbon Microcapsules Containing Phase-Change Material with Enhanced Thermal Properties. *the Scientific World Journal* 2014.

López-García, R., Ganem-Rondero, A.,2015. Solid Lipid Nanoparticles (SLN) and Nanostructured Lipid Carriers (NLC): Occlusive Effect and Penetration Enhancement Ability. *Journal of Cosmetics, Dermatological Sciences and Applications* 5:62-72.

Maji, R., Dey, N.S.,. 2014. Preparation and characterization of Tamoxifen citrate loaded nanoparticles for breast cancer therapy. *International Journal of Nanomedicine* 9(3):3017-3118.

Manjunath, A., Deepa, T., Supreetha, N.K., Ifan, M.,2015. Studies on AC Electrical Conductivity and Dielectric Properties of PVA/NH<sub>4</sub>NO<sub>3</sub> Solid Polymer Electrolyte Films. *Advances in Materials Physics and Chemistry* 2015 5: 295-301.

Miller, D., Smith, N., Bailey, M., Czarnota, G., Hynynen, K., Makin, I.,2012.Overview of Therapeutic Ultrasound Applications and Safety Considerations. *Journal of Ultrasound Med.* 31(4):623–634.

Mountzious, G., Soultati, A., Pectasides, D., Dimopoulos, M.A., Papadimitriou, C.A.,2013.Novel Approaches for Concurrent Irradiation in Locally Advanced Cervical Cancer: Platinum Combinations, Non-Platinum-Containing Regimens, and Molecular Targeted Agents. *Obstetrics and Gynecology International* 2013(5):536765.

Nair, K.L., Jaqadeeshan, S., Kumar, J.S.,2011. Biological evaluation of 5-fluorouracil nanoparticles for cancer chemotherapy and its dependence on the carrier, PLGA. *International Journal of Nanomedicine* 6:1685-1697.

Narala, A., Veerabrahma, K.,. 2013. Preparation, Characterization and Evaluation of Quetiapine Fumarate Solid Lipid Nanoparticles to Improve the Oral Bioavailability. *Journal of Pharmaceutics* 2013.

Olukman, M., Sanli, O., Solak,E.K.,2012. Release of Anticancer Drug 5-Fluorouracil from Different Ionically Crosslinked Alginate Beads. *Journal of Biomaterials and Nanobiotechnology*. 3:469-479.

Patel, M.N., Lakkadwala, S., Majrad, M.S., Injeti, E.R., Gollmer, S.M., Shah, Z.A., Boddu, S.H.S., Nesamony, J., 2014. Characterization and Evaluation of 5-Fluorouracil-Loaded Solid Lipid Nanoparticles Prepared via a Temperature-Modulated Solidification Technique. *AAPS PharmSciTech* 15(6):1498-1508.

Rahangdale, L., Lippmann, Q.K., Garcia, K., Budwit, D., Smith, J.S., van Le, L., 2014. Topical 5-fluorouracil for treatment of cervical intraepithelial neoplasia 2: a randomized controlled trial. *American Journal of Obstetrics and Gynecology* 4: 3141-3148.

Rapoport, N., Payne, A., Dillon, C., Shea, J., Scaife, C., Gupta, R., 2013. Focused ultrasound-mediated drug delivery to pancreatic cancer in a mouse model. *Journal of Therapeutic Ultrasound* 1-11.

Safari, J., Zarnegar, Z., 2014. Advanced drug delivery systems: Nanotechnology of health design A review. *Journal of Saudi Chemical Society* 18:85–99.

Sharma, D., Maheshwari, D., Philip, G., Rana, R., Bhatia, S., Singh, M., Gabrani, M.R., Sharma, S.K., Ali, J., Sharma, R.K., Dang, S., 2014. Formulation and Optimization of Polymeric Nanoparticles for Intranasal Delivery of Lorazepam Using Box-Behnken Design: *In Vitro* and *In Vivo* Evaluation. *BioMed Research International* 2014: 1-14.

Shi, L., Li, Z., Yu, L., Jia, H., Zheng, L., 2011. Effects of Surfactants and Lipids on the Preparation of Solid Lipid Nanoparticles Using Double Emulsion Method. *Journal of Dispersion Science and Technology* 32(2): 254-259.

Thakor, A.S., Gambhir, S.S., 2013. Nanooncology: The Future of Cancer Diagnosis and Therapy. *CA : Cancer Journals for Clinicians* 63(6):395–418.

Wolinsky, J.B., Colson, Y.L., Grinstaff, M.W., 2012. Local Drug Delivery Strategies for Cancer Treatment: Gels, Nanoparticles, Polymeric Films, Rods and Wafers. *Journal of Controlled Release* 159(1):34.

Xu, J., Wang, J., Xiangting Dong, J., Guixia Liu, G., Yu, W., 2011. Preparation of PVP/PLLA Ultrafine Blend Fibers by Electrospinning. *International Journal of Chemistry* 3(4):57-60.

Yadav, N., Khatak, S., SINGH SARA, S., 2013. Solid lipid nanoparticles- a review. *International Journal of Applied Pharmaceutics* 5(2):8-18.

Yuan, Q., Han, J., Cong, W., Ge, Y., Ma, D., Dai, Z., Li, Y., Bi, X., 2015. Docetaxel-loaded solid lipid nanoparticles suppress breast cancer cells growth with reduced myelosuppression toxicity. *International journal of Nanomedicine* 9:4829—4846.

## CHAPTER 5

### CONCLUSIONS AND RECOMMENDATIONS

---

---

#### 5.1 Conclusions

Cervical cancer is rated one of the most prominent and lethal cancers among women and is strongly attributed to HPV. Precancerous stages of cervical cancer (CIN I, II, III) are an important part of early diagnosis. There are many types of HPV viruses and a great number of these are due to sexual contact and therefore has recently been affecting the younger population, males and females. If not treated, HPV may progress to CIN eventually leading to cervical cancer. HPV vaccines are available as a preventative measure but not every individual has the means of acquiring the vaccine due to factors such as social issues and the cost of living, thus alternative approaches are essential.

The continuous expansion of drug delivery has opened doors of opportunities for enhancement of diagnosing and treating procedures, including the augmentation of medical procedures such as HIFU application for tumoural ablation. Stimuli-responsive delivery systems are being developed everyday and are moving toward nanotechnological designed systems for advanced and synergistic treatment in medical conditions including cancer. Extensive research has been done on thermoresponsive and ultrasound-responsive delivery systems. These two responses complement each other in the presence of ultrasound owing to frequencies and heat that is produced by the ultrasound. Many polymers that do not respond to ultrasound may be modified in formulation delivery systems to become ultrasound responsive. Ultrasound has shown to alter pH in some cases and may be used in a variety of modified stimuli-responsive systems in the future. These systems can be termed as being 'Pseudo-ultrasonic' responsive.

Combinations of thermoresponsive and ultrasound responsive polymers were employed to formulate organogels with a minute concentration of DMSO and additional solvents that are less toxic, to determine the responsive properties of the gel. The TIO's presented with different degrees of responses to heat and ultrasound stimuli. However, TIO 3 shows minimal physical changes under stimuli response. This dual response system combining antineoplastic, heat and ultrasound should synergistically increase the overall therapeutic outcome for a patient. The Images of the gels show that they have a very dense network but also accommodate for loading of other substances that is; drugs or carriers of bioactives such as SLN's. The SLN's will prevent unnecessary leakage of the drug to reduce the side effects associated with the chemotherapeutic agents. The amorphous nature of the TIO's

adds an advantage towards delivery of drugs and has been proven non-cytotoxic below 5mg/mL.

It has been previously established in clinical trials that 5-fluorouracil is efficient in treating cervical cancer intravaginally. The SLN's have proven by a large scale to fall within the nano range through SEM and Zeta sizing and possess reasonable drug entrapment. An increased polymer concentration during formulation leads to an increase in size of the SLN's. The TINO's showed both swelling and erosive properties during degradation studies. The drug release profiles for the SLN alone showed a greater sustained release whereas the SLN incorporated into the TIO allows for a higher concentration of drug release. TINO 1 and TINO 2 provides the desired response for drug release i.e. TINO's exposed to ultrasound as well as thermal stimuli depict greater drug release profiles in comparison to thermal stimuli alone. However, TIO 3 did not provide the same response. It can be concluded that TINO 1 and TINO 2 in conjunction with ultrasound application are potential delivery systems that may be further investigated for cervical cancer.

## **5.2 Recommendations**

- a) The TIO's properties could be optimized to improve its injectability and responsiveness to body temperature and HIFU via polymer proportion.
- b) The SLN's maybe optimised to increase the concentration of the 5-FU for maximum entrapment.
- c) The TINO delivery system could be optimised with the proportions of SLN:TIO for adequate drug delivery.
- d) The TINO's may undergo animal studies to determine the optimised quantity that would deliver the desired outcome.
- e) It may be studied in the management of Human PapillomaVirus (HPV) by decreasing the size of the lesion gradually in combination with ultrasound such as HIFU and ultimately ablation of the lesion.
- f) It may be studied in the treatment of Cervical Intraepithelial Neoplasia or cervical dysplasia by ultrasound application targeting the mutated tissue solely, leaving healthy tissue unharmed and increase repairing time.
- g) It could be studied for management of cervical cancer through preventing the progression of the staging and grading of the lesion.
- h) It could be studied as treatment of cervical polyps by decreasing the size of the polyps until they completely regress in order for healing to commence.

## APPENDICES

### APPENDIX A

---

---

#### **A Review of Thermo- and Ultrasound-Responsive Polymeric Systems for Targeted Delivery of Chemotherapeutic Agents**

**Zardad A., Choonara Y. E., du Toit L. C., Kumar P., Mabrouk M., Kondiah P. P. D., Pillay V.\***

*<sup>1</sup>Wits Advanced Drug Delivery Platform Research Unit, Department of Pharmacy and Pharmacology, School of Therapeutic Sciences, Faculty of Health Sciences, University of the Witwatersrand, Johannesburg, 7 York Road, Parktown, 2193, South Africa*

Correspondence: [viness.pillay@wits.ac.za](mailto:viness.pillay@wits.ac.za)

#### **Abstract**

There has been an exponential increase in research into the development of thermal and ultrasound-activated delivery systems for cancer therapy. The majority of researchers employ polymer technology that responds to environmental stimuli some of which are physiologically induced such as temperature, pH, as well as electrical impulses, which are considered as internal stimuli. External stimuli include ultrasound, light, laser and magnetic induction. Biodegradable polymers have interesting properties that have proven to be thermo-responsive or ultrasound-responsive that can complement cancer therapy through sonoporation and hyperthermia by means of High Intensity Focused Ultrasound (HIFU). Thermo-responsive and other stimuli-responsive polymers have been used in drug delivery systems, activated via ultrasound stimulation. polyethylene oxide/polypropylene oxide cblock or triblock polymers and Poly methacrylate(PMA) are thermal- and pH-responsive polymers, respectively but have proven to have successful activity and contribution in chemotherapy when exposed to ultrasound stimulation. This review focused on collating thermal and ultrasound-responsive delivery systems, and combined thermo-ultrasonic responsive systems, and elaborating the advantages, as well as shortcomings, of these systems in cancer chemotherapy. The mechanisms of these systems are explicated through their physical alteration when exposed to the corresponding stimuli. The properties they possess and the modifications that enhance the mechanism of chemotherapeutic drug delivery from systems are discussed and the concept of pseudo-ultrasound responsive systems was introduced.

**Facile Green Synthesis of Thermo-sonic injectable Organogels (TIO's)**

**Zardad A., Choonara Y. E., du Toit L. C., Kumar P., Mabrouk M., Badhe R.V., Cheraja  
D.R., Kondiah P. P. D., Pillay V\***

*<sup>1</sup>Wits Advanced Drug Delivery Platform Research Unit, Department of Pharmacy and Pharmacology, School of Therapeutic Sciences, Faculty of Health Sciences, University of the Witwatersrand, Johannesburg, 7 York Road, Parktown, 2193, South Africa*

Correspondence: [viness.pillay@wits.ac.za](mailto:viness.pillay@wits.ac.za)

**Abstract**

The purpose of this study was to design TIO's moving towards thermal and ultrasonic stimuli. The TIO's were non-cytotoxic and biocompatible, with properties of gellation in response to tumoral temperature as well as being responsive to ultrasound stimuli. These TIO's were formulated through a simplistic open ring polymerization process integrating green chemistry principals. Fourier Transformed Infrared Spectroscopy (FTIR), Differential Scanning Calorimetry (DSC), X-Ray Diffraction (XRD), Rheological tests, Scanning Electron Microscopy (SEM), Textural analysis and cell proliferation studies were performed on the TIO's in order to obtain the results. Open ring polymerization was achieved in <15 minutes. SEM images convey the density and microscopic structures seen within the TIO's such as striations and pores which permits facilitated storage for drug loading. New bands are observed at  $770.9\text{cm}^{-1}$ ,  $1037\text{cm}^{-1}$  and  $1080\text{cm}^{-1}$  that represent the presence of aromatic rings, -CH deformation vibrations and C-O carbonyl groups attached to an aromatic ring. Gels showed an amorphous nature by representation of shallow broad peaks from the sharp concise peaks given by the parent monomers. Rheological temp ramp tests depicts the storage modulus  $G'$  to be higher than loss modulus  $G''$  where  $G'$  increases at a faster rate than  $G''$  when heat is applied. The compressive strength of the gels was recorded at 4Pa, 3.25Pa and 4.4Pa. TIO 1, TIO 2 and TIO 3 formulations are non-cytotoxic when used at concentrations of 6mg/mL, 7.8mg/mL and 7mg/mL respectively and promote cell proliferation within a 5 day period. The design of TIO's was successfully formulated to respond to thermal and ultrasound stimuli.

### **Synthesis, Characterization and the Assembly of Solid Lipid Nanospheres into the Thermosonic Injectable Organogel (TINO's)**

**Zardad A., Choonara Y. E., du Toit L. C., Kumar P., Mabrouk M., Kondiah P. P. D., Pillay V\***

*<sup>1</sup>Wits Advanced Drug Delivery Platform Research Unit, Department of Pharmacy and Pharmacology, School of Therapeutic Sciences, Faculty of Health Sciences, University of the Witwatersrand, Johannesburg, 7 York Road, Parktown, 2193, South Africa*

Correspondence: viness.pillay@wits.ac.za

#### **Abstract**

The objective of this study was to design Solid Lipid Nanospheres (SLN's) with a Poly Vinyl Alcohol coat, which serves as a carrier of 5-Fluorouracil and load. These SLN's were added to a TIO's to form TINO's with thermosonic properties and releases a higher dose of drug on ultrasound stimulus command. FTIR, DSC, XRD, zeta sizing, zeta potential and SEM were carried out for the SLN's while degradation and dissolution studies were undertaken on the combined system. FTIR for the SLN's presented with a broad band between  $3027\text{-}3614\text{cm}^{-1}$  and prominent bands at  $2942\text{cm}^{-1}$  and  $1729\text{cm}^{-1}$ . Furthermore, the addition of 5-FU in the formulation increases the intensity of the bands. The thermal activity of the SLN's show a slightly lower melting point than PVA ( $323.29^\circ\text{C}$ ) and the drug loaded SLN's formulations show thermal activity that may represent degradation of the SLN's. The XRD results for the SLN's convey that 1:1 PA: PLA is semi crystalline as it presents with a broad peak at an average intensity of 5528.32a.u. at approximately  $35.5^\circ$  while 2:1 convey an amorphous nature of the SLN's. SEM images depicts that with an increase in polymer concentration and addition of 5-FU, the size of the particles increase. The zeta potential of the SLN's are between  $-23.2$  and  $-26.2\text{mV}$  however the PDI of the SLN's are all below 0.6 and therefore can be said to possess a fair to good stability with an accepted size distribution. The degradation profiles show that the combined system undergoes swelling and degradation and loading of SLN's into the TIO's may prolong degradation of the TINO. Drug release profiles depict that TINO's assist with drug release from the SLN and with higher concentrations of SLN's the release profiles are more sustained.